NAT'L INST. OF STAND & TECH R.I.C.
A11105 102441

NIST
PUBLICATIONS

NISTIR 5904

ANNUAL CONFERENCE ON FIRE RESEARCH: Book of Abstracts October 28 - 31, 1996

Kellie Beall, Editor

Building and Fire Research Laboratory
Gaithersburg, Maryland 20899

QC
100
.U56
NO.5904
1996

United States Department of Commerce
Technology Administration
National Institute of Standards and Technology

NISTIR 5904

ANNUAL CONFERENCE ON FIRE RESEARCH: Book of Abstracts October 28 - 31, 1996

Kellie Beall, Editor

October, 1996
Building and Fire Research Laboratory
National Institute of Standards and Technology
Gaithersburg, MD 20899

U.S. Department of Commerce
Michael Kantor, *Secretary*
Technology Administration
Mary L. Good, *Under Secretary for Technology*
National Institute of Standards and Technology
Arati Prabhakar, *Director*

TABLE OF CONTENTS and
CONFERENCE PROGRAM

MONDAY, OCTOBER 28, 1996

Opening Remarks: 8:30 - 9:00 a.m.

SESSION 1:
FIRE SUPPRESSION - WATER SPRAYS
9:05 a.m. - 12:40 p.m.

SESSION 2:
SOOT AND HEAT
9:05 a.m. - 12:40 p.m.

Break: 10:35 - 10:55 a.m.

Lunch: 12:40 - 1:45 p.m.

SESSION 1:
FIRE SUPPRESION - WATER SPRAYS
1:45 - 5:15 p.m.

SESSION 2:
POOL AND JET FIRES
1:45 - 5:15 p.m.

Adjourn: 5:15 p.m.

Buses Leave for Smokey Glen Farm: 6:00 p.m.

Barbeque Dinner, Smokey Glen Farm: 6:30 p.m.

TUESDAY, OCTOBER 29, 1996

SESSION 1:
FIRE SUPPRESSION - HALON ALTERNATIVES
8:35 a.m - 12:40 p.m.

SESSION 2:
FIRE PLUMES

8:35 a.m. - 12:40 p.m.

Break: 10:35 - 10:55 a.m.

Lunch: 12:40 - 1:45 p.m.

WEDNESDAY, OCTOBER 30, 1996

THURSDAY, OCTOBER 31, 1996

INTRODUCTION

The NIST Annual Conference on Fire Research has long been the prime forum for the presentation and discussion of the latest advances in the science of fire and the engineering of fire safety. Hundreds of billions of dollars of products and services are involved in fire safety decisions each year. New technology is changing the way those products are developed, manufactured, evaluated, and used.

This conference enables all interested parties to hear of and discuss advances in fire science, with the intent of stimulating (a) new products that are more fire-safe and (b) new ways to capture that value in the ways products are tested and approved for use. The Conference scope includes all fire research performed within Federal laboratories or sponsored by Federal agencies, as well as work from laboratories around the world.

This booklet contains the abstracts of the 76 papers focussing on the phenomenology of fire: fire extinguishment, chemistry and physics of material and product combustion, flame spread, flame structure, soot, pool fires, fire-induced flows, fire plumes, combustion product generation and measurement, and fire detection. Discussion session will consider the status of our knowledge and the most important understanding yet to be developed. With this, we hope to continue cross-pollinating the elements of the fire research community while stimulating our members to new understanding that will lead to more fire-safe products and practices.

Richard G. Gann, Conference Chair
Chief, Fire Science Division
Building and Fire Research Laboratory
National Institute of Standards and Technology

THE DYNAMICS OF WATER DROPLETS IN A COUNTERFLOW FIELD AND ITS EFFECT ON FLAME EXTINCTION

Andrea M. Lentati and Harsha K. Chelliah
Department of Mechanical, Aerospace and Nuclear Engineering
University of Virginia
Charlottesville, VA 22903

Introduction

Efficient suppression of flames by condensed-phase agents (e.g. dry powder, water, etc.) requires a basic understanding of the rate-controlling physical, thermal and chemical processes. A steady, laminar, non-premixed flame, established within the mixing layer of a counterflow of methane and air, is used here to numerically determine the rate controlling processes associated with flame extinction by fine water droplets. Although experiments are planned to validate the model, only the numerical results with water droplets introduced with the air stream are reported here.

Numerical Calculations

In implementing particle effects to the existing quasi one-dimensional flame code [1], Eulerian-Eulerian formulation can, in theory, be adopted to describe the gas-phase and particle-phase interactions [2]. However, for large particles, the "push back" effect (i.e. if the particles are large enough to penetrate through the stagnation plane, then the on coming methane stream can reverse their direction of motion) gives rise to a singularity in the particle number density equation [3]. To overcome such singular points, it is found convenient to implement a hybrid Eulerian-Lagrangian formulation for gas-particle phases. The resulting Lagrangian equations for mass, momentum, energy and particle flux fraction (normalized by that at the air nozzle exit) are integrated in time to determine the particle location and source terms contributing to the gas-phase conservation equations. The two sets of equations are then iterated until a predetermined convergence criterion is reached. Using this modified counterflow nonpremixed flame code, the water particle dynamics in a reacting counterflow field with and without mass evaporation are performed and are presented here.

Results and Discussion

When a single droplet is introduced with the air stream to a counterflow flame, the temperature and the velocity of the droplet can be different from that of the local gas-phase. The resulting thermal and momentum lag will control the heat transfer rate to the droplet and the subsequent cooling of the gas, leading to different extinction characteristics at different particle loading and size.

If interactions between particles and the gas-phase is neglected, then the integration of Lagrangian equations controlling the dynamics of a *single* water particle gives trajectories as shown in Fig. 1, for particle sizes ranging from 10-70 μm. The 10 μm particle is seen to track the gas velocity closely, while the large particles show the "push back" effect, with several crossings of the stagnation plane. Depending on whether the mass evaporation and gas-particle interactions are included or not, the dynamics of the particles can differ slightly. The mass evaporation process itself is coupled to the droplet temperature and to that of the gas mixture. As the droplet enters the thermal mixing layer, there is a short transient period in which the droplet temperature approaches the boiling point, T_b [the actual droplet temperature, T_s ($< T_b$), can be estimated by using the Clausius-Clapeyron Equation]. During this transient time a thermal wave will propagate from the surface of the droplet to the interior of the droplet, with increasing surface temperature. The temperature of the droplet will eventually reach a steady value, T_s. The total duration for the droplet temperature to achieve this value T_s starting from the room temperature, T_∞, is strongly related to the original particle size, thermal diffusivity, and net heat flux from the gas-phase to the droplet. Accurate modeling of this transient droplet heating process plays a critical role in determining the mass evaporation, especially of large particles.

As far as fire suppression by the water mist system is concerned, the total mass released by the water

droplets plays a major role. Clearly, this has an important thermal effect and a chemical effect (because of the modification of the gas temperature and the presence of water vapor which can modify the finite-rate chemistry). Instead of a single water droplet, if a group of noninteracting monodisperse droplets are introduced with the air stream, then the integration of the "particle equation" indicate that the number density of the droplets changes along the axis of symmetry because of the flow straining effect. Assuming no particle interactions, the variation of particle flux fraction (particle number density normalized by that at the air stream exit) as a function of the axial location, for various monodisperse particles, is shown in Fig. 2. The total mass evaporation by such a group of noninteracting monodisperse droplets depends on the physical location, as shown in Fig. 1, and the number density variation due to the flow straining, as shown in Fig. 2. These two coupled effects on total mass evaporation, for water droplets of 10-70 μm are shown in Fig. 3. It is seen that 10 μm droplets vaporize completely before they reach the reaction front and cool the convective-diffusive zone on the air side. However, the water evaporated in this zone gets convected through the flame because the flame is located in the air-side of the stagnation plane. For droplets greater than 10 μm, evaporation occurs over a wider region; however, the total mass evaporation (area under the curve) can be a non-monotonic function of droplet size. Therefore, when the gas-particle interactions are included, the flame extinction condition is observed to be a non-monotonic function of particle size, but the exact role of thermal and chemical effects needs to be analyzed carefully.

Acknowledgment: This work is supported by National Institute of Standards and Technology, with Dr. W. L. Grosshandler serving as the scientific officer.

[1] Smooke, M.D., Puri, I.K., and Seshadri, K., *Twenty-first Symposium (Int.) on Combustion*, p. 1783, 1986.
[2] Lacas, F., Darabiha, N., Versaevel, P., Rolon, J.C., and Candel, S., *Twenty-Fourth Symposium (Int.) on Combustion*, The Combustion Institute, p. 1523, 1992.
[3] Chen, N.-H., Rogg, B., and Bray, K.N.C., *Twenty-Fourth Symposium (Int.) on Combustion*, The Combustion Institute, p. 1513, 1992.

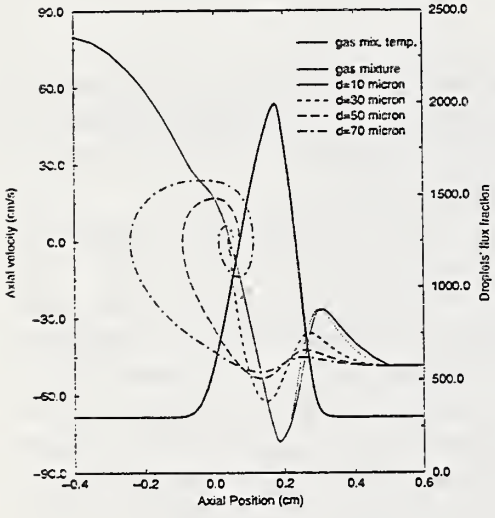

Figure 1: Particle velocities within the mixing layer, for selected particle sizes.

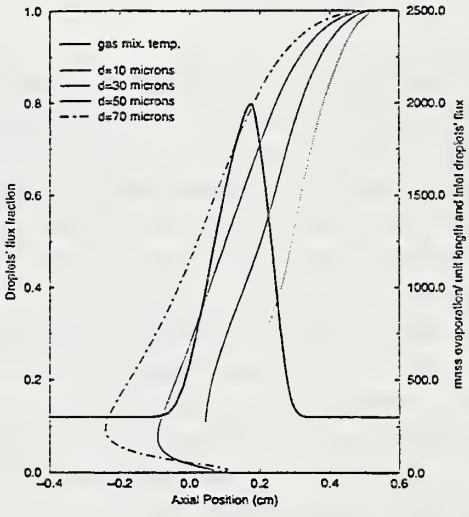

Figure 2: Change in particle flux fraction, for selected particle sizes.

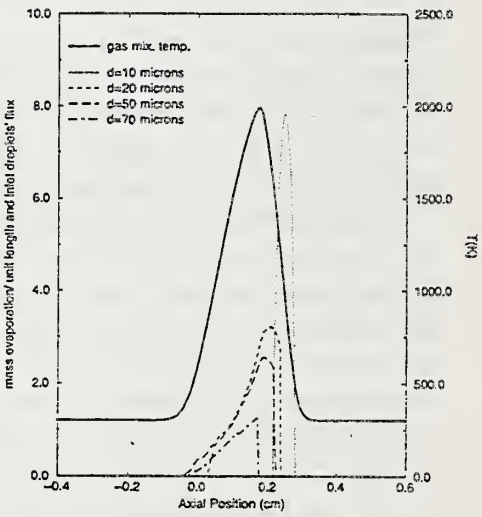

Figure 3: Net mass evaporation, for selected particle sizes.

For submission to the Annual Conference on Fire Research
Gaithersburg, Maryland October 28 - 31, 1996

Evaporation of a Small Aqueous Suppressing Agent Droplet

W. Chien, J.C. Yang, M. King, and W.L. Grosshandler

Building and Fire Research Laboratory
National Institute of Standards and Technology
Gaithersburg, Maryland 20899 U.S.A.

Abstract

Due to its ozone-depleting potential, halon 1301 (CF_3Br) has been banned from production under the Montreal Protocol. The research for halon replacement(s) has led to the reconsideration of using water in certain applications. However, under cold storage conditions (below 0 °C) water will freeze, thus posing a limitation in low temperature operations. Certain additives, if selected properly, not only can suppress the freezing point of water but also can improve its fire suppression effectiveness. Some water-based agents have recently been proven to be more effective than pure water when used in the form of mist to suppress a small JP-8 pool fire (Finnerty *et al.*, 1996). Among the thirteen agents they tested, potassium lactate (60% w/w) and potassium acetate (60% w/w) were found to be far superior than pure water and other candidate solutions.

When a fine mist is formed in a nozzle, the majority of the droplets are unlikely to penetrate to the base of the fire because the droplet momentum is small enough that they are deflected away from the rising plume (Downie *et al.*, 1995). The deflected mist droplets subsequently experience a cooler environment outside the hot gas plume, thus resulting in slow droplet evaporation. Some of the slowly vaporizing droplets will impinge upon the enclosure surfaces wherein the fire is located or obstacles within the enclosure. The droplets will eventually be vaporized on the heated surfaces.

The evaporation of suspended droplets containing dissolved solids was first studied by Charlesworth and Marshall (1960). The formation of a solid crust and various appearance changes during the course of evaporation under a wide range of experimental conditions were observed. Three major evaporation stages were identified: (1) evaporation before the formation of the solid phase, (2) progressive formation of the solid phase about the droplet, and (3) evaporation during the solid phase formation. Several studies on droplets with dissolved solids have since been conducted (Nešić and Vodnik, 1991; Kudra *et al.*, 1991). It is the objective of this work to examine the evaporation characteristics of some of these water-based agents and pure water on a heated surface. Previous studies (*e.g.*, Chandra and Avedisian, 1991) have been focused on relatively large drops (above 1 mm in diameter). Droplets with diameters less than 0.5 mm (to simulate mist droplets) are used in the present work.

Figure 1 is a schematic of the experimental apparatus. It consists of a droplet generator, a solution reservoir, a nickel-plated copper block equipped with two small cartridge heaters, a stainless steel surface, a temperature controller, and a CCD camera. The droplet generator has a chamber, a piezoelectric ceramic disc, and a glass nozzle (Yang *et al.*, 1990) and is based on the drop-on-demand ink-jet technique. A small droplet is ejected from the nozzle as a result of the deflection of the piezoelectric ceramic disc upon application of a squared pulse with controlled amplitude and duration to the disc. The use of this droplet generator enables the production of smaller droplets and repeatable operation. The surface on which the droplet is vaporized is made of 5 cm x 3 cm x 0.5 cm polished stainless steel (SS 304). The 5 cm x 3 cm x 1.25 cm nickel-plated copper block is used to heat the surface to the desired temperature (between 50 °C and 150 °C). Surface temperature is maintained within $\pm$ 1 °C by using a temperature controller. The CCD camera is used to record the evaporation histories of the droplets. The evaporation times of the droplets can be determined by using frame-by-frame analysis of the video records. The experimental procedure involves the delivery of a single droplet from

the droplet generator to the heated surface located 6.5 cm below the nozzle tip and the recording of the droplet evaporation processes. No shattering of droplets due to impact on the surface was observed within the range of surface temperatures tested. The Weber number ($\rho U^2 D/\sigma$) of the droplets was less than 80.

Figure 2 is a comparison between the evaporation time of pure water, 5 % (w/w), 10 %, and 20 % potassium acetate droplets as a function of surface temperature. The initial droplet diameter is estimated to be 360 μm $\pm$ 20 μm from the 35 mm single-strobe flash photographs taken near the nozzle tip. Note that the evaporation times for the potassium acetate solutions reported in the figure refer to the times immediately before the formation of solid phase. It is assumed that the amount of water vaporized before solid formation constitutes the bulk of the initial water content. The assumption appears to be reasonable for small droplets (Charlesworth and Marshall, 1960). Addition of potassium acetate does not change the evaporation time significantly (within the experimental uncertainties) at high surface temperatures. Results on other water-based agents will be presented and discussed.

References

Chandra, S., and Avedisian, C.T., "On the Collision of a Droplet with a Solid Surface," *Proc. Roy. Soc. London A 432*, 13 (1991).

Charlesworth, D.H. and Marshall, W.R., Jr., "Evaporation from Drops Containing Dissolved Solids," *A.I.Ch.E. Journal 6*, 9 (1960).

Downie, B., Polymeropoulos, C., and Gogos, G., "Interaction of a Water Mist with a Buoyant Methane Diffusion Flame," *Fire Safety Journal 24*, 359 (1995).

Finnerty, A.E., McGill, R.L., and Slack, W.A., "Water-Based Halon Replacement Sprays," ARL-TR-1138, U.S. Army Research Laboratory, Aberdeen Proving Ground, July 1996.

Kudra, T., Pan, Y.K., and Mujumdar, A.S., "Evaporation from Single Droplets Impinging on Heated Surfaces," *Drying Tech. 9*, 693 (1991).

Nešić, S. and Vodnik, J., "Kinetics of Droplet Evaporation," *Chem. Eng. Science 46*, 527 (1991).

Yang, J.C., Jackson, G.S., Avedisian, C.T., "Combustion of Unsupported Methanol/Dodecanol Mixture Droplets at Low Gravity," 23rd Symp. (Int.) on Combustion, The Combustion Institute, pp. 1619-1625, 1990.

Acknowledgments

The authors would like to thank Prof. S. Chandra of the University of Toronto for many helpful suggestions and discussions.

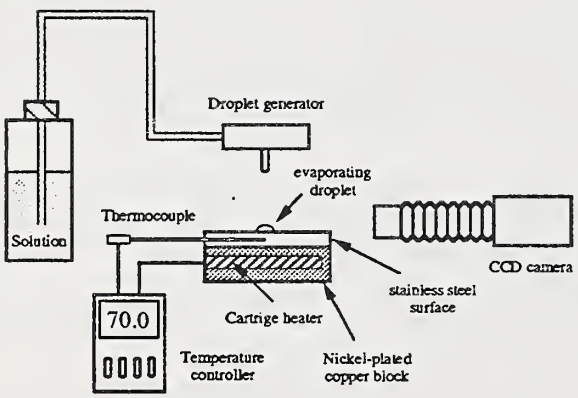

Figure 1. Experimental set-up.

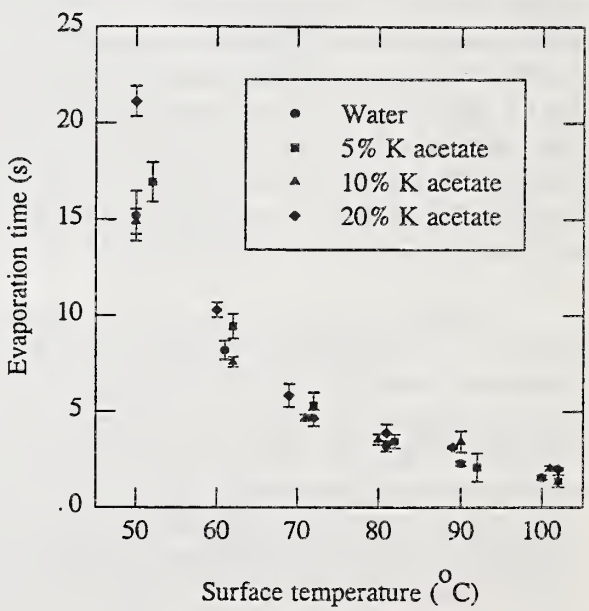

Figure 2. Evaporation time as a function of surface temperature.

A Numerical Study on Water Mist Suppresion of Methane-Air Diffusion Flames.

Chiping Li, Kuldeep Prasad[1] and K. Kailasanath
Laboratory for Computational Physics and Fluid Dynamics
Naval Research Laboratory, Washington DC.

The use of water mist for fire suppresion has been an active area of research and development in recent years. The need for low weight impact replacement sprinkler systems on commerical ships has been driven by International Maritime Organization (IMO) regulations requiring retrofit of fire suppression systems on most commerical marine vessels. This gave immediate impetus to the development of low water demands, high efficiency mist systems to replace sprinkler systems. The phaseout of halons and the search for alternative technologies that preserve most of the benefits of a clean total flooding agent without adverse environmental impact has sparked recent interests in water mist technology.

Fine water mist relies on relatively small droplet sprays to extinguish fires. The mechanisms of extinguishment include gas phase cooling (evaporation and heat capacity), oxygen displacement by steam, wetting of fuel surfaces, and attenuation by radiative heat transfer. Although the potential efficacy of water mist fire suppresion systems has been demonstrated in a wide range of applications and by numerous experimental programs, the underlying physical processes involved in the suppression and their relative impact have not been clearly understood. Factors that contribute to the success or failure of a water mist system for a particular application include droplet size, velocity, the spray pattern geometry as well as the momentum and mixing characteristics of the spray jet. At this time, the effect of these factors on fire suppresion and system effectiveness is not well known.

A numerical model has been developed to obtain a detailed understanding of the various physical and chemical processes involved during the combustion of methane air diffusion flames stabilized above a Wolfhard-Parker burner and the inhibition of these flames by water sprays. The conservative form of the full compressible Navier-Stokes equations for a multi-component chemically reacting fluid flow are solved. Chemical reactions are described by a single step finite rate arrhenius kinetics or a flame sheet model. A real gas thermodynamic model is employed and allowances are made for variable transport properties. For a detailed understanding of the process of spray vaporization, it is necessary to have knowledge of the mechanism of vaporization of the individual droplets and the size and spatial distribution of the droplets that make up the spray. A hybrid Eulerian-Lagrangian sectional approach is used to analyze spray vaporization. The method is based on dividing the droplet size domain into sections and dealing only with one integral quantity in each section such as surface area or total volume. The advantage of this approach is that the integral quantity is conserved within the computational domain and the number of conservation equations is substantially reduced to be equal to the number of sections.

Numerical simulations have been performed to obtain detailed structure of the temperature contours obtained above a methane air diffusion flame burner and have been found to compare favourably with experimental results. Parametric studies on the effect of nitrogen dilution have been completed and are compared with experimental results. Detailed simulation have been performed to investigate the effect of 100 million water droplets (150 micron diameter) introduced as a co-flow in the air stream. Figures a and b show the temperature profiles obtained above a methane air diffusion flame burner with and without water droplets. Simulations have been performed to compute the relative importance of gas phase thermodynamic cooling and oxygen displacement. The fraction of water droplets that interacts with the flame sheet (based on streamline profiles) are computed for various initial droplet diameters. The presentation will attempt to quantify the effect of water droplet size, droplet number density and velocity of the jet spray on methane air diffusion flames.

---

[1] Science Application International Corporation, VA.

Effect of Water Mist Suppresion on Methane Air Diffusion Flames

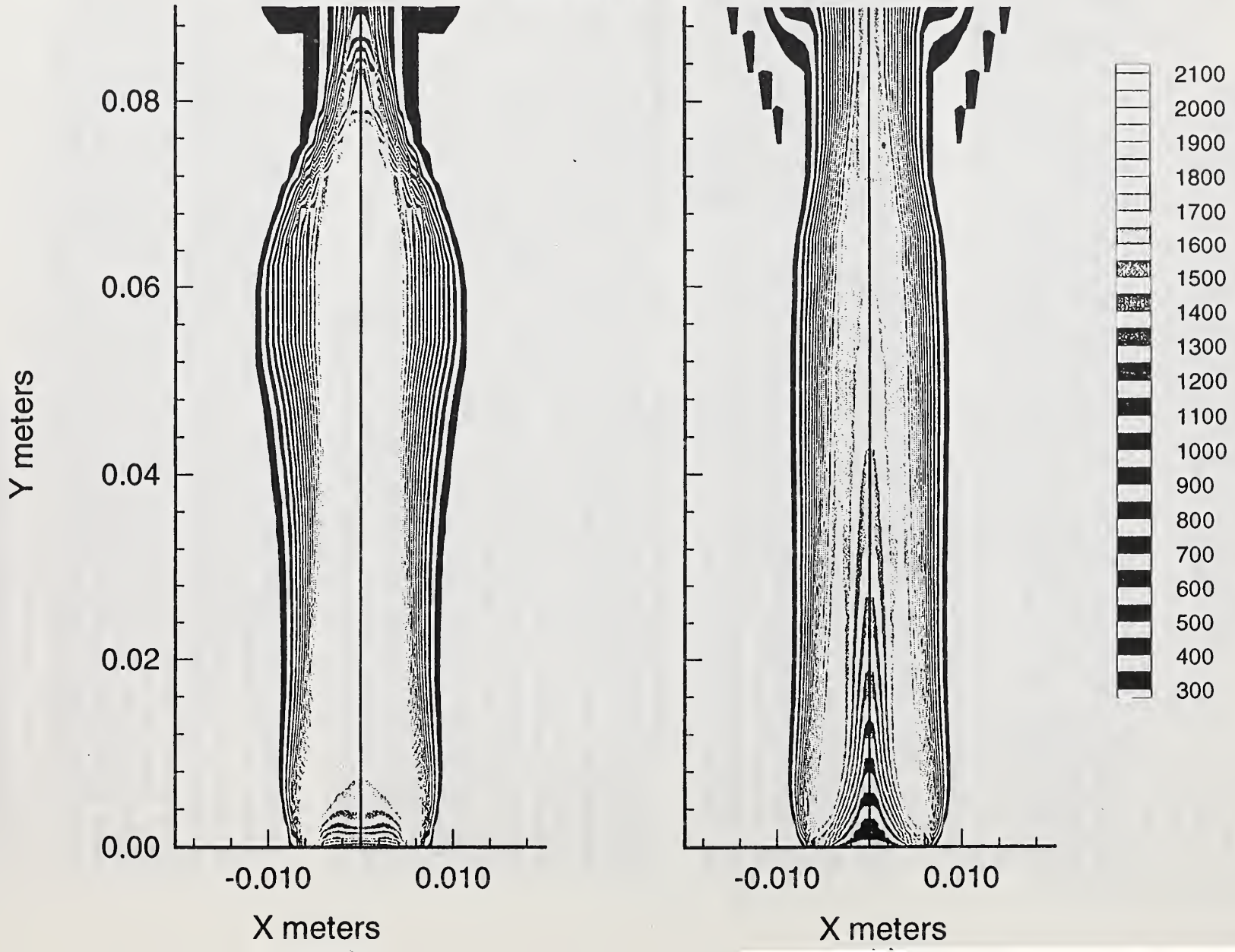

Experimental and modelling studies of Compartment Jet Fire Suppression Using Water Spray

K. Alageel , BCR Ewan and J Swithenbank

Chemical Engineering and Fuel Technology

Mechanical and Process Engineering Department

University of Sheffield

Mappin Street

Sheffield, S1 3JD, UK

The safe design and operation of process plants requires an ability to predict hazard consequences reliably. A particular hazard is a jet fire that might arise from the ignition of an accidental release of pressurised gas or liquid. Mitigation systems involving agents such as Halon, which are perceived to be environmentally damaging, are currently out of favour and interest has revived in the use of water sprays.

The objective of this study is to assess the effect of fine water spray droplets on a propane jet fire which burns at 0.1 kg/s inside a compartment 6 m long, 2.5 m wide and 2 m high (fig.1). The total volume is 30 m^3 with reduced ventilation to simulate accidental fires in offshore modules. The vertical jet nozzle size is 1.5 cm. in diameter.

Mathematical modelling was done by using the computational fluid dynamics programme FLUENT. The modelling approach used divided the domain of interest (i.e. the compartment) into a number of discrete cells (25000) and the conservation equations was solved for each cell to obtain the field variables such as the fluid density, species concentrations, and temperature. The geometry was specified to be open at one end with induced ventilation arising from the jet entrainment.

In the initial stages of this study, the modelling of the development of the jet fire and the associated movement of combustion products within closed system of inter-connected compartment was carried out. This was followed by the development of the model for the dispersion of water spray droplets.

The simulation starts by first running the code without combustion to do the cold flow calculations in the compartment. Following that, the jet fire is ignited and the calculation was resumed until the dispersion of water spray is activated, the code tracks the flow of water droplets in the compartment and the interaction between the droplets in terms of mass, momentum and heat transfer. The water flow rates used in the studies were 0.05, 0.075,0.1, 0.15 or 0.2 kg/s in each time for different spray(s) locations.

For propane flame, fuel dilution due to water evaporation decreased the CO_2 and CO production rate and the O_2 depletion rate, figures 2-6. Less hydrocarbons were burned and the hydrocarbon percentage was observed to increase as the water application rate was increased with further increase in the water application rate, dilution effects become dominant and the flame gets extinguished.

The result shows that, for this study, oxygen depletion is not the main cause of extinguishment as there is still enough oxygen in the compartment to sustain the combustion.

The result of this work will be validated with experimental result.

References:

1. Cowley LT, Behaviour of oil and gas fires in the presence of confinement and obstacles, Health and Safety Executive; Steel Construction Institute, ISBN 0118820354, HMSO Books, United Kingdom, 1992. 307p.

2. Dinenno P.J,..et al, The SFPE handbook of fire protection engineering, first edition, 1993, National Fire Protection Association and Society of Fire Protection Engineers.

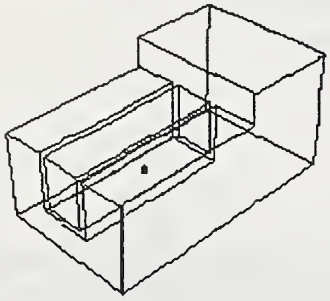

fig. 1 compartment geometry.

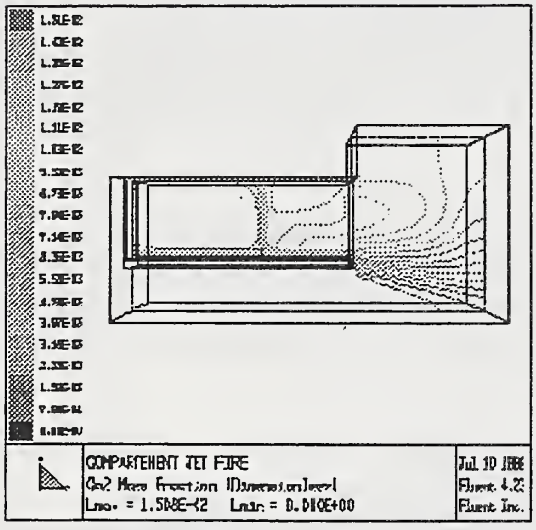

fig. 3. CO_2 mass fraction inside the compartment.

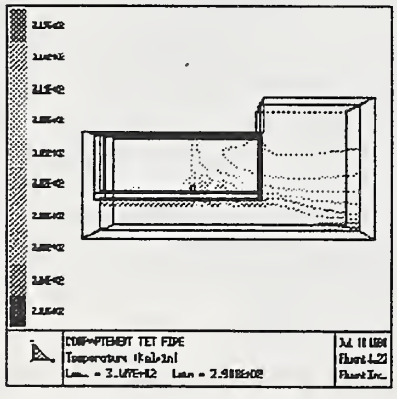

fig.5 temperature contours.

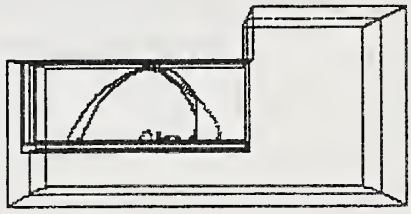

fig. 2. water spray droplet trajectories.

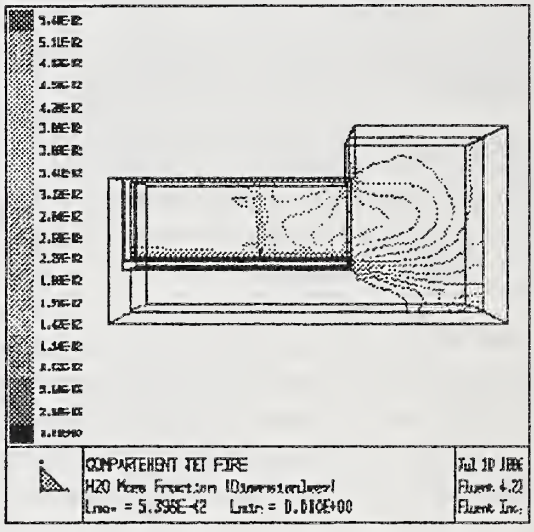

fig. 4. H_2O mass fraction inside the compartment.

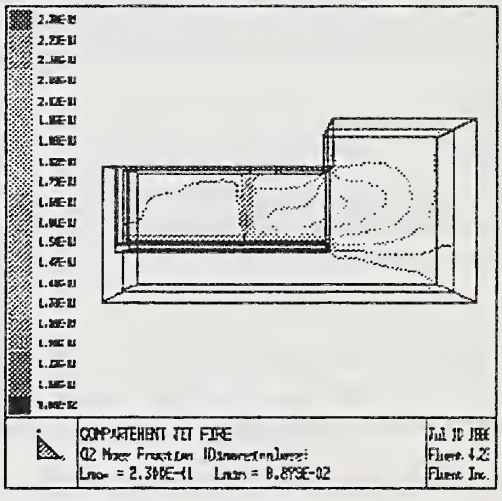

fig. 6. O_2 mass fraction inside the compartment.

PARAMETRIC STUDY WITH A COMPUTATIONAL MODEL SIMULATING INTERACTION BETWEEN FIRE PLUME AND SPRINKLER SPRAY

Soonil Nam

Factory Mutual Research Corporation, 1151 Boston-Providence Turnpike, Norwood, Massachusetts 02062, USA

A parametric study to improve sprinkler performance is being carried out using numerical models predicting actual delivered densities (ADDs) of early suppression fast response (ESFR) sprinklers in heptane-spray fire scenarios. The computational models were developed through the following stages.

First, in order to supply input data for development of numerical models and experimental data for validation of the models, four sets of measurements were carried out. The measurements were momentum and water flux distribution of two ESFR sprinkler sprays without fire, temperature and axial velocities along the axis of free-burn fires, and actual delivered densities. Then, a numerical model for a sprinkler spray was completed by assigning representative drop size, mass flow rate, discharge speed, and discharge angle of 275 trajectories in such a way that they produce reasonable agreement with the measured water flux distribution and spray momentum in absence of fire. A numerical model for the free-burn fire was created by assigning a heat flux distribution on the horizontal surface and simulating a central, vertical air jet used in the experiment, varying parameters until a reasonable match was established with the measured temperatures and the axial velocities along the axis.

Numerical computations of actual delivered densities were carried out by combining the water spray model and the free-burn fire model of predetermined fire sizes for different water flow rates of the sprinklers. ADDs obtained from the simulations compared reasonably well with those from the measurements. Figure 1 shows the ADDs with 1.88 l/s flow at 500, 1000, 1500 kW fires.

Once the models were completed, routine computations using the models are being carried out to study the impact of parameters in sprinkler performance. The most significant parameters dictating the penetration capability of water spray from a sprinkler are drop size distribution, spray momentum, ceiling clearance, and fire size. The performance will be compared in terms of sprinkler penetration ratio, the ratio of ADD without a fire to ADD with the fire, with different combinations of the parameters.

Preliminary results with varying water flow rates at an invariant fire size show the trend that Heskestad[1] observed during his experiment. When a fire intensity remain constant regardless of the water flow rates applied, the penetration ratio decreases as the flow rate increases up to a critical flow rate, after which the trend reverses itself. Figure 2 shows that the dominant parameter shifts from the drop size at relatively low flow rates to spray momentum as the flow rate increases, as indicated from the experiment[1].

References

1. Heskestad, G., "Sprinkler Performance as Related to Size and Design: Volume I–Laboratory Investigation," FMRC Serial No. 22437, RC79–T–1, Factory Mutual Research Corporation, Norwood, MA, 1979.

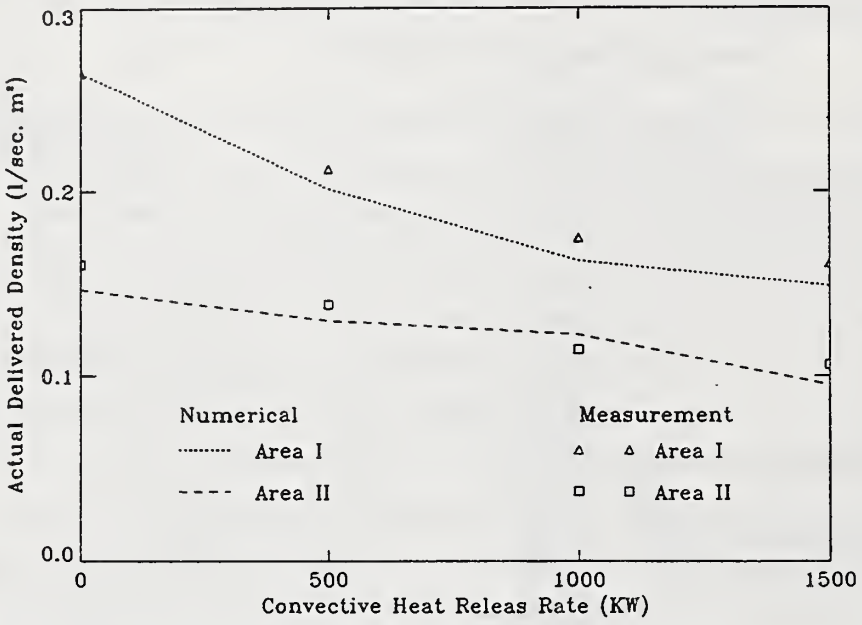

Figure 1. Actual delivered densities: 1.88 l/s flow at 0.5, 1.0, 1.5 MW fire.

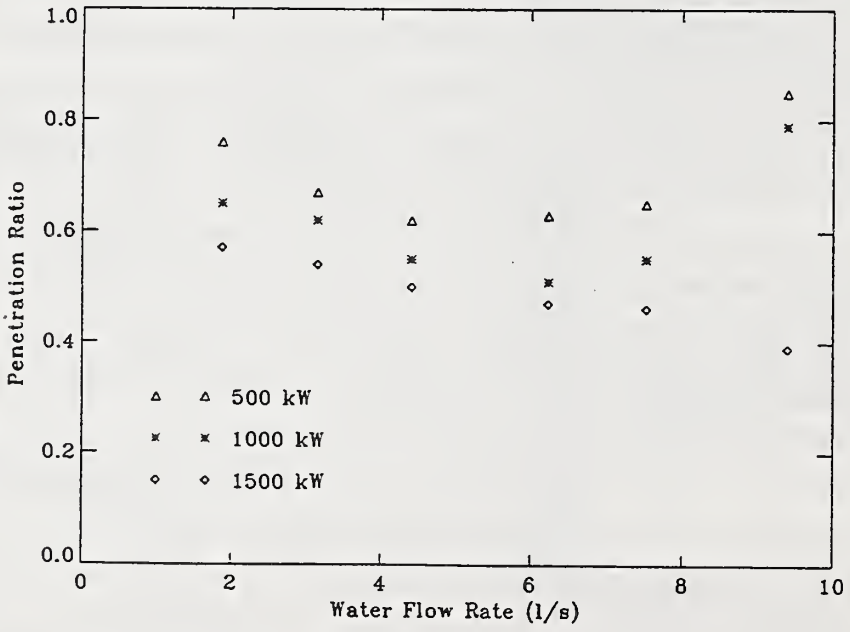

Figure 2. Penetration ratio vs. water flow rate (comp.).

Experimental Investigation of the Water Mist Impacting Phenomenon on Horizontal Wires

L. S. Hung and **S. C. Yao**
Department of Mechanical Engineering
Carnegie Mellon University
Pittsburgh, Pennsylvania
Telephone: (412)-268-2508

The phenomenon of water mist impacting on horizontal wires has been experimentally investigated. This process is relevant to the water mist intercepting and penetrating into the openings of compartment. The impaction of droplets on wires provides a basis for the understanding of the similar processes on more complicated structures such as screens, etc.

The mono-size water droplets are generated using the principle of Impulsed Spray Generator which was invented and patented by Yao and Ashgriz [1]. Figure 1 shows the cross-section schematic of this spray generator. It consists of a piezoelectric plate, a fluid chamber, and an orifice plate. The pressure pulses generated from the piezoelectric plate force the liquid jets to break up into mono-size droplets. Since any residual air bubbles trapped into the chamber would diminish the effect of pressure pulses, special inlet and exit channels of water flow are implemented in the generator for the bubbles to be swept away naturally.

The images of the impacting phenomenon are recorded using the strobe lighting, a CCD camera, and a video recorder. The CCD camera is equipped with stereomicroscopic lens for magnification.

Yao et al [2] studied the process of droplet impaction on rectangular strips. They illustrated that the controlling parameters of impacting phenomenon are the droplet Weber number (We_o), the offset of droplet relative to wire (Δ), and the ratio of incoming droplet diameter to the wire diameter (R) with the following definitions:

$$We_o = \frac{\rho_l V_o^2}{(\sigma/d)} \qquad \Delta = \frac{\delta}{(d+D)/2} \qquad R = \frac{d}{D}$$

where, d = diameter of droplet D = diameter of the wire
V_o = incoming droplet velocity ρ_l = density of droplet
δ = distance between the centers of the droplet and wire
σ = surface tension of the droplets

Generally, the impaction phenomenon consists of a combination of cutting, splashing, disintegrating, and regrouping. The diameters of shattered droplets usually appear as a spectrum with bimodal type distribution. Usually, the offset of the centers of the incoming droplet and the wire affects the result of impaction substantially. Figure 2 shows the typical images of this process. The incoming droplet Weber number is 47.4. The diameter of the wire is about 760 μm while the droplet diameter is about 600 μm (i.e., R= 0.789). As the droplets are approaching at a larger offset (i.e., $\Delta = 0.882$) at the right side of the wire, a large fragment is formed on the right side while many small satellite droplets are disintegrated at the left side. At a smaller offset ($\Delta = 0.551$), the droplet splits into 2 equally large segments, one at each side. However, when the droplet is approaching at zero offset ($\Delta = 0.0$), it splashes onto the wire, warps around it, and then regroups together again to form a large elongated fragment of liquid. This fragment detaches from the wire and drips off downward vertically. It is expected that the corresponding phenomenon at higher Weber number could be different in nature.

Acknowledgment

This research is funded by the Department of Commerce, NIST, Building and Fire Research Laboratory, under Grant No. 60NANB5D0093.

Reference

[1] Yao, S.C., and Ashgriz, N., "Multi-Orifice Impulsed Spray Generator," U.S. Patent Serial No. 4 667 877, 1986.

[2] Yao, S.C., Hochreiter, L.E., and Cai, K.Y., "Dynamics of Droplets Impacting on Thin Heated Strips," *J. Heat Transfer*, (**110**), pp. 214-220, 1988.

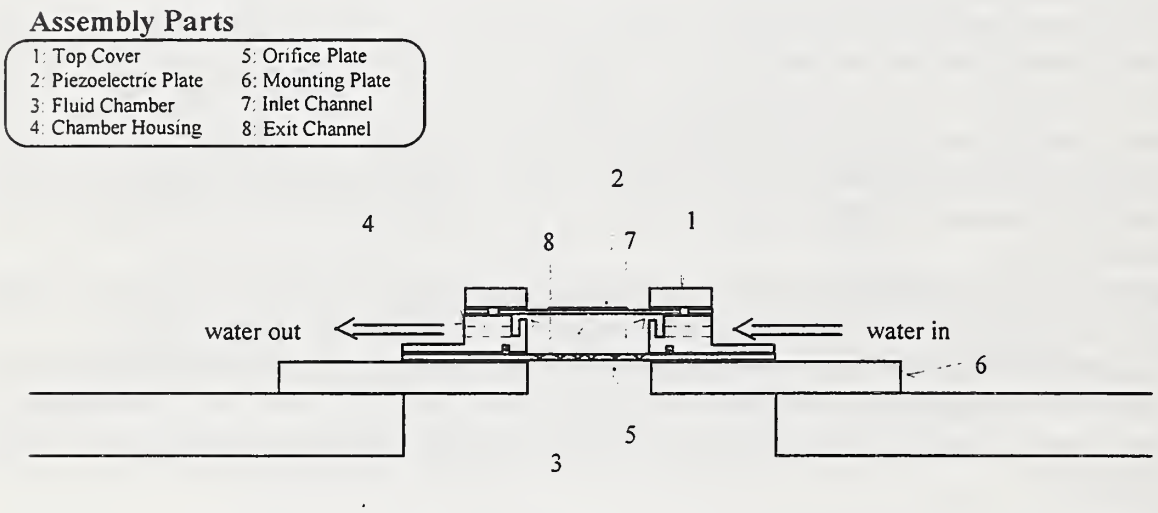

Figure 1 Schematic of the Impulsed Spray Generator (Cross Section)

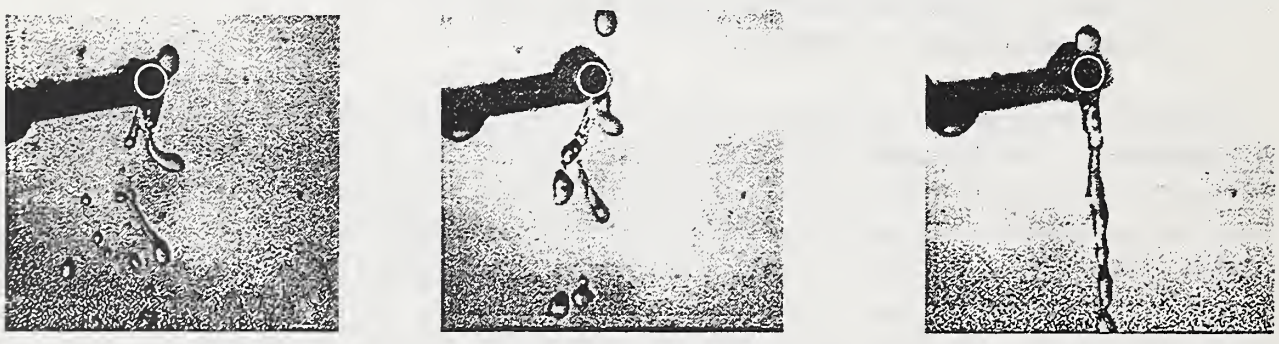

(1) (2) (3)

Figure 2 Images of droplets impacting on the horizontal wire
(R = 0.789, We_o = 47.4)
(1) - Larger offset from the right side (Δ = 0.882)
(2) - Smaller offset from the right side (Δ = 0.551)
(3) - Zero offset (Δ = 0.0)

Numerical Studies on the Deposition and Transport of Water Mist Normal to a Horizontal Plate

L.S. Hung and **S.C. Yao**
Department of Mechanical Engineering
Carnegie Mellon University
Pittsburgh, Pennsylvania
Telephone: (412)-268-2508

The deposition and transport of fine droplets in a water mist flowing downwards onto a horizontal plate are modeled numerically in this study. It reveals the aerodynamic process of droplets impacting to the top of a compartment or an object. The nature of the droplets transport phenomenon in the wake region behind an object is also investigated.

The computation is conducted in a 2-D flow field. The turbulent gas flow is modeled using the two-equation k-ε method in an Eulerian coordinate; however, the droplets are traced stochastically in a Lagrangian coordinate. Droplet dispersion is obtained by considering the interaction (2-way coupling) between the gas turbulent eddies and droplet trajectories.

The plate, where deposition occurs, is positioned horizontally with the gas streams coming from the top. In this study, the length of the plate is 0.75 m and the incoming gas velocity is 1 m/s. Droplets are introduced at the top of the flow field, which is primarily a stagnation-point flow. Both 50 μm and 200 μm droplets are studied for comparison.

In stagnant air, the terminal velocities for both the 50 μm and 200 μm droplets are found to be 0.075 m/s and 0.579 m/s, respectively, due to their difference in mass (inertia). Even though droplets are injected at the same rate, 200 μm droplets would move faster across the flow field.

Figure 1 shows a typical result of the deposition pattern of 50 μm droplets on the horizontal plate. It indicates higher mass flux depositions at both edges. It is also found that the deposition near the edges of the plate are mostly in the form of tangential impactions.

Below the plate, a flow recirculation zone appears with its size comparable to the plate. Figure 2 shows the gas flow streamlines together with the instantaneous distribution of the droplets in the field. Right below the plate, very little number of droplets can be swept into the recirculation zone due to their inertia effects.

The flow wake also shows oscillatory motion in time. In the wake, turbulent diffusion shall allow droplets to migrate toward the centerline and eventually may merge together to close the spray wake. However, the droplets in the spray may not follow the flow wake closely depending upon the size of the droplets and the flow condition. As shown in Figure 2, small droplets of 50 μm tend to follow the gas streams closely behind the wake than the large droplets of 200 μm. This is because when the droplet size is increased, its inertia effect becomes important that they do not follow closely to the gas streamlines. It can also be found that the number of 200 μm droplets in the flow field is considerably less than that for the 50 μm droplets because of the effect of terminal velocity.

Acknowledgment

This research is funded by the Department of Commerce, NIST, Building and Fire Research Laboratory, under Grant No. 60NANB5D0093.

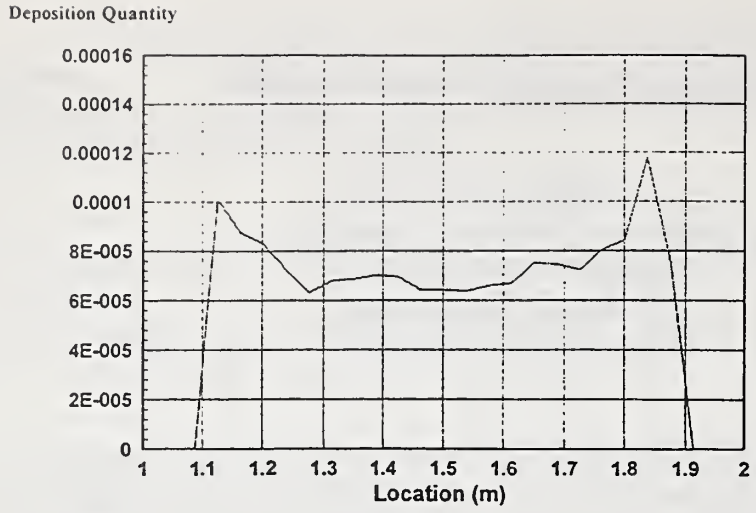

Figure 1 Deposition pattern of droplets onto a horizontal plate

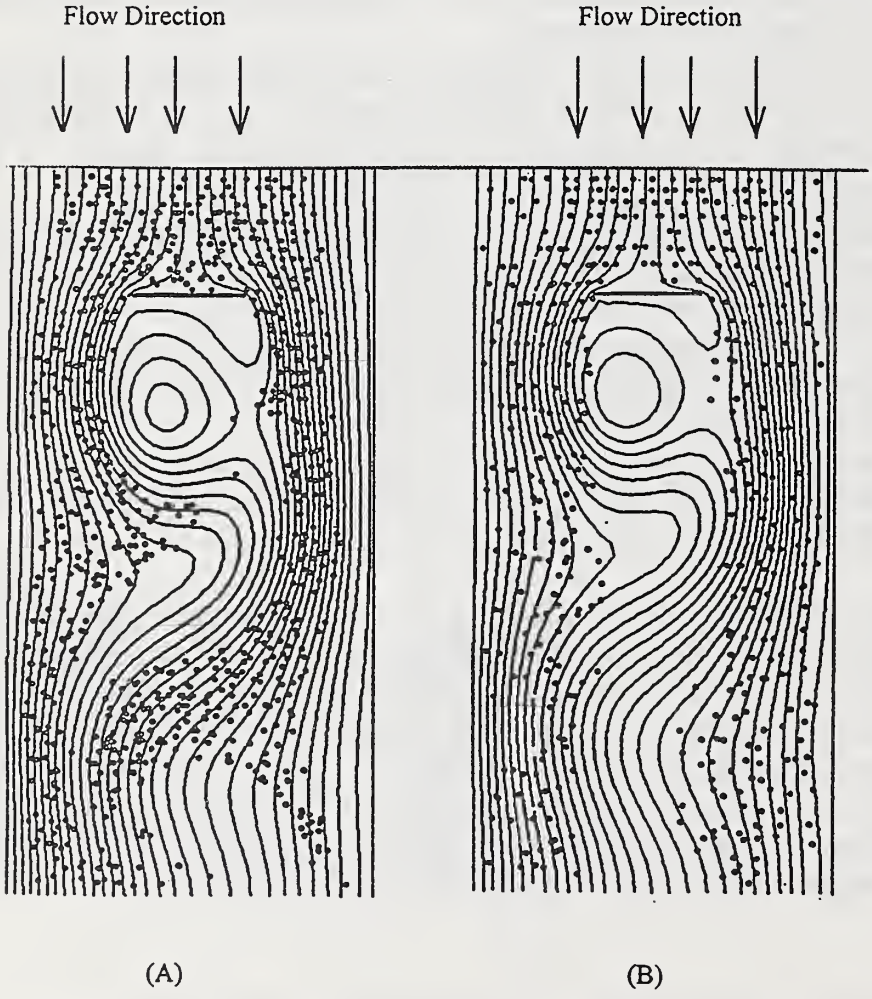

Figure 2 Effect of droplet size in the wake zone behind the plate
(A) 50 μm (B) 200 μm

THE EFFECT OF DISSOLVING A SURFACTANT IN WATER SPRAYED ON A HOT SURFACE

Y. M. Qiao & S. Chandra

Department of Mechanical & Industrial Engineering
University of Toronto
Toronto, Ontario M5S 3G8
Canada

Water sprays are widely used for fire suppression, both to extinguish flames on burning objects and to prevent flame spread by cooling surfaces that have still not ignited. Recently there has been renewed interest in water as an environmentally benign alternative to halons for fire extinguishment on board aircraft and vehicles, where the weight of liquid that can be carried on board is limited and it is important to minimize water requirements. One method that has proved effective in improving the fire suppression capabilities of water has been to add "wetting agents", which are typically surfactant solutions that reduce surface tension and promote foaming (Bryan 1993). Large scale tests have shown that addition of a wetting agent reduces by up to 60% the volume of water required to extinguish fires on wood, cotton bales and rubber tires. Though wetting agents have been used for about 40 years, little information is available on the mechanism by which surfactants enhance heat transfer from a hot surface to impinging droplets in water sprays. We therefore studied experimentally the effect of adding a surfactant (sodium dodecyl sulfate) to a water spray impinging on a heated surface. The experiments, so far, have been done using a non-burning metal surface. The intent has been to gain insight into the effect of surfactant addition on surface-liquid heat transfer.

Figure 1 is a schematic diagram of the apparatus used for spray cooling experiments. The spray nozzle and test surface were enclosed in an aluminum chamber (152 mm long x 152 mm wide x 254 mm high) which was mounted on a rotation stage so that the orientation of the test surface with respect to gravity could be varied. Water was supplied by a turbine pump to the spray nozzle via stainless steel tubing. The cooled surface was the flat face of a 25.4 mm diameter copper cylinder, electroplated with a 10 μm thick layer of nickel to prevent oxidation. It was placed at a distance of 50 mm from the nozzle tip, centered along the axis of the spray. Four 0.5 mm diameter Chromel-Alumel (type K) thermocouples were inserted into holes drilled 6.4 mm apart along the axis of the cylinder, with the top hole positioned 0.4 mm below the spray cooled surface. The lower end of the cylinder was bolted to a copper heater block that housed two 500 W cartridge heaters.

Two full-cone commercial nozzles (Unijet TG 0.6 and 0.7, Spray Systems Co., Wheaton, Illinois) were employed to achieve several combinations of three spray parameters: liquid mass flux, mean droplet diameter, and impact velocity, which have been identified as the main variables influencing spray cooling heat. Spray cooling experiments were done using both pure water and solutions containing 100 PPM by weight of surfactant (sodium dodecyl sulfate (SDS)). Adding 100 PPM of SDS reduces the surface tension of water by only 4% (Qiao & Chandra 1995), and has negligible influence on other physical properties such as density and viscosity. Therefore, adding a surfactant was expected to have no appreciable effect on the diameter, velocity, or mass flux distribution of droplets in the spray.

A transient spray cooling experiment was started by switching on power to the heaters until the surface temperature, as measured by the uppermost thermocouple, reached 240°C. The heaters were then switched off and the water pump activated. Water impinging on the test surface quenched it to a temperature below 100°C in a period of 10 s – 100 s, depending on the spray parameters used. Signals from the thermocouples inserted into the surface were amplified and recorded using a data acquisition system during spray cooling. Spray impingement on the hot surface was also recorded using both a 35 mm camera and a video camera.

Fig. 2 shows the surface temperature (T_W) variation during spray cooling of a surface using pure water with a mass flux m_l = 0.5 kg/m^{2}s. Time t=0 marks the instant that the spray was turned on. The surface heat flux (q), calculated from the interior temperature measurements using a finite difference model of heat transfer in the copper cylinder, is also shown. At an initial surface temperature of 240°C spray droplets were in a state of film boiling, bouncing off the surface after impact, and the heat flux was

low (q =0.8 MW/m^2). Heat transfer to the spray was in the transition boiling regime for 140°C < T_W < 200°C, and surface heat flux increased rapidly until it reached its maximum value, called the critical heat flux (CHF), at T_W = 140°C. Heat transfer at lower surface temperatures was by nucleate boiling, and q decreased with further reductions in surface temperature.

The effect of adding a surfactant on spray cooling heat transfer is shown in Fig. 3, where the measured variation of surface heat flux with surface temperature is plotted for both pure water and surfactant solution, at two different mass fluxes (m_1 = 2.8 kg/m^{2}s and 0.5 kg/m^{2}s). The most notable effect of adding a surfactant is to significantly increase both nucleate boiling and CHF during spray cooling: for surface temperatures between 100°C and 120°C the surface heat transfer rate was increased by 50% to 300%. The increase in nucleate boiling heat transfer was observed at all mass fluxes and impact velocities in our experiments. Photographs taken of the surface show that the surfactant greatly enhanced formation of foam during nucleate boiling on the surface. This agrees with observations made during experiments with single droplets evaporating on a hot surface (Qiao & Chandra 1995) that nucleation promotion and foaming by a surfactant are the most important mechanisms responsible for enhancing nucleate boiling heat transfer.

References

Bryan, J. L. (1993) *Fire Suppression and Detection Systems.* pp. 331-334, Macmillan Publishing Co, New York.

Qiao, Y. M. and Chandra, S., "Evaporative cooling enhancement by addition of surfactant to water drops on a hot surface", ASME HTD Vol. 304-2, pp. 63-71, (1995).

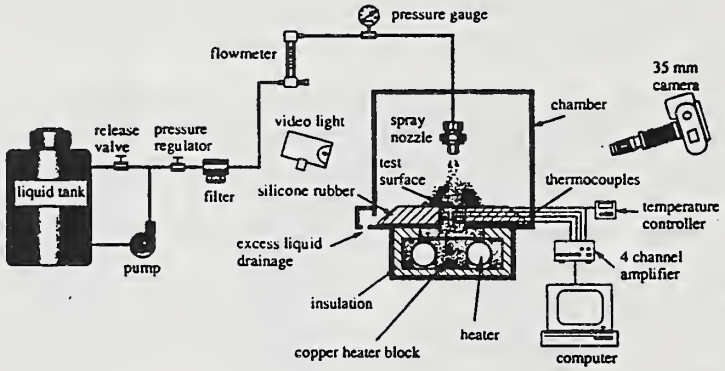

Figure 1 Schematic diagram of the spray cooling apparatus

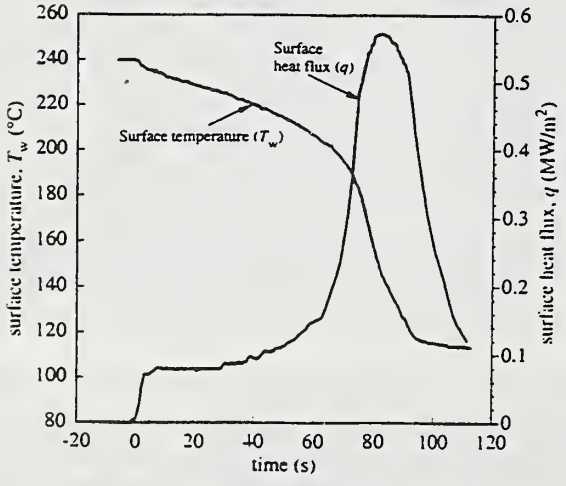

Figure 2 Calculated surface heat flux and temperature during spray cooling with pure water (mass flux = 0.5 kg/m^{2}s).

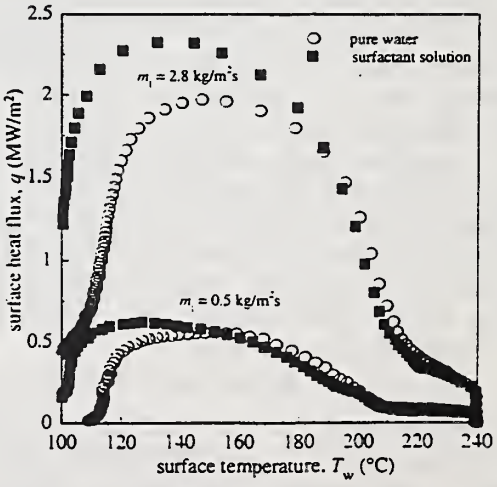

Figure 3 Effect of a surfactant on spray cooling heat transfer at two different mass fluxes.

FINE SPRAY PROTECTION OF SHIPBOARD ENGINE ROOMS

Robert G. Bill, Jr.*, Richard L. Hansen**, and Kevin Richards***

*: Factory Mutual Research Corporation (FMRC), Norwood , MA, 02062 **: U.S. Coast Guard Research and Development Center,Groton, CT, 06320 and ***: Worcester Polytechnic Institute (WPI), Center for Firesafety Studies, Worcester, MA, 01609

Twenty-three fire tests were conducted to determine the ability of current fine water spray (mist) technologies to extinguish fires in the International Maritime Organization (IMO) fire test procedure[1] for engine rooms greater than 500 m^3 in volume. The fire tests were conducted using nozzles installed at a 5 m height and 1.5 m spacing in the FMRC Test Center (2800 m^2 in area and 18 m in height). Two types of nozzles were used: a low pressure commercial nozzle operating between 1.2 MPa and 1.5 MPa with a flow per nozzle between 12.0 and 13.4 lpm and a high pressure multi-nozzle prototype consisting of seven nozzles operating at 6.9 MPa, flowing 5.3 lpm. These nozzles were selected because they had previously been shown to be capable of extinguishing the IMO engine room test fires in an enclosure with a protected area of 83 m^2 and a ceiling height of 4.5 m (see Reference 2). The fire tests selected from the IMO fire test procedure included 6 MW diesel spray fires on top of the IMO engine mock-up, a 6 MW shielded spray fire adjacent to the engine mock-up, a 1 MW shielded diesel spray fire at the same location, and a wood crib within a 2 m^2 pan filled with heptane. The IMO engine mock-up is shown in Figure 1.

Sixteen fire tests were conducted in which no additional enclosure surrounded the fine water spray nozzles other than the large test facility as required in the IMO test method for Class III engines (volumes greater than 3000 m^3). Using either the low pressure nozzles or high pressure prototypes, the IMO test fires were not significantly affected by the fine water spray when 36 nozzles (protected coverage area of 81 m^2) were installed. Increasing the number of nozzle to 100 for the low pressure nozzles or 90 for the high pressure nozzles did not improve the performance of the fine spray systems.

To further investigate fine spray system capabilities, a ceiling was then placed directly over the nozzles covering an area of 188 m^2. Using 90 high pressure prototypes, the IMO test fires were not extinguished. A 940 m^3 enclosure was then formed by dropping tarpaulins to the floor from the ceiling. A 4 m^2 vent was placed in the wall. The 6 MW diesel spray fire on top of the mock-up was then extinguished with the 90 high pressure prototypes (see Figures 2 and 3). When the 6 MW fire was shielded beside the mock-up, the fire was not extinguished. Closing the vent resulted in extinguishment of the 6 MW shielded spray fire. Under the same test conditions, a 1 MW shielded diesel spray fire and a 0.1 m^2 heptane pool fire were not extinguished. The fire test results suggest that protection of engine rooms with volumes of about 1000 m^3 is possible by optimizing current fine spray technology; while larger volumes will require significantly improved discharge characteristics. Complete details of the study are given in Reference 3.

ACKNOWLEDGEMENTS

This work was supported by the U.S. Coast Guard Research and Development Center under delivery order DTCG39-95-F-E00280. We wish to thank Professor Robert G. Zalosh for his support through the WPI Center for Firesafety Studies. The plans for the IMO engine mock-up were developed by Mr. William Brown of FMRC. Mr. Donald Charlebois and Mr. Dennis Waters were in charge of fire testing at the FMRC Test Center.

REFERENCES

1. "Interim Test Method for Fire Testing Equivalent Water-Based Extinguishing Systems for Machinery Spaces of Category A and Cargo Pump Rooms, IMO, MSC/Circ 668 Annex, Appendix B, 4 Albert Embankment, London, UK, December 30, 1994.

2. Back, G.G., DiNenno, P.J., Hill, S.A., and Leonard, J.T., "Full-Scale Testing of Water Mist Fire Extinguishing Systems for Machinery Spaces on U.S. Army Watercraft," Naval Research Lab. NRL/MR/6180-96-7814, February 1996.

3. Bill, R.G., Jr., Charlebois, D.E., Waters, D. L., and Richards, K., "Water Mist Fire Tests for Class II & III Engine Rooms," Final Report, Delivery Order DTCG39-95-F-E00280, U.S. Coast Guard Research and Development Center, Groton, CT, February 1996.

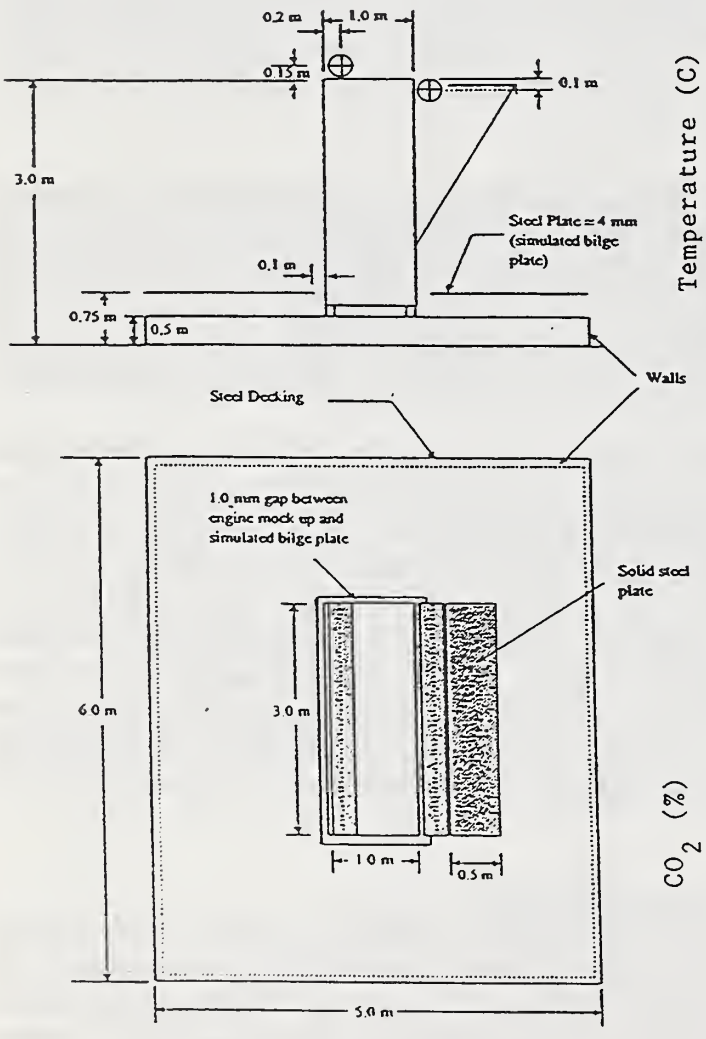

Figure 1. IMO Engine Mock-Up (West Side and Plan View)

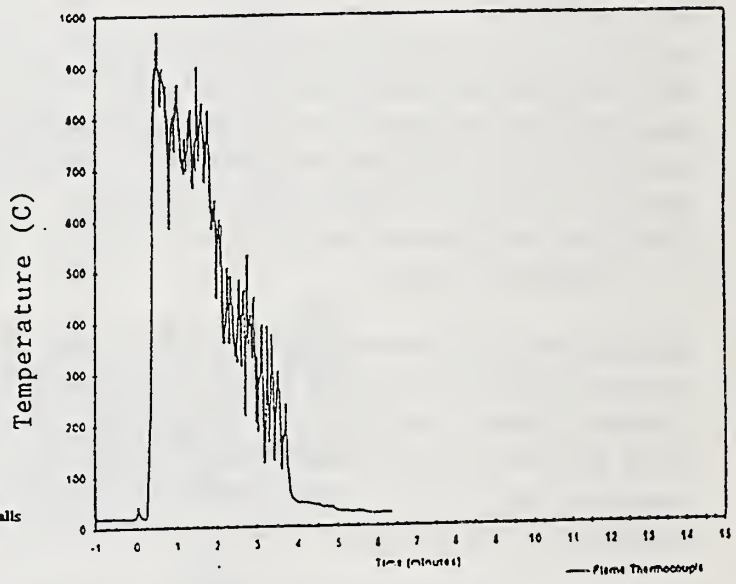

Figure 2 Flame temperature in a 6 MW diesel spray fire (Test 19) with Spraying Systems seven-nozzle head

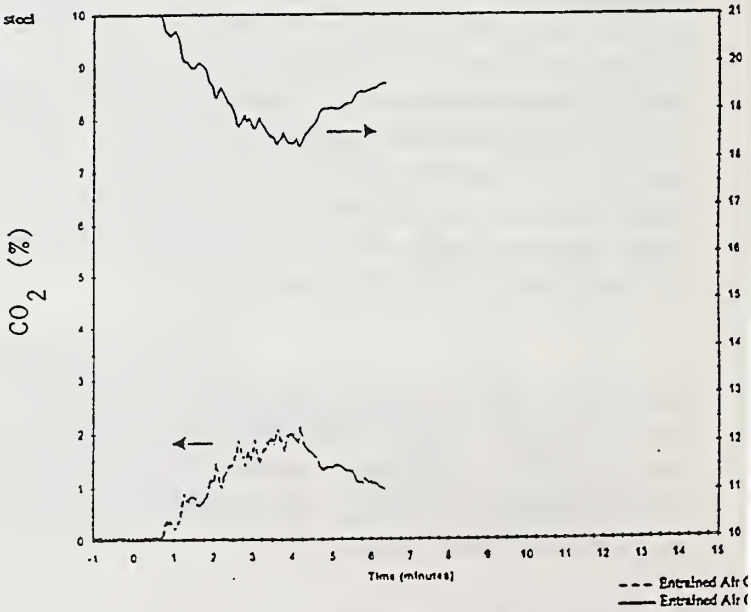

Figure 3 Oxygen and carbon dioxide concentrations adjacent to a 6 MW diesel spray fire (Test 19) with Spraying Systems seven-nozzle head

Wet Bench Fire Suppression with Fine Water Spray

by
P.K. Wu, T. Taylor and R.B. Harriman
Factory Mutual Research Corporation
Norwood, Massachusetts

Introduction

Fires involving polypropylene wet benches in cleanroom environments have caused significant losses in the semiconductor industry. This abstract concerns with the suppression of wet bench fire with a Fine Water Spray System. Previous work and the initial "free-burn" test with a polypropylene wet bench under a fire products collector strongly suggested that detection and suppression of wet bench fire could and should be carried out in the early stage of the fire (Ref. 1 and 2). A full-scale simulated cleanroom facility was built and a series of fire suppression tests were conducted with a fine water spray system. The results show that a fine water spray system can be used effectively to extinguish wet bench fire in its early stage.

The Simulated Cleanroom Facility

The simulated cleanroom facility was designed to provide a realistic flow environment around the wet bench. The inside dimensions of the room were 3.7 m wide x 5.5 m long x 3.7 m high. The floor was raised about 1.2 m to accommodate two nominal 8,000 CFM blowers to generate a downward flow of about 60 FPM in the room. On the roof, a porous steel plate with 6.3 mm perforations and 6% open area was placed on the cross beams. An identical layer of porous plate was also placed below the floor. The floor was constructed with close mesh 12 gauge steel grating. A conventional fire retardant polypropylene wet bench was used near the center of the wall. A third blower was connected to the wet bench to provide a secondary flow rate of up to about 1,000 CFM. The wet bench has dimensions of 1.4 m wide x 2.3 m long x 2 m high. The surface area was replaced by a 1/4 inch thick aluminum plate. The plenum has dimensions of 0.8 m wide x 2.3 m long x 0.6 m high. About 45% of the secondary flow went through the slots on the surface area and the remainder entered the slots on the back wall behind the surface area.

Results

The fire source was represented by a polypropylene pool fire with pan diameter ranging from 4 in. to 12 in. Polypropylene can be ignited with a 100 watts heating source. The ignition was simulated with a 12 V battery and a diesel engine glow plug. The ignition typically took 15 - 30 seconds. The mass loss from the burning was monitored by a loadcell. After ignition, all polypropylene fires have a long period of slow growth (an incubation period) and then accelerate to steady state burning. A sample of mass loss history (for a 6 in. polypropylene pool fire) is given in Figure 1. For the 6 in. fire, the incubation period was about 25 minutes and the steady state burning rate was 6 kW.

Instrumentation included thermocouples, optical probes for measuring smoke density at various locations, a loadcell and an FTIR multiple gas analyzer. For the present study, polypropylene pool fires were placed either in the plenum or on the surface area of the wet bench. To examine the possibility of fire detection by gas sampling, the increases of concentration for CO and CO_2 due to a fire were measured at various locations in and around the wet bench when either a 4 in. or 8 in. polypropylene pool fire was placed in the plenum or on the surface area. The rise in CO concentration was too small

to be measured. The rise in CO_2 concentration was also negligible except in the exhaust duct. With a fire in plenum, the rise in CO_2 concentration was about 65 PPM for a 4 in. fire and 650 PPM for an 8 in. fire. With a fire on the surface area, the rise was approximately 44 PPM for a 4 in. fire and 400 PPM for an 8 in. fire.

For protection of the plenum, two nozzles were used (one on each end wall). The pool fire was placed in the middle with two nominal 7 in. cylinders on each side to block the direct impingement of water mist. Tests were carried out with various fire sizes and results are shown in Figure 2. The extinguishment time is less than 10 seconds for both 4 in. and 12 in. fires. It rises to above 10 seconds for 6, 8 and 10 in. fires. This suggests that there are at least two competing fire suppression mechanisms. The fine water spray system was also tested for surface area protection and the extinguishment time is less than 10 seconds.

References

1. Fisher, L.F., Williamson, R.B., Toms, G.L., and Crinnion, D.M., "Fire Protection of Flammable Work Stations in the Cleanroom Environment of a Microelectronic Fabrication Facility," Fire Technology, Vol. 22, NO.2, May 1986.

2. Wu, P.K., Chaffee, J., and Knaggs, B., "A Wet Bench Free-Burn Test Under FMRC Fire Products Collector," Technical Note, Factory Mutual Research Corporation, Norwood, MA, April 1995.

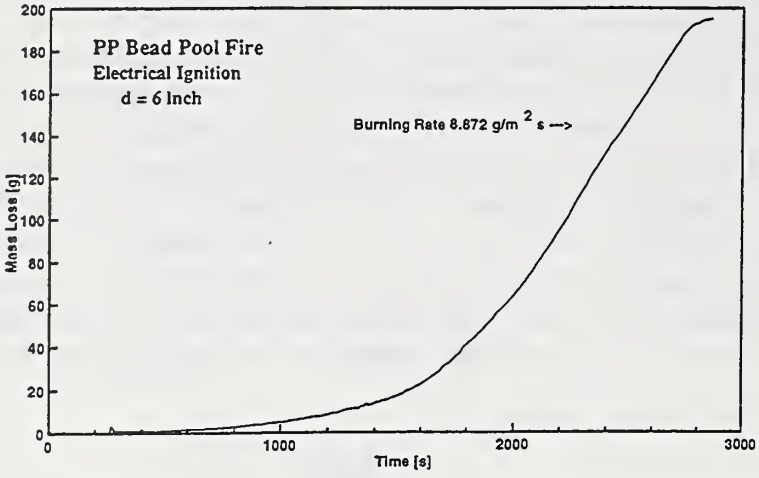

Figure 1. Mass Loss History of a 6 inch Polypropylene Pool Fire

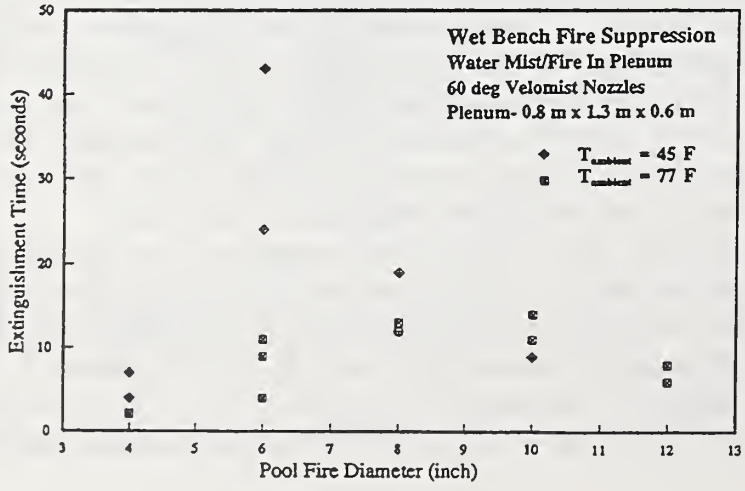

Figure 2. Extinguishment Time vs Pan Diameter For Plenum Fire Tests

Residence Time Effects on Soot Growth Processes

O.A. Ezekoye and Z. Zhang
University of Texas at Austin
Austin, TX 78712

Soot growth processes affect both the radiative heat transfer distribution in a fire as well as the smoke properties. While it is difficult to achieve long residence time effects in laboratory scale flames at normal gravity, it is relatively easier to produce these conditions in microgravity flames. Within a novel microgravity burner configuration used by Atreya and coworkers[1] 2 and 3 seconds of residence time are achieved in a relatively small microgravity flame (cf. figure 1). We have performed computational and theoretical investigations of the soot growth processes within this geometry as well as investigations of the convective and radiative coupling on the total radiative transfer and burner characteristics [2,3].

By coupling the soot and gas phase chemistry with radiative heat transfer processes, detailed effects of radiation from both the soot and gas phase species on the kinetics can be examined in a quasi-steady state microgravity spherical acetylene-air diffusion flame. The gas phase reaction is modeled by either single step or two step chemical kinetics. The soot reaction mechanism includes nucleation, surface growth, oxidation and coagulation steps. The radiation from both soot and the gas phase are calculated by employing a spherical harmonics (P-1 approximation) model. The local Planck mean absorption coefficients of the computed species are specified in the computations.

As a benchmark for these calculations, figure 2 shows the computational soot mass as a function of time as compared with experimental data. Basic soot agglomeration models assume that soot aggregates into volume effective spheres which was shown in Ezekoye and Zhang [2] to predict a low soot specific surface area prediction. In figure 2 we contrast the predicted soot mass time history by assuming volume effective agglomeration and then by assuming no agglomeration at all. It is not surprising that the prediction based on the non-agglomerating assumption over-predicts the soot net growth rate. The finite connection area between soot primary particles ensures that the actual soot surface area is between these two limiting assumptions.

Figure 3 shows the calculated flame radius (defined by the maximum reaction rate) compared with experimental measurements by Atreya et al. There is relatively good agreement between the predicted flame radius and the experimentally measured radius. Two experimentally measured temperatures are compared with the calculated temperatures and are presented in figure 4. The surface area per unit volume in the absence of agglomeration achieves maximum values of approximately 50 cm^{-1} which compare favorably with the measurements of Dobbins et al.[4] where surface area per unit volume estimates are approximately 20 cm^{-1} . By not allowing the particles to agglomerate as spherical objects, the total number of primary particles within the system increases with time. Figure 5 presents the soot number density in mixture fraction space at various times and shows that in the flame region the number densities are significantly larger for the non-agglomerating mechanism, and that on the air side of the flame that the number densities are independent of the agglomeration model. Examination of figure 5 shows that the number of primary particles per aggregate increases from order 10 near the flame sheet to a maximum value of order 10,000 and then decreases to order 1 in the fuel rich region of the flame. These extremely large primary particle numbers (i.e., order 10,000) are consistent with recent soot morphology measurements by Ito et al. [5] in a micro-gravity diffusion flame suggesting that in the absence of strong convection (i.e., cases where the soot has long residence times) the number of soot primary particles per aggregate is significantly larger than in a normal gravity flame. Finally figure 6 presents the growth budget for this flame and shows the volume averaged contributors to the soot growth process as a function of time. For this particular flame, it is evident that only at very short times ($t < 0.1$ ms) does soot nucleation add mass to the soot mass at a larger rate than soot surface growth. For constant absorption coefficient conditions, soot oxidation by OH is always larger than soot oxidation by O_2, and at approximately 10 ms, soot oxidation begins to consume more mass than nucleation adds to the system. Finally, it is shown that only at very long times (approximately 1 second) is there a net decrease in soot mass associated with oxidation processes.

Acknowledgments: This work is supported by the National Institute of Standards and Technology (NIST) under Grant No. 60NANB3D1436, with Dr. K. Butler serving as Scientific Officer.

References:
1. Atreya, A., Agrawal, S., Shamim, T., Pickett, K., Sacksteder, K. R., and Baum, H. R., "Radiant Extinction of Gaseous Diffusion Flames", NASA Microgravity Workshop, Cleveland OH, 1995
2. Ezekoye and Zhang Z. *Combustion and Flame* in review 1996.
3. Ezekoye and Zhang Z. *AIAA Journal of Thermophysics and Heat Transfer* in review 1996.
4. Dobbins, R.A., Santoro, R.J., and Semerjian, H.G., "Analysis of Light Scattering from Soot using Optical Cross Sections for Aggregates," Twenty-Third Symposium (International) on Combustion. 1990
5. Ito, H., Fujita, O., and Ito, K. *Combustion and Flame* 99:363-370, 1994.

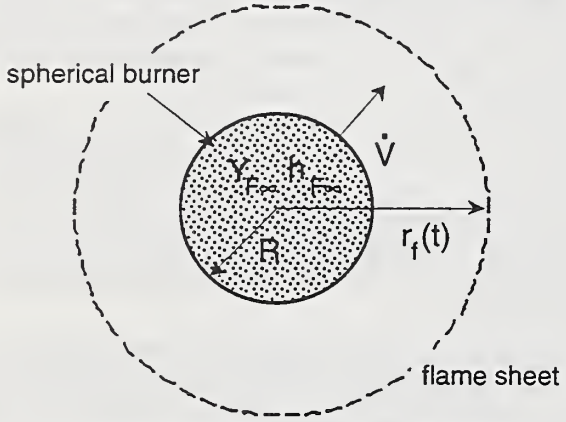

Fig.1 Schematic of computational domain

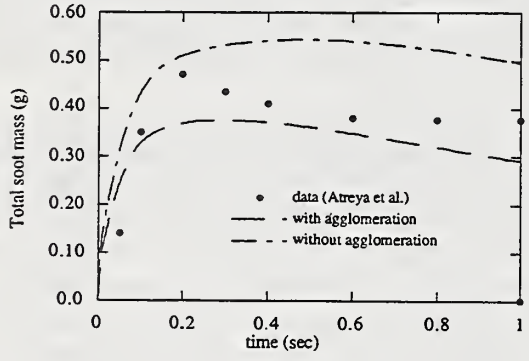

Fig.2 Soot mass predictions compared to expts.

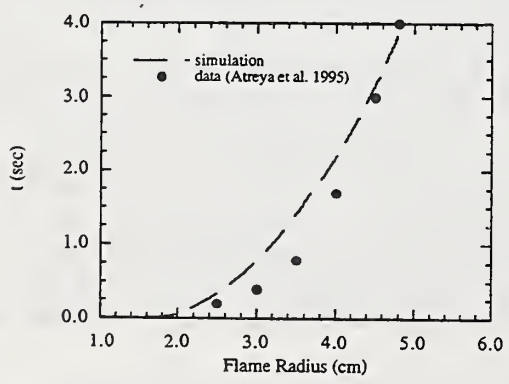

Fig. 3 Flame radius compared to expts.

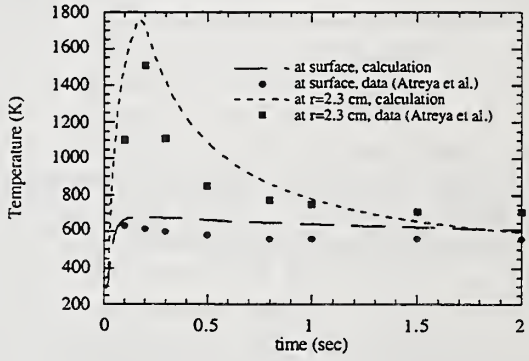

Fig. 4 Flame temperature predictions and expts.

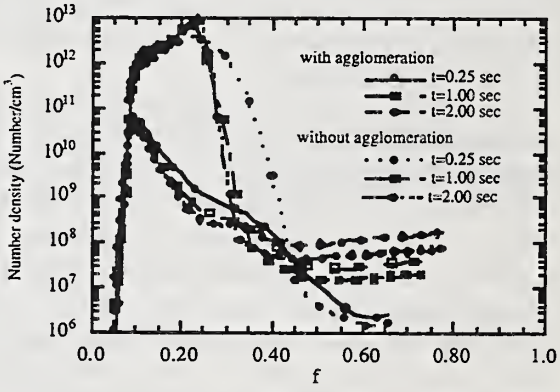

Fig. 5 Soot number concentration predictions

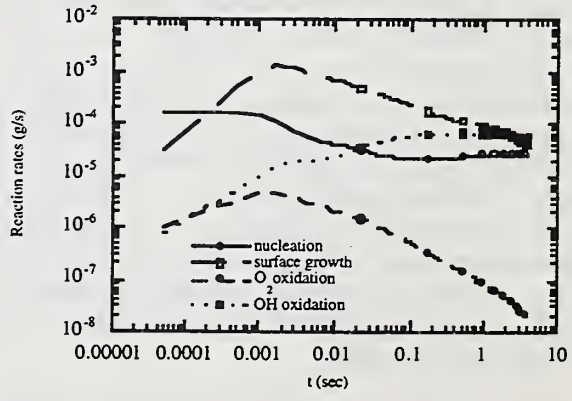

Fig. 6 Growth budget for soot species

REFRACTIVE INDICES OF OVERFIRE SOOT IN LARGE BUOYANT TURBULENT DIFFUSION FLAMES

by

J.-S. Wu, S.K. Krishnan, K.-C. Lin and G.M. Faeth
Department of Aerospace Engineering
The University of Michigan
Ann Arbor, Michigan 48109-2118

Introduction. Information about the optical properties of soot is needed in order to develop reliable nonintrusive measurements of soot physical properties and estimates of soot radiation properties in flame environments. Unfortunately, current estimates of soot optical properties are limited by excessive uncertainties about soot refractive indices [1]. Motivated by this observation, the objective of the present investigation was to experimentally determine soot refractive indices at visible wavelengths (350-800 nm). Soot in the overfire region of buoyant turbulent diffusion flames in the long residence time regime (where soot properties are independent of position and residence time [2]) was studied, considering flames fueled with acetylene, propylene, ethylene and propane burning in still air.

Experimental Methods. The soot was produced by a round, water-cooled burner exhausting into a large collection hood (heated to minimize soot deposition) followed by a short exhaust duct. Soot properties were measured at the exit of the exhaust duct. Soot physical properties were found by collecting samples thermophoretically and analyzing them by pychnometry to find soot density, by ultimate analysis to find elemental composition and by transmission electron microscopy (TEM) to find soot structure. Soot volume fractions were measured by weighing soot collected on a filter while measuring the volume flow of gas over the collection period; this information, combined with the known soot density, yields soot volume fractions at the test location.

Soot refractive indices were found from measurements of soot scattering properties in conjunction with the gravimetric determination of soot volume fractions. Measured scattering patterns were successfully correlated using Rayleigh-Debye-Gans scattering theory for polydisperse fractal aggregates (denoted RDG-PFA theory) that has been shown to be effective for soot optical properties [1-4]. These results then yielded the real and imaginary parts of the refractive indices and the dimensionless extinction coefficients of soot in a straightforward manner [5].

Results and Discussion. Present measurements confirmed that RDG-PFA theory was effective for treating the optical properties of soot for the present conditions; this is important because the test range reached primary particle optical diameters as large as 0.42, which severely tests the approximations of RDG-PFA theory [5].

Present measurements of the real and imaginary parts of the refractive indices of soot are plotted as a function of wavelength, with fuel type as a parameter, in Fig. 1. Also shown on the figure are *ex situ* reflectometry measurements for soot in fuel-lean regions of acetylene and propane/air diffusion flames [6,7], *in situ* measurements for soot in fuel-lean plexiglass/air diffusion flames [8], and *in situ* measurements for soot in the post-flame region of fuel-rich premixed propane and ethylene/air flames [9,10]. Present soot refractive indices do not vary significantly with fuel type and are in reasonably good agreement with the often criticized early measurements of Dalzell and Sarofim [6]. On the other hand, the other measurements [7-10] can be criticized because they involve questionable models of the optical and aggregate properties of soot, while some use questionable approximations when applying Drude-Lorenz dispersion models or Kramers-Krönig causality relationships to close procedures to find soot refractive indices. In particular, present results do not approach a resonance condition typical of graphite as the uv is approached, which is assumed in some refractive index determinations; instead, refractive indices decline continuously similar to the observations of Vaglieco et al. [10] for amorphous carbon and soot.

Present measurements of dimensionless extinction coefficients are plotted as a function of wavelength, with fuel type as a parameter, in Fig. 2. Also shown on the figure are earlier measurements

of this parameter for soot in the overfire region of crude-oil/air diffusion flames [11] and in the post-flame region of premixed fuel-rich acetylene/air flames [12]. Present measurements exhibit little variation with fuel type and wavelength and yield a mean value of 5.1 [5]; this value is smaller than the values of 8.1-9.4 found earlier [11,12], however, for reasons that still must be explained.

Acknowledgments. This research was supported by NIST Grant No. 60NANB4D1696 with K.C. Smyth of BFRL serving as Scientific Officer.

References

1. Faeth, G.M. and Köylü, Ü. Ö., Combust. Sci. Tech. 108:207 (1995).
2. Köylü, Ü. Ö. and Faeth, G.M., Combust. Flame 89:140 (1992).
3. Köylü, Ü. Ö. and Faeth, G.M., J. Heat Trans. 116:152 (1994).
4. Farias, T. et al., J. Heat Trans. 117:1152 (1995).
5. Wu, J.-S. et al., J. Heat Trans., submitted.
6. Dalzell, W.H. and Sarofim, A.F., J. Heat Trans. 91:100 (1969).
7. Batten, C.E., Appl. Optics 24:1193 (1985).
8. Lee, S.C. and Tien, C.L., Eighteenth Symposium (International) on Combustion, The Combustion Institute, Pittsburgh, 1980, p. 1159.
9. Chang, H.Y., and Charalampopoulos, T.T., Proc. R. Soc. London A 430:577 (1990).
10. Vaglieco, B.M. et al., Combust. Flame 79:259 (1990).
11. Dobbins, R.A. et al., Atmos. Environ. 28:889 (1994).
12. Choi, M.Y. et al., Combust. Flame 102:161 (1995).

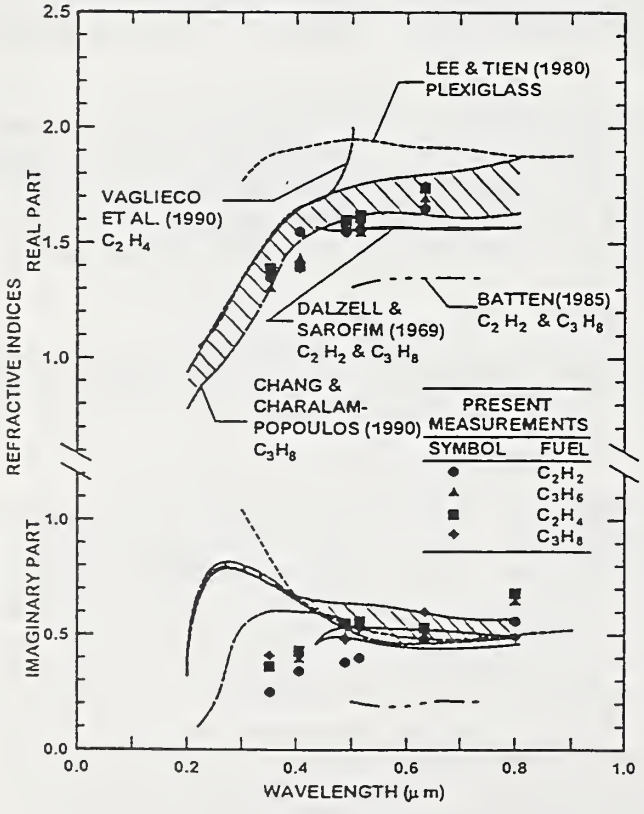

Fig. 1 Measured soot refractive indices.

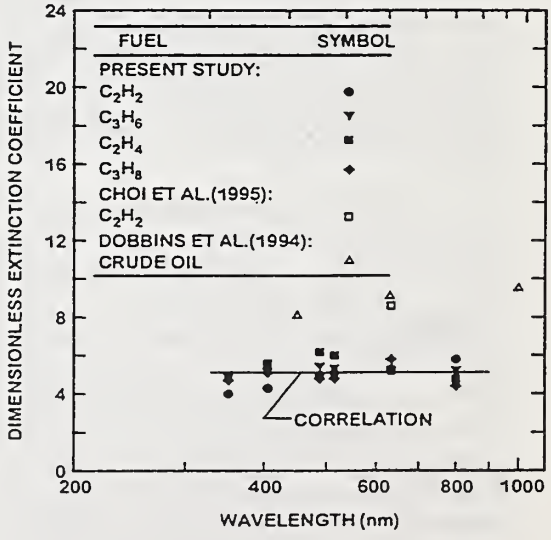

Fig. 2 Measured soot dimensionless extinction coefficients.

A Study of Soot and PAH Oxidation in Post-Flame Gases

M.P. Tolocka and J.H Miller
Department of Chemistry
The George Washington University
Washington DC 20052

The incomplete combustion of gas phase hydrocarbons can lead to toxic emissions from both unwanted fires (Pitts *et al.*, 1994; Zukoski *et al.* 1991) and from industrial processes (You *et al.*, 1994). Typically, both acute toxins such as carbon monoxide (Pitts, 1994) and chronic toxins, such as Polycyclic Aromatic Hydrocarbons (PAH) are simultaneously emitted. Carbon monoxide present in enclosure fires is believed to be responsible for roughly 2/3 of deaths in those situations(Harwood and Hall, 1989). Because of its threat to human health, CO is regulated by the EPA as a criteria pollutant by the Clean Air Act.

PAH are hazardous in their own right; these pollutants exhibit mutagenic and carcinogenic properties (Blakeslee, 1983, Bhatt and Coombs, 1990). In light of the biotoxicity of this class of compounds (see Zaia and Biemann, 1994) , PAH are listed as Hazardous Air Pollutants (HAP) under Title III of the 1990 Clean Air Act Amendments (CAAA). However, PAH may contribute to acute toxicity as well. These molecules are thought to be the key intermediates in the formation of particulate carbon. Both they and the particles that form from them participate in the formation of CO from fires through both the direct oxidation and indirect processes such as radical quenching.

Prediction of heat release rates, opacity of the combustion products, and the amount of CO and other products of incomplete combustion formed in fires have been addressed using hood experiments (see Beyler, 1986; Tewarson and Steciak, 1983; Zukokski *et al.* 1991) and enclosure fires (Grand *et al.* 1986; Morikawa and Yanai, 1986). The composition of the fire emissions in these studies seems to be well correlated with the amount of oxidizer supplied. In many of these studies, the Global Equivalence Ratio, or GER (Cooper, 1994) has been used to quantify the level of ventilation defined as the moles of carbon divided by the moles of oxygen normalized by the stoichiometric ratio (Pitts, 1994). Therefore GERs greater than one are designated underventilated, GERs less than one are overventilated.

However, in a review by Pitts (1994), results from Morehart (1990) show the equilibrium concentrations of CO increase by a factor of two from 900 - 1500 K for all of the underventilated fires investigated. This suggests that CO formation is a kinetically controlled process. Pitts concludes that the correlation between post-flame temperature and the composition of the gases is not well understood, especially for intermediate temperatures, or where the fires generate copious amounts of smoke.

In our laboratory at GWU a system to study the emissions from overventilated and underventilated diffusion flames has been constructed (Skaggs *et al.* 1996). Both the production of gas phase products(methane, acetylene, carbon monoxide, carbon dioxide, and oxygen) and condensed phase compounds (PAH and soot) from these flames can be followed. The product composition was measured using tunable diode laser absorption spectroscopy, mass spectrometry, laser light extinction, and gas chromatography. The temperature of the effluent stream was varied up to 1300 K using a tube furnace, allowing us to investigate the kinetics of post-flame oxidation.

Some of the key results of our measurements have been:

- The concentrations of the products of incomplete combustion all increase with increases in GER.

- For lean global stoichiometries, the oxidation chemistry proceeds at a greater rate with increasing tube furnace temperature.
- For rich stoichiometries, evidence exists that chemical processes which include pyrolytic growth and oxidation occur at all furnace temperatures. However, these chemistries undergo a marked change in intensity at temperatures near 900 K.
- The magnitude of the soot oxidation rate agrees qualitatively with what may have been expected from high temperature extrapolations (e.g. Park and Appleton, 1973). However the activation energies for our rates are substantially lower. (Figure 1)

References

Beyler, C.L. (1986) *Fire Safety J.* **10**, 287
Bhatt, T.S. and Coombs, M.M. (1990) *Polycyclic Arom. Comp.* **1**, 51.
Blakeslee, J.R., Elliot, A.M. and Carter, L.J. (1983) Polynuclear Aromatic Hydrocarbons: Formation, Metabolism and Measurement. Battelle Memorial Institute, MA. 123.
Cooper, L.Y. (1994) *Fire Safety J.* **23**, 245
Harwood, B. and Hall, J.R. (1989) *Fire J.* **83**(3), 29
Morehart, J.H. (1990) *Ph.D. Thesis*
Park, C. and Appleton, J.P. (1973) *Combust. and Flame* **20**, 369.
Pitts, W.M. (1994) NIST Monograph 179 (Washington, DC) and references therein
Skaggs, R.R., Tolocka, M.P., and Miller, J.H. (1996) *Combustion Sci. and Tech.* in press.
Tewarson, A. and Steciak, J. (1983) *Combust and Flame* **53**, 123.
You, J.H., Chiang, P.C., Chang, K.T., and Chang, S.C. (1994). *J. Haz. Mater.* **36**, 1.
Zaia, J. and Biemann, K. (1994) *J. Am. Chem. Soc.* **116**, 7407.
Zukoski, E.E., Morehart, J.H., Kubota, T., and Toner, S.J. (1991) *Combust. and Flame* **83**,325.

Figure 1: Comaprison of surface soot oxidation rates from literature values and current measurements. (see Park and Appleton, 1973).

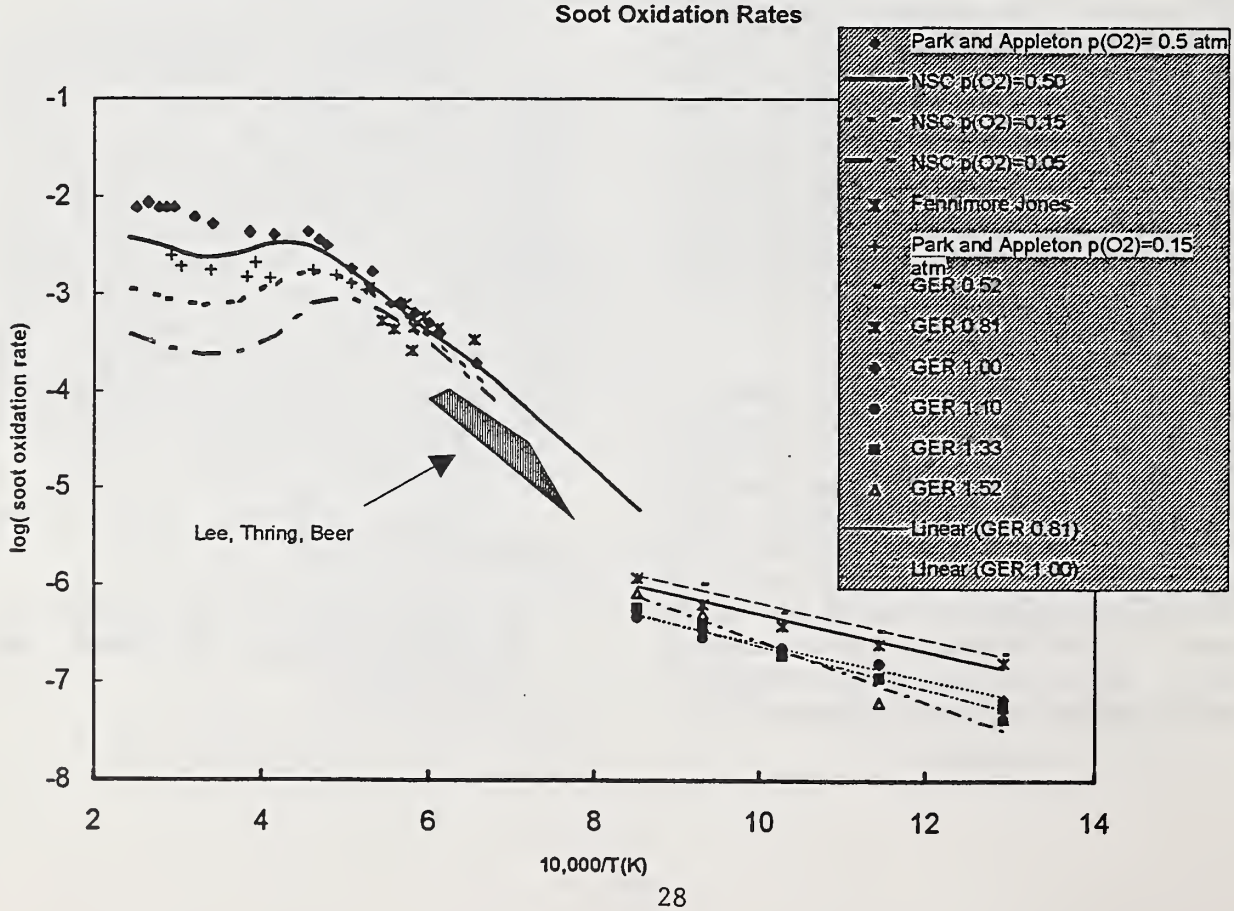

Proposed for Presentation at
The Annual Conference on Fire Research
Gaithersburg, MD, October 28-31, 1996

Absorption/Emission Spectroscopy Measurements of Soot Volume Fraction and Soot Emission in Large Fires*

Louis A. Gritzo*, Yudaya Sivathanu**, Walt Gill***, and T.Y. Chu****
*Unsteady and Reactive Fluid Mechanics, Department 9116
***Thermal and Mechanical Environments, Department 9735
****Severe Accident Phenomenology, Department 6423
Sandia National Laboratories, P. O. Box 5800
Albuquerque, NM 87185-0836

** - En'Urga Inc. West Lafayette, IN

The hazard posed by a large, fully turbulent (i.e. > 1.3m diameter) hydrocarbon fuel fire is defined by the history of the net heat flux from the fire to the system of interest. Due to the large amounts of soot (~10-15% total yield, [1]) and the relatively low velocities (on the order of 1-10 meter/second [2]) which characterize these fires, heat fluxes incident on most systems of interest are primarily due to participating media radiative transport. It is therefore necessary for the temperature of the *media* (as opposed to the temperature of a thermocouple exposed to the media) and the media radiative properties to be known within a hemispherical region with a minimum diameter of 4 optical path lengths to determine the heat flux at a point in the fire. Radiative emission and absorption from small (10-100 nm), spherical soot particles are thought to dominate radiative transport within the flame zone of large fires. Radiative scattering (as occurs in highly agglomerated soot, [3]) and gas band emission and absorption (as becomes increasingly important for smaller flames [4]) are typically neglected. Although the radiative transport depends on the knowledge of soot absorption and emission within the fire, relevant data have not been obtained for large fires. Data are therefore needed to validate soot generation and combustion submodels presently employed in fire field model. Due to the turbulent nature of these environments, highly time-resolved measurements are required.

To satisfy these requirements, a new optical fiber-based soot probe has recently been developed at Sandia in collaboration with En'Urga, Inc. and Purdue University to perform highly-transient measurements of the soot extinction coefficient, soot emission temperature, and soot volume fraction. The fundamental technique has been employed previously [5] in laboratory scale fires. A description of the technique employed in large fires, as well as recently acquired data, are presented. These data lend unique insight into the actual soot radiative properties and temperature which could previously only be indirectly inferred from "grab samples" (which tend to suffer from low sampling rates and alteration of soot topography in transit) or estimated based on combined thermocouple temperature and heat flux data.

Soot extinction coefficients are determined by measuring the attenuation of laser light though a small, cylindrical (~1.2 cm dia. X 2.5 cm long) sample volume. The soot emission temperature is measured using the ratio of the intensities at the 900nm and 1000nm wavelengths. Soot volume fraction can be

*This work was supported by the Sandia Model Validation Project, the Sandia Engineering Sciences Research Foundation, and the Defense Nuclear Agency and was performed at Sandia National Laboratories, Albuquerque, NM, managed by Lockheed-Martin Corp. for the U.S. Department of Energy under Contract DE-AC04-94AL85000

obtained from the soot probe data in two different manners. By assuming that the soot particles are small and round (thought to be a reasonable assumption in the interior of the flame zone but presently not validated) the soot volume fraction can be determined directly from the soot extinction measurements and the tabulated soot indices of refraction [6]. The relative strength of the intensities at 900 and 100 nm can also be used to calculated the soot volume fraction subject to the same assumption, but also subject to the assumption that the temperature is uniform throughout the sample volume.

Presently, the soot diagnostic technique uses two water-cooled, insulated, probe heads equipped with collimating and focusing lenses and a nitrogen purge to avoid soot deposition. The two-probe system allows simultaneous stationary and traversing measurements to be performed for spatial distribution data to be inferred. Stainless-steel fiber optic bundles (100 m length, capable of being immersed in water for the last 25 m) transmit the signal to and from the probe head from portable (0.6 m X 1.0 m) sending and receiving optics boxes. Portable, rack-mounted signal processing hardware is employed in conjunction with a high speed data acquisition system or a portable lap-top computer which is used to digitize and store the data.

Newly acquired data for 5 m diameter pool fires obtained using this technique will be presented. These data render the following advances in our understanding of large fires:

- Unique characterization of soot radiative properties in large fires.
- Assessment of soot volume fraction as needed for comparison with soot generation and combustion models.
- Assessment of small-scale variations in soot temperature.
- Characterization of the differences inherent in thermocouple temperature and actual emission temperature.
- An assessment of the time scales associated with radiative emission for the purposes of assessing the effects of radiative turbulence in large fires.
- The time-resolved correlation between soot volume fraction and soot emission temperature.

Further studies are expected to focus on in-situ soot measurements in larger (18.9 m diameter) fires, fires which include the effects of winds, and in the vicinity of engulfed, objects. The end goal is to advance our understanding of the dominant physical phenomena and to improve the fidelity of fire simulations through physically-based models which are validated with full-scale data.

References

1. Notarianni, K. A., Evans, D. D., Walton, W. D., and Koseki, H. "Smoke Production from Large Oil Pool Fires," Proceedings of INTERFLAM '93, pp. 111-119, 1993.
2. Koski, J. A., Gritzo, L. A., Kent, L. A., and Wix, S. D. "Actively Cooled Calorimeter Measurements and Environment Characterization in a Large Pool Fire," *Fire and Materials*, Vol 20, pp. 69-78, 1996.
3. Koylu, U. O., and Faeth, G. M. "Optical Properties of Soot in Buoyant Laminar Diffusion Flames," *Journal of Heat Transfer*, Vol 116, pp. 971-979, 1994.
4. Grosshandler, W. L. "RADCAL: A Narrow-Band model for Radiation Calculations in a Combustion Environment, NIST Technical Note 1402, 1993.
5. Sivathanu, Y. R., and Gore, J. P. "Simultaneous Multiline Emission and Absorption Measurements in Optically-Thick Turbulent Flames," *Combustion Science and Technology*, Vol. 80, pp 1-21, 1991.
6. Tesner, P. A., Snegiriova, T. D., Knorre, V.G. "Kinetics of Dispersed Carbon Formation," Combustion and Flame, Vol. 17, pp. 253-260, 1971.

HEAT FLUX CALIBRATION FLOW AND CONDUCTION FACILITIES: STATUS REPORT

K. Steckler and W. Grosshandler
Building and Fire Research laboratory
National Institute of Standards and Technology

ABSTRACT

Standard methods exist at NIST for calibrating thermal radiation detectors up to 10 kW/m^2 using blackbody cavities, and up to 40 kW/m^2 using a monochromatic laser source. Heat flux transducers, however, are often used under conditions where convection dominates, where radiation emanates from a source with a different spectral character, or where flux levels exceed 40 kW/m^2. The objective of this project is to extend NIST heat flux calibration capabilities to, at least, a limited range of the latter conditions. Convective and conductive heat transfer facilities are being designed and constructed for this purpose.

Channel-Flow Facility

A laboratory-scale, 3.2 m-long, low speed wind tunnel, having a 0.2 m (l) x 0.3 m (w) x 0.01 m (h) test section, will be used to calibrate heat flux gauges under convective heat transfer, boundary-layer flow conditions. The test section will have a heated wall in which a heat flux gauge can be mounted flush. Cooler flow-conditioned air will pass through the test section. Air temperature and velocity will be variable, with heat fluxes at the surface designed to be preset between 0.5 and 5.0 kW/m^2 with an uncertainty of less than ± 5 percent. Flow visualization, hot-wire probing, thermocouples, and temperature-sensitive liquid crystals will be used to measure the temperature fields in the air and on the surface adjacent to the flux gauge.

The 3.0 m-long flow-conditioning part of the wind tunnel has been designed, fabricated, and assembled. This part contains heat exchangers, honeycomb and screen turbulence-control sections, and a 30/1, two-dimensional, contraction section. The test section is being designed. Its heated surface will contain an array of guarded, foil, resistance heaters designed to maintain the surface at a uniform temperature. Numerical simulations by co-workers in other NIST laboratories (CSTL and EEEL) of the energy transfer are being used to refine the design and minimize uncertainties. The final design will be included in this presentation.

The tools necessary for the hot-wire velocity measurements have been gathered and shakedown experiments are underway. Subsequently, the velocity field at the exit of the contraction will be mapped.

Gas-Phase Conduction Facility

A guarded hot-plate concept has been extrapolated to produce heat fluxes up to 100 kw/m^2. Figure 1 shows a 1.0 mm-thick layer of helium separating two flat, polished, copper plates maintained at a temperature difference of several hundred degrees. This arrangement avoids contact-resistance on the helium side of the gauge and should produce the necessary high level of conductive flux with trivial radiative component. The conduction apparatus has been designed and fabrication is about 75 percent complete. Details of the design and, if available, preliminary shakedown results will be included in this presentation.

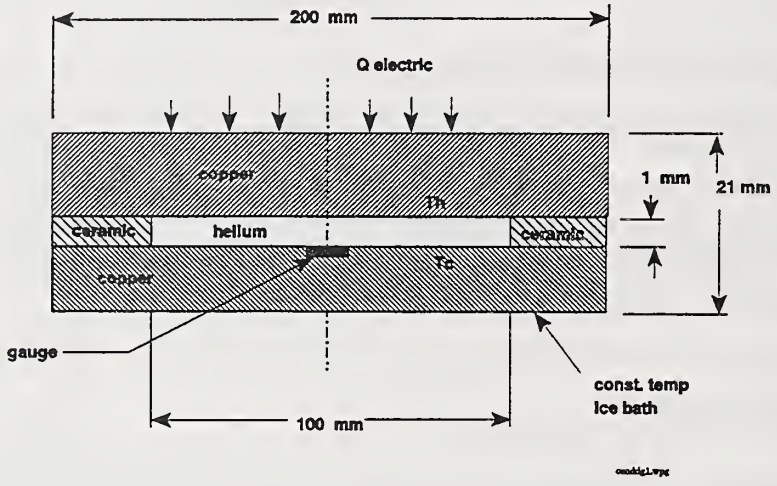

Figure 1. Schematic of conduction apparatus (elevation).

Proposed for Presentation at
The Annual Conference on Fire Research
Gaithersburg, MD, October 28-31, 1996

Fuel Temperature Distribution and Burning Rate in Large Pool Fires*

Louis A. Gritzo, Edward A. Boucheron
Unsteady and Reactive Fluid Mechanics, Department 9116
Sandia National Laboratories, P. O. Box 5800
Albuquerque, NM 87185-0836

Doug Murray
Code 528220D
Naval Air Weapons Center
China Lake, CA 93555

Many scenarios of interest in fire science and fire safety involve the burning of liquid fuels in the form of large, fully turbulent (i.e. > 1.3 m diameter) fires. Included in these scenarios are instances where the fuel forms a pool which can be considered as "thermally deep", i.e., the fuel layer is of sufficient depth that thermal penetration is confined to an upper layer and, therefore, the substratum does not interact thermally and has a negligible effect on the fire. Examples include the burning of fuel in an open tank during an industrial accident, burning from a fuel-filled pit as a consequence of a transportation accident, and the gathering and subsequent burning of crude oil on the surface of a waterway for environmental impact mitigation. Other relevant scenarios, not thermally deep, include cases where fuel is spilled and spreads to form a thin liquid layer on a impermeable surface such as a concrete runway, aircraft carrier deck or facility floor. If the surface is flat and the spill is continuous, the mass flow rate of the spill and the mass flux of vapor from the pool surface combine to define the size and duration of the resulting fire.

Large pool fire scenarios are often roughly characterized by the maximum total chemical heat release rate given by $\dot{Q} = \dot{M}_{avg} H_c$, where $\dot{M}_{avg}$ is the average fuel vaporization rate and H_c is the fuel heat of combustion. The total heat release rate defines an important upper limit on the thermal potential of the fire and limited success has been achieved in estimating large fire hazards based on this quantity [1]. The actual thermal hazard large fires pose to critical systems and personnel is determined by the heat flux from the fire to the object of interest. The heat flux distribution within the fire and the distribution of radiative heat flux from the exterior of the flame zone are both strongly affected by the efficiency of combustion within the flame zone. Variations in combustion efficiency are possible due in part to the spatial distribution of fuel which is vaporized from the surface of the liquid and the subsequent transport and mixing of the gaseous fuel with air.

Measurements of fuel vaporization rates and fuel temperature distributions were recently performed as part of a series of large (18.9 m diameter) JP-8 pool fire experiments at the Naval Air Weapons Center (NAWC) CT-4 test facility at China Lake. This work is of particular interest since the majority of the studies performed to date are limited to fires with diameters significantly smaller than the lower limit of the fully turbulent regime. Several important distinguishing features are noted between the mechanisms present in the previous studies and those present in the large fires discussed here. The difference in these mechanisms is primarily due to the magnitude and distribution of the heat flux to the fuel surface. Smaller fires are characterized by spatially uniform heat fluxes to the fuel surface of approximately 30 kW/m^2 [2,3]. Data acquired from large pool fires [4] shown significant variations in the heat flux to the fuel surface with values ranging from 20kW/m^2 near the oxygen-starved interior, to fluxes of 100kW/m^2 directly below the primary flame zone.

---

*This work was supported by Defense Nuclear Agency and the Sandia Engineering Sciences Research Foundation and was performed at Sandia National Laboratories, Albuquerque, NM, managed by Lockheed-Martin Corp. for the U.S. Department of Energy under Contract DE-AC04-94AL85000

Data were acquired at locations of high and low heat flux for each of eight tests with wind conditions ranging from 1.3 m/s to 10.9 m/s. The same general trends were observed in all of the data sets. Inspection of the data reveals the following:

- After the initial transient associated with fire growth (~60 s), the fuel recession rate is steady and equal to 4.4 mm/min; the same value was reported by Blinov and Khudyakov [5] for burning of kerosene and gasoline in 9 m and 23 m diameter fires.
- Heating of the fuel is limited to the top 1.5 cm (which greatly exceeds the penetration depth for pure 1-D conduction).
- The heated depth appears to be slightly greater in regions of reduced heat flux.
- The temperature at the free surface of the fuel is spatially uniform and approximately 510K (nearly equal to the mean of the distillation curve for JP8).
- There are very significant fluctuations observed in the data which increase in magnitude near the fuel surface.

The preceding trends, in conjunction with the distributions of heat flux to the fuel surface observed in previous studies, imply lateral mixing of the liquid fuel primarily due to the maintenance of a free surface in the presence of a non-uniform heat flux distribution. In addition, the potential exists for convection resulting from uneven heating. The construction of a submodel suitable for fire field model implementation depends on the extent to which lateral transport occurs, between the limits of "well-mixed" and "non-mixed". Reduced-scale experiments with well-defined uniform and non-uniform heat flux distributions, complemented by Fourier Transform Infrared (FTIR) measurements of fuel radiative properties, are presently underway to satisfy these requirements.

For large, fully turbulent fires, the heat flux distribution to the fuel surface, which affects the fuel gasification rate and the transport of gaseous fuel within the fire, is strongly influenced by scenario-specific parameters such as; fuel type, fuel pool shape, wind, topology in the neighborhood of the fire, and the presence of engulfed and nearby objects. Present fire field models are capable of representing the effect of varying these parameters on fire behavior in reasonable detail. With improved understanding and quantification of the dominant physical mechanisms governing the burning of liquid fuels in large fires, phenomenological models of the fuel pool thermal transport and gasification processes can be developed for use in numerical simulations. The end goal is to improve the fidelity of fire simulations through physically based models which are validated with full-scale data.

References

1. Mudan, K. S. and Croce, P. A. "Fire Hazard Calculations for Large, Open Hydrocarbon Pool Fires," Section 2-4, *The SFPE Handbook of Fire Protection Engineering, First Edition*, National Fire Protection Association, Quincy, MA.
2. Hamins, A., Fischer, J, Kashiwagi, T., Klassen, M.E. and Gore, J.P., "Heat Feedback to the Fuel Surface in Pool Fires," *Combustion Science and Technology,* Vol 97, pp. 37-62, 1994.
3. Inamura, T., Saito, K., and Tagavi, K.A., "A study of Boilover in Liquid Pool Fires Supported on Water. Part II: Effects of In-depth Radiation Absorption," *Combustion Science and Technology*, Vol. 86, pp. 105-119, 1992.
4. Gritzo, L.A., Nicolette, V.F., Tieszen, S.R., and Moya, J.L. "Heat Transfer to the Fuel Surface in Large Pool Fires," *Transport Phenomenon in Combustion*, S.H. Chan, ed, Taylor and Francis, 1996.
5. Blinov, V.I., and Khudyakov, G. N. "Diffusion Burning of Liquids," English Translation: U.S. Army Engineering Research and Development Labs, Fort Belvoir, VA, Report AERDL-T-1490-A, 1961.

PRE-BOILOVER BURNING OF A SLICK OF OIL ON WATER

S. Gandhi, J. L. Torero,
Department of Fire Protection Engineering, University of Maryland
College Park, MD20742-3031, USA

J. P. Garo and J. P. Vantelon
Laboratoire de Combustion et de Detonique, ENSMA-Universite de Poitiers
86960 Futuroscope Cedex, FRANCE

ABSTRACT

The burning of oil in water is of great interest as a result of off-shore exploration, production and transportation of petroleum. This combustion phenomenon may constitute a hazard, i.e. and accidental burning slick drifting towards a platform, but it may also serve as a measure to minimize the environmental damage of an oil spill [1,2]. The available information on this phenomena is quite limited. Although great effort has been devoted to the understanding of pool fires [3] and flame spread over liquid pools [4] the specific issues related to a fuel burning over a water bed have deserved little attention. Most of the work being related to fires in fuel tanks and the phenomena commonly referred as "boilover" [5,6]. Only a few studies have dealt with the burning of a thin layer of fuel on a water bed. A good summary of existing knowledge is provided by Evans et al. [2].

The burning rate of a slick of oil on a water bed is calculated by a simple expression derived from a one-dimensional heat conduction equation. Heat feedback from the flame to the surface is assumed to be a constant fraction (χ) of the total energy released by the combustion reaction ($\dot{q}''_S = 4\chi\,\dot{Q}/\pi d^2$). The total heat release, as a function of the pool diameter ($\dot{Q} = \rho_\infty C_p (T_\infty g (T_f - T_\infty))^{1/2} d^{5/2}$) is obtained from existing correlations [3,7]. It is assumed that radiative heat is absorbed close to the fuel surface, that conduction is the dominant mode of heat transfer in the liquid phase and that the fuel boiling temperature remains constant. By matching the characteristic thermal penetration length scale for the fuel/water system and an equivalent single layer system, a combined thermal diffusivity can be calculated ($\alpha_{EQ} = \frac{r\,y_{S,i}}{\alpha_F}(\sqrt{\alpha_W} + \sqrt{\alpha_F})^2$) and used to obtain a solution for the burning rate.

$$r = \frac{1}{H_v \rho_F}\left[\chi\left(\frac{4\,\rho_\infty\, C_p (T_\infty g (T_F - T_\infty))^{1/2}}{\pi}\right) d^{1/2} - \frac{\alpha_F \lambda_F (T_S - T_\infty)}{y_{S,i}(\sqrt{\alpha_F} + \sqrt{\alpha_W})^2}\right]$$

Theoretical expressions were correlated with experiments for crude oil (63% Kittiway, 33% Arabian Light and 4% Oural) and heating oil (a mixture of hydrocarbons ranging from C_{14} to C_{21}), for a number of pool diameters and initial fuel layer thickness [8] (figure 1). Experiments were also conducted with emulsified and weathered crude oil [9]. The simple analytical expression describes well the effects of pool diameter and initial fuel layer thickness permitting a better observation of the effects of weathering, emulsification and net heat feedback to the fuel surface. Experiments showed that only a small fraction of the heat released by the flame is retained by the fuel layer and water bed ($0.001 < \chi < 0.004$), that the effect of weathering on the burning rate decreases with the weathering period (figure 2) and that emulsification results in a linear decrease of the burning rate with water content (figure 3). Deviations from the predicted values arise from the assumptions used in the model and from the uncertainties in the experimental results for an initial fuel thickness smaller than 5 mm.

REFERENCES

1. Twardus, E.M. and Brzustowski, T.A., *Archivum Combustionis*, Polish Academy of Sciences, **1**, 1-2,49-60, 1981.
2. Evans, D., Walton, W., Baum, H., Lawson, R., Rehm, R., Harris, R., Ghoniem, A. and Holland, J., *Proceedings of the Third Arctic And Marine Oil Spill Program Technical Seminar,* pp. 1-38, 1990.
3. Drysdale, D.D., *An Introduction to Fire Dynamics*, John Wiley and Sons, 1985.
4. Ross, H.D. Progress in Energy and Combustion Science, 20, pp.17-63, 1994.
5. Ito, A., Inamura, T. and Saito, K., *ASME/JSME Thermal Engineering Proceedings*, 5: 277-282, 1991.
6. Arai, M., Saito, K. and Altenkirch, R.A., *Combustion Science and Technology*, 71, pp.25-40, 1990.
7. McCaffrey, B. J., NBSIR 79-1910, National Bureau of Standards, Washington D.C., 1979.
8. Garo, J. P., Vantelon, J. P. and Fernandez-Pello, A.C., *Twenty-fifth Symposium (International) on Combustion*, The Combustion Institute, **1481-1488**, 1994.
9. Garo, J.P., "*Combustion d'Hydrocarbures Repandus en Nappe sur un Support Aqueux. Analyse du Phenomen de Boilover*", Ph.D. Thesis, University of Poitiers, France, 1996.

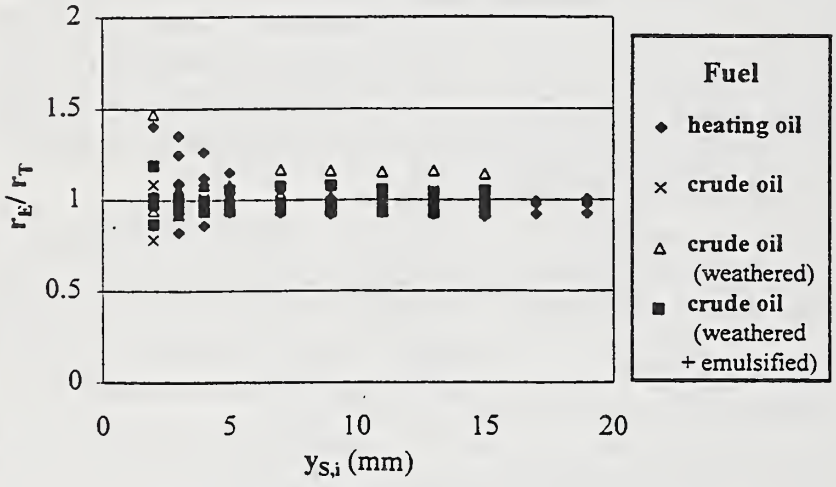

Figure 1. Comparison between experimental (r_E) and calculated (r_T) regression rates

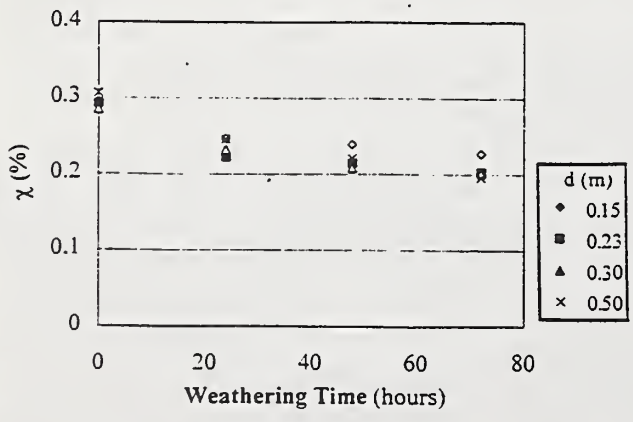

Figure 2. Efficiency constant as a function of the weathering period for crude oil

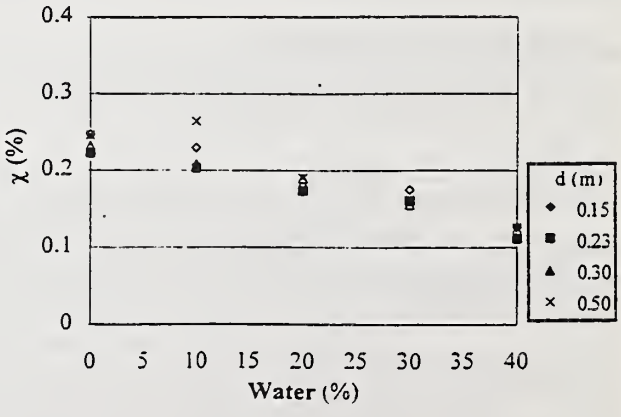

Figure 8. Efficiency constant as a function of water content period for emulsified crude oil (weathered 24 hours)

WHY ARE POOL FIRES ANCHORED?

S. Venkatesh, A. Ito, and K. Saito

Combustion and Fire Research Laboratory
Department of Mechanical Engineering
University of Kentucky
Lexington, KY 40506–0108

ABSTRACT

This paper attempts to answer the question, "Why are small scale pool fires anchored?" by providing and interpreting a new set of experimental data. For momentum–controlled, high Reynolds (Re) number turbulent–jet diffusion flames, the formation of a premixing zone is suggested as the primary reason for the flame anchoring. For buoyancy–controlled pool fires, however, the existence of the premixing zone at the flame base is not clear because both Re and Fr (Froude number) are low. To improve our understanding of the flame anchoring mechanism and structure of buoyancy–controlled liquid pool fires, we employed small scale pool fires whose diameters range between 1.5 – 20 cm. Our measurements include flow visualization by a particle–track laser–sheet technique (PTLS) combined with a high speed video camera and temperature profiles by a fine thermocouple. We found from those measurements that major air entrainment occurred through the primary anchoring zone, PAZ, which consists of a small area covering approximately 1 cm high and around the circumference just above the dark zone; while air entrainment through the quenching zone (a dark zone formed between the visible flame edge and the burner port) was negligible. The structure of the PAZ was found to be premixed flame (another interpretation may be it is similar to counter–diffusion flame). This enables the pool fires to anchor at the burner port. In addition, we visualized the existence of a vortex ring at a stagnation zone in the fuel vapor phase for both propanol and hexane pool fires, in agreement with qualitative observation by other workers.

OBJECTIVES

(1) Understanding the mechanism of flame anchoring in pool fires. We investigate if and how the PAZ controls the flame anchoring. The cross–sectional area of PAZ is at most 1 cm high x 1 cm wide in radial direction consisting of the pan's brim surface, a sub–millimeter size dark (quenching) zone, a millimeter–size visible leading flame edge, and an extended (believed to be diffusion controlled) flame zone. We divided McCaffray's continuous flame zone into three subzones: the quenching zone, PAZ, and post PAZ, and studied each zone thoroughly. Figure 1 shows a schematic of the five–zone structure.

Much work has been conducted on the stability and liftoff of laminar and turbulent jet diffusion flames. The common understanding is that premixing occurs near the base and is responsible for anchoring and stabilization. The results by Takahashi et al. on turbulent jet diffusion flames show mixing of the fuel and air through a circulation zone established at the burner rim due to strong shear stresses, leading to flame anchoring. For liquid pool fires, Bouhafid et al suggested the formation of a premixed reaction zone as the mechanism of flame anchoring due to the observed strong radial component of the air velocity induced by the plume. We think that in a pool fire, the fuel and oxidizer velocities at PAZ are much smaller, perhaps insufficient to produce shear stress induced circulation zones observed for the turbulent jet diffusion flames.

(2) Understanding of the mechanism of air entrainment at PAZ and other heights. According to Bouhafid et al and this study, convective air entrainment likely occurs at PAZ in order to satisfy mass conservation because of the rapid acceleration of the

buoyant gases in the flame interior. In the intermittent region, however, air entrainment occurs mainly by relatively large–scale buoyancy–induced mixing as explained by Weckman et al, Zhou and Gore and Cetegen. In the post–PAZ region where the flame is a pseudo laminar continuous flame, air streamlines are parallel to the visible flame surface (to be shown in Fig. 3), and air transport to the flame surface is by diffusion.

(3) Experimental confirmation of the stagnation and re–circulation zone. Based on thermocouple temperature and CO, CO_2 concentration measurement data, Bouhafid et al predicted the existence of a stagnation and re–circulation zone in the fuel–vapor phase just above the liquid fuel surface. Yet there is no experimental data to directly verify their prediction; therefore, flow–visualization experiments were conducted in order to examine the proposed stagnation and re–circulation zones.

SUMMARY AND CONCLUSIONS

(1) Based on our experimental measurements on pool fires in diameter of 1.5 – 20 cm of propanol and hexane, and finite–rate chemistry concepts, the entire flame sheet of a pool fire is established to have a triple flame structure. The structure of the flame at the base was established from PTLS data and through a comparison of the location of the flame sheet in the convective–air entrainment zone for fuels with different stoichiometric fuel–air requirements.

(2a) Air entrainment through the quenching zone was found to be a small fraction of the net air entrainment near the base for the pool fires. Our data show that the ratio of the total mass of air entrained into the flame interior through PAZ to the total mass of air entrained through the quenching zone was 0.05.

(2b) The fluid–dynamic structure of the anchoring mechanism of a buoyancy–dominated small scale pool fire and a momentum–dominated jet diffusion flame is different. In a jet diffusion flame, the Reynolds shear stress near the rim of the burner induces a stagnant re–circulation zone where the fuel and the oxidizer are mixed and the flame anchors. To the contrary, in a pool fire the shear stresses at the rim are two orders of magnitude lower and turbulent mixing does not occur. Finite–rate chemistry establishes the presence of a molecular–diffusion mixing zone. Therefore, the flame anchors at the base.

(3) For both propanol and hexane pool fires with their diameter range between 1.6 cm and 10 cm, the formation of the stagnation re–circulation zone predicted by Bouhafid et al was experimentally confirmed.

ACKNOWLEDGEMENTS

We would like to thank F.A. Williams, A.S. Gordon and T. Hirano for their valuable comments. This study was supported in part by the National Institute of Standards and Technology under grant #60NANB1D1123, in part by NASA–Kentucky EPSCoR program and in part by the Center for Manufacturing Systems at the University of Kentucky.

REFERENCES

Venkatesh, S., Ito, A., Saito, K., and Wichman, I.S., Twenty–sixth International Symposium on Combustion, The Combustion Institute, 1996. to appear.

Qian, C., Tashtoush, G., Ito, A., and Saito, K., Proc. International Conference on Fire Research and Engineering, Edited by D.P. Lund., Society of Fire Protection Engineering, 1995.

Tashtoush, G., Narumi, A., Ito, A., Saito, K., and Cremers, C.J., Proc. Eight International Symposium on Application of laser Techniques to Fluid Mechanics, Lisbon, Portugal, 1996.

SCALING FLAME LENGTHS OF LARGE DIFFUSION FLAMES

E. E. ZUKOSKI

CALIFORNIA INSTITUTE OF TECHNOLOGY

The scaling laws for flame length of large buoyant diffusion flames have not been established on any basis except simple correlations and the correct parameters to be used in these have not been clearly established. Several possible parameters are discussed and a set of experiments is described in which the effects on the flame length of changing these parameters are investigated. The changes in the parameters are accomplished by diluting natural gas fuel with nitrogen and by heating and diluting the ambient air with products of combustion.

Variables and Parameters: The variables that control the flame height Z_f for large buoyancy controlled diffusion flames stabilized on circular burners with horizontal surfaces include: the acceleration of gravity, g; the density, specific heat at constant pressure and specific heat ratios, and temperature of the ambient gas, $\rho_\infty, Cp_\infty, \gamma_\infty,$ *and* T_∞; and the corresponding values for the fuel at the source, subscript U_f, and the gas in the flame, subscript f. Other variables include: the total heat release rate of the fire, $\dot{Q}$, the loss from the fire due to radiation from soot, convective heat transfer to the burner, and etc., $\dot{Q}_{loss}$, and the net heating rate of the gas in the fire plume $\dot{Q}_c \equiv \left(\dot{Q} - \dot{Q}_{loss}\right)$ the heat added to the plume flow by the fire; the fuel velocity, U_f, at the surface of the burner or of a solid or liquid fuel; the chemical heat released by complete oxidation of the fuel per mass of fuel, ΔH_f, the stoichiometric fuel to air ratio, f_s, and the heat released per mass of air, $\Delta H_a \equiv f_s \Delta H_f$. Here the heating value for the fuel ΔH_f is defined as the heat release when a kilogram of the fuel is completely oxidized to carbon dioxide and water vapor in standard air.

However, important factors concerning combustion processes in turbulent diffusion flames, such as the turbulence intensity, the rate of fuel consumption per unit volume of the flame or the production and combustion of soot, are ignored and the influence of the various density ratios have not been considered as separate parameters.

These variables can be arranged in a number of dimensionless parameters, and the changes produced in these parameters during the experiments are discussed in detail in the paper. The parameters include:

$$\left(Q^*\right) \equiv \left(\frac{\dot{Q}}{\rho_\infty Cp_\infty T_\infty \sqrt{gD}\,D^2}\right),\quad H_f \equiv \left(\frac{\Delta H_f}{Cp_\infty T_\infty}\right),\quad H_a \equiv \left(\frac{f_s \Delta H_f}{Cp_\infty T_\infty}\right) \text{ and } X_L \equiv \left(1 - \frac{\dot{Q}_c}{\dot{Q}}\right).$$

Experiments: Two sets of experiments were carried out. In the first, the parameters were changed by diluting a fixed flow rate of natural gas fuel with up to five moles of nitrogen per mole of fuel and the effects on the flame height were determined for a fixed flow rate of the natural gas fuel. In the second set of experiments, the flame was contained within a hood and the ambient gas was produced by recirculation of a mixture of air diluted with the products of combustion of the flame. This arrangement allowed the ambient gas temperature to be increased to 400° K and the oxygen mole fraction to decrease to 10% to 12% system. In both experiments, flame heights were determined using the methodology discussed in Cetegen et al (1984) where about 50 flame heights were measured. In a typical set of experiments, the fuel flow rate was held fixed while the dilution was increased from zero to the flammability limit.

In both experiments, the flame height was almost constant and increased less than 10% as the dilution was increased from zero to the flammability limit. In both experiments, the radiant flux from the fires was decreased smoothly from about 30% to about 10% of the chemical heat release; soot production was reduced to

almost zero near the flammability limit. Part of the observed 10% increase in flame height was a result of the increase in the heating rate of the plume due to this reduction in radiation heat loss as the dilution was increased.

In the second set of experiments, an increase in ambient gas temperature from 320^{o} to 400^{o} K had no systematic effect on flame height.

Conclusions: These results were compared with the predictions of the model of Steward (1972), and correlations of Cetegen et al (1982), Zukoski et al (1984) and Heskestad (1996). The results show that the Q^* scaling proposed in Cetegen et al (1984) does a satisfactory job as a scaling parameter and suggests that $\dot{Q}_c$ rather than $\dot{Q}$ is the appropriate heat release parameter to use in Q^*. Froude number scaling is certainly inappropriate here, and the model of Steward and correlation of Heskestad that depend on the heating value parameters, H_f and H_a, predicted much larger changes than were observed in the experiments.

In summary, Q^* scaling, based on the convective heat release, is only weakly affected by either the dilution of the air or fuel, and is in reasonable agreement with the present results.

References

Cetegen, B. M., Zukoski, E. E. and Kubota, T., (1984) "Entrainment in the Near and Far Field of Fire Plumes," *Comb. Sci. & Tech.*, 39, pp 305-331.

Heskestad, Gunnar (1981) "Peak Velocities and Flame Heights of Buoyancy-Controlled Turbulent Diffusion Flames," *Eighteenth Sym. (Int.) on Comb.*, The Comb. Institute, pp 951-960.

Steward, F. R. (1970) "Prediction of the Height of Turbulent Diffusion Flames," *Comb. Sci and Tech.*, 2, pp 203-212.

Zukoski, E. E., Kubota, T. and Cetegen, B. (1984), "Visible Structure of Buoyant Diffusion Flames," Twentieth Symp. (Int.) on Comb., The Comb. Institute, pp 361-366.

Acknowledgment

Much of the work discussed here was supported by grants from the Building and Fire Research Laboratory, NIST, the Department of Commerce, under the guidance of Dr. Len Cooper and Dr. Walter Jones of the Building and Fire Research Laboratories of NIST.

VISIBLE AND CHEMICAL FLAME LENGTHS OF ACETYLENE/AIR JET DIFFUSION

Wade, R. W. and Gore, J. P.
School of Mechanical Engineering
Purdue University
West Lafayette, IN 47907-1288

Introduction

The lengths of turbulent diffusion flames have been widely studied experimentally and theoretically. Flame lengths are typically defined in terms of the mean temperature, chemical composition or luminosity along the axis. For many flames, the interchangeable use of the different definitions, that frequently occurs in the literature, may cause qualitative and quantitative discrepancies amongst data and confusion regarding the importance of different physical processes. There are several existing models for flame length correlations [1-6]. The significant assumption in most of the flame length correlation is that the visible flame length is proportional to local chemical state. One complication that these existing models do not address is that of soot. If a large fraction of the fuel mass is converted to soot, then the visible flame length would be determined by radiation emitted by the hot soot particles. The radiation transferred from the hot soot particles to the surroundings lowers that temperature of the soot and flame gas mixtures making the flame non-luminous. Gore et al. [7] have shown that the peak temperature along the centerline occurs much closer to the injector exit in strongly radiating flames than in weakly radiating flames. Therefore, the definition of flame length based on this visible luminosity is inconsistent. Based on the above, the objective of the present work was to obtain flame lengths based on measurements of axial gas species concentrations.

Experimental Methods

The visible and chemical flame heights for acetylene/air diffusion flames ranging from 1 to 40 kW issuing from three burner diameters were measured during this study. Visible flame length (H_f) was measured by averaging 40 video frames obtained using a CCD camera, with a shutter time of 1 ms. A neutral density filter was placed in front of the camera to avoid pixel blazing. The axial concentrations of the major gas species within the flames were measured using a water cooled stainless steel probe and gas chromatography. The chemical flame length ($H_{f,c}$) was taken as the axial location at which X_{fuel} drops to 0.0005 [1], which is the lower detection limit of the instrument.

Results and discussion

The lower flow rate acetylene/air diffusion flames stabilized on the burner exit, while the higher flow rate flames were lifted from the burner. The visible flame length increased monotonically with increasing heat release rate. At low heat release rates, significant amounts of dark soot leave the cooler orange tip of the flames. As the heat release rate increases, large amounts of soot continue to exit the tip of the flame but the center of the flame becomes very bright, indicating high temperatures. When the flames are lifted, the whole length appears bright white and virtually no dark soot is visible above the flame. Similar behavior is observed for all three burner diameters, with the transitions described above occur at relatively low heat release rates for the lower diameter burners. The variation in visible flame length discussed above for a gaseous flame suggests that soot formation and radiation phenomena affect the visible flame length of both types of flames. The chemical flame length remains almost constant when compared to the visible flame length. No discontinuity occurs in the visible or the chemical flame length across the transition from attached to lifted flames. Differences in visible and chemical flame lengths are most pronounced at high heat release rates on the 2.1 mm diameter burner where $H_{f,v}$ is more than one and a half times $H_{f,c}$. For lower flow rates on the 4.8 mm burner, $H_{f,c}$ is longer than $H_{f,v}$ which may be attributed to the use of the neutral density filter. In all cases, the visible flame length data in this study were shorter than those predicted by the correlations in the literature [2,4,6]. This can be attributed to the use of a neutral density filter over the video camera lens which blocks out the less luminous flame tip.

Becker and Liang [2] obtained their correlations as curve fits for methane, ethane, and propane visible flame lengths. Acetylene flame length data obtained by Becker and Liang [2] themselves show that momentum dominated flames follow their stabilized flame correlation. As the flames become more buoyant, they become shorter than those predicted by the correlation. The visible flame length data from this study are similar to those of Ref [2], and both are overestimated by the correlations. The visible and chemical flame lengths from the present study are plotted according to the correlation by Delichatsios [4] in fig. 1. The acetylene flames tested in the present study are all in the "purely momentum turbulent" regime according to the classification given by Delichatsios [4]. The data fall into regions of both momentum and buoyancy control, as shown in fig. 1. Delichatsios predicts a smooth transition between the two regimes, but $H_{f,v}$ is qualitatively similar to the buoyancy dominated prediction at all fire Froude numbers. The chemical composition based flame length is not similar to the correlation in the buoyancy regime but qualitatively similar to the trend in the momentum controlled

regime. However, there is a factor of two difference between the momentum dominated limiting values measured in the present work and those predicted by Delichatsios [4].

The most recent dimensional analysis of turbulent jet flames is given by Blake and McDonald [5,6] and the resulting correlations are plotted in fig. 2 with the present data. The data for visible flame length are in qualitative agreement with the buoyancy dominated correlation. The correlation also classifies all of the present flames as buoyancy dominated. However, the present chemical composition based flame length data show that most of the present flame lengths are almost constant or increase very slowly with increases in Froude number, even in this buoyancy regime. The correlations were developed with the fundamentals of turbulent mixing and reaction but were calibrated using visible flame length data. However, for the present acetylene flames the correlations do not even qualitatively predict the chemical composition based flame length. The differences between $H_{f,v}$ and $H_{f,c}$ are attributed to the sooting characteristics of acetylene. Soot causes the bright yellow color in the flame, reduces the amount of fuel that reacts to form gaseous products, and cools the flame radiatively, which reduces the length for which the soot is visible. Transport of high temperature and high concentration soot further along the axis causes the visible flame length to increase. Visible flame length correlations for luminous flames should include soot chemistry and radiative cooling considerations.

Conclusions

This investigation shows that visible flame length and chemical flame length are not the same and do not follow the same scaling with flowrate in acetylene flames. The use of general non-dimensional flame correlations to predict the chemical behavior of highly sooting flames could be hampered without this understanding of the difference between chemical length and visible length. Flame length would be further clarified by more investigation into soot transport and chemistry.

Acknowledgments

This work was supported by the National Institute of Standards and Technology, Building and Fire Research Laboratory under Grant No. 60NANB1D1172 with Dr. D. D. Evans serving as NIST Scientific Officer.

References

1. Hawthorne, W. R., Weddell, D. S., and Hottel, H. C., *Third Symposium on combustion and Flame and Explosion Phenomena*, Williams and Wilkins, Baltimore, 1949, pp. 266-288.
2. Becker, H. A. and Liang, D., *Combust. Flame* 32:115-123 (1978).
3. Becker, H. A. and Yamazaki, S., *Combust. Flame*, 33: 123-150 (1978).
4. Delichatsios, M. A., *Combust. Flame*, 92:349-364 (1993).
5. Blake, T. R. and McDonald, M., *Combust. Flame* 94: 426-432 (1993).
6. Blake, T. R. and McDonald, M., *Combust. Flame* 101: 175-184 (1995).
7. Gore, J. P., Ip, U.-S., and Sivathanu, Y. R., *Journal of Heat Transfer*, 114:487-493 (1992).

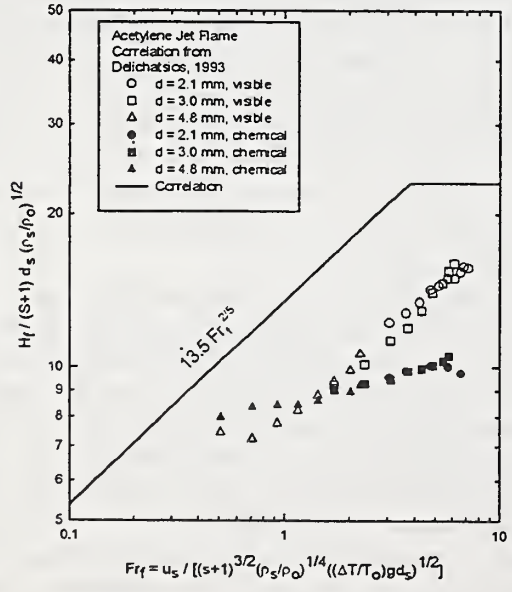

Figure 1. Jet Flame Correlation from Delichatsios [4].

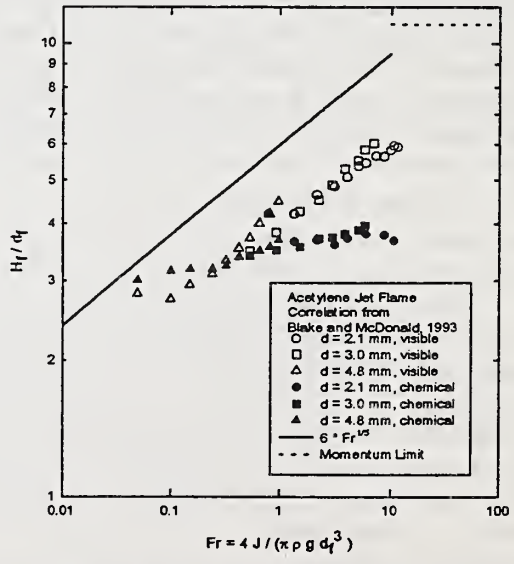

Figure 2. Jet Flame Correlation from Blake and McDonald [6].

A NEW RISK ASSESSMENT METHOD FOR EVALUATING ALTERNATIVE FIRE SUPPRESSION AGENTS

Robert Zalosh
Center for Firesafety Studies
Worcester Polytechnic Institute
Worcester, MA 01609

The development of new fire suppression systems has created a need for criteria that will facilitate the evaluation of these new systems in comparison to traditional systems. Fire suppression system evaluation criteria are developed in this paper from a risk analysis perspective that combines historic incident data with new fire test data and with considerations of the toxicity of the suppression agent, its decomposition products, and combustion products of the fire itself.

The various probabilistic measures of suppression system performance to be considered are: 1) expected times-to-fire-suppression, 2) probabilities of re-ignition, 3) the expected numbers of injuries and fatalities associated with their operation (including inadvertent operation); and 4) expected maximum fire size before the fire is suppressed or controlled. Each of these measures needs to account for the various fire scenarios and for personnel exposure scenarios applicable to the facility in question.

If we denote the time-to-fire-suppression as t_s, time from ignition to the actuation of the suppression system as t_{do}, and the time to suppression from initiation of system discharge as t', then

$$t_s = t_{d0} + t' \qquad (1)$$

All three variable in Eqn 1 are treated as random variables with probability distributions to be determined from historic and/or test data and analysis. For example, t_{do} can be determined from historic data in the case of manually actuated suppression systems, from calculations in the case of thermally actuated systems (for which numerous computer models are available), or from test data in the case of smoke and other nonthermal detectors. Values for t' are most readily obtained from fire tests using the different suppression systems accounting for the pertinent engineering design parameters such as agent concentration or density, ceiling height or enclosure volume, fire size and perhaps oxygen concentration at system actuation. Of course, some of these parameters are dependent on t_{d0}. Results can be compared in terms of the mean (expected) value; $E(t_s)$, i.e.

$$E(t_s) = E(t_{d0}) + E(t') \qquad (2)$$

which is valid whether or not t_{d0} and t' are independent.

The probability of re-ignition, $p_{re\text{-}ig}$, after the fire is temporarily suppressed is a particular concern in the case of special suppression systems such as gaseous agents and aqueous foams. It can be determined either by

extensive fire testing for new suppression systems, or by historical loss data for existing suppression systems and fire scenarios. It, too, is often a function of t_{d0}, and the oxygen and agent concentrations.

The expected numbers of injuries and fatalities is perhaps the most difficult challenge in this approach. However, it is a challenge requiring pursuit for suppression systems that create a personnel hazard during discharge (e.g. carbon dioxide systems and the newly developed pyrogenic propellant suppression systems) or as a result of the agent decomposition products formed during chemical suppression (e.g. fluorinated gseous agents). The expected number of fatalitites, N_{fi}, occurring during either a discharge for a toxic agent or following a suppressed fire for an agent that forms toxic decomposition products, can be written as

$$N_{fi} = n_i \, p_f(D_i) \qquad (3)$$

where n_i is the number of people being exposed to the toxic gas in scenario i, p is the probability of a fatality given the exposure dosage D_i, defined as

$$D_i = \int_{t_{d0}}^{t_{fi}} c_i \, dt \qquad (4)$$

and c_i is the toxic gas concentration history in scenario i.

If f_i is the frequncy of incidents of type i per facility-year, and if calculations are performed for various scenarios, comparisons between alternative suppression systems can be made in the form of plots of f_i versus N_{fi}. A frequency versus fatality curve can, in principle, also be conducted for the baseline case of no suppression system. In the baseline case, the fatalities would be due either to carbon monoxide or lethal temperatures or heat fluxes generated in the fire. Correlations of p_f versus D for carbon monoxide, hydrogen fluoride, and other gases are available, for example, in reference 1, which describes the use of toxic gas and fire/explosion incident risk assessments in the chemical industry.

A progress report on the implementation of this methodology for the case of shipboard machinery space fires was presented recently [2], and an update will be presented in this paper. The alternative suppression agents being considered in this application are carbon dioxide (currently used in commercial ship engine rooms), Halon 1301, FM-200™, PFC-410™, FE-13™, and representative water mist systems.

1. Guidelines for Chemical Process Quantitative Risk Assessment, AIChE Center for Chemical Process Safety, 1989.

2. Zalosh, R., "Risk Analysis Evaluation of Alternative Fire Suppression Agents for Machinery Space Fires," Fire Risk and Hazard Assessment Symposium, National Fire Protection Research Foundation, San Francisco, June 26-28, 1996.

This work has been sponsored by the U.S. Coast Guard under Delivery Order 7 of contract DTCG39-92-D-E38K37.

Halon Alternatives Testing in Combat Vehicle Engine Compartments

John F. McFassel, U.S. Army Aberdeen Test Center, Aberdeen Proving Ground, MD, USA

Terrance J. Treanor, U.S. Army Aberdeen Test Center, Aberdeen Proving Ground, MD, USA

Historically fire suppression testing and live fire vulnerability testing for the Army has been conducted by the U.S. Army Aberdeen Test Center (ATC), at Aberdeen Proving Ground, MD. This testing ensures the safety and reliability of equipment being issued to DOD personnel. These tests have often shown the need for vehicle redesign to enhance crew survivability. An area of special emphasis has been assessing the reliability and performance of Automatic Fire Extinguishing Systems (AFES). AFES tests may be conducted on an entire system or on single components such as a sensor.

Halon 1301 has been the fire suppression agent of choice because of its ability to effectively control fires at concentrations which will not adversely impact the crew. Therefore, it is widely used in occupied spaces of combat vehicles, watercraft, and aircraft. Halon 1301 is also used because of its excellent handling qualities over a broad range of conditions and its ease of distribution. These same characteristics have caused Halon to be used in a variety of civilian applications such as computer room asset protection and civil aviation. Unfortunately recent scientific studies have linked the release of Halon 1301 with depletion of the stratospheric ozone layer. The U.S. Army Acquisition Pollution Prevention Support Office (AAPPSO) is seeking alternatives for all Ozone Depleting Chemicals currently used by the Army. The Program Manager for Armored Systems Integration (PM-ASI) in cooperation with the Tank-Automotive Research Development and Engineering Center (TARDEC) is overseeing the Halon replacement program for ground combat vehicles.

Typically fire suppression testing has been divided into two separate types: those fires which occur during peacetime and those which result from perforations by overmatching threat munitions during time of war. Fires occur in one of two distinct areas of the vehicle, the crew compartment and the engine compartment. This separation is made because peacetime fires usually occur in the engine compartment as a result of electrical shorts or fuel line rupture and crew compartment fires usually result from perforating impacts during combat. Halon 1301 is currently used in the engine and crew compartment AFES as well as hand held fire extinguishers (HHFE).

TARDEC has requested that ATC conduct a series of test programs demonstrating the performance of Halon 1301 replacements in the engine and crew compartments of ground combat vehicles as well as HHFE. The engine compartment program has been going on much longer due to the fact that the Army has designated only the crew compartment as a mission critical use for

Halon 1301. Therefore there is a more pressing need to find an alternative agent for the engine compartment.

This engine compartment test program is to be conducted in four major phases. Phases I and II were conducted by ATC in two modified M60 tank fixtures over a two year period. Phase I testing was conducted using a non-operational power pack and Phase II was conducted using an operational power pack. Fourteen potential replacement agents were studied in Phase I, while only four candidates proceeded to Phase II. The objective of these phases was to screen potential Halon 1301 replacement agents quickly and economically. Tests were conducted using bilge and simulated fuel spray fires with and without airflow. The result of these phases was a narrowing of the potential field of alternate agents down to two candidates: FM-200 and a dry chemical system.

Phase III testing consists of refining the alternate agent delivery system for individual vehicles using the two replacement agents still under consideration. Separate test programs are being set up by the individual vehicle program managers. The first two vehicles, the M1 Abrams Main Battle Tank and the M2 Bradley Infantry Fighting Vehicle, are currently undergoing testing. The end result of Phase III will be a decision on which of the two agents still under consideration to use.

Once a single agent is chosen, a limited ballistic validation test will be conducted at ATC. In this phase of testing, actual anti-tank weapons will be fired to impact the fuel tanks of operational M60 and M1A1 Main Battle Tanks. All of the tests conducted in the previous phases used peacetime fire scenarios. The results of this testing will indicate whether agent delivery systems intended to suppress non-ballistically initiated fires will be effective against the types of fires expected to be encountered in combat.

Testing on replacement agents has proceeded rapidly and economically while allowing for maximum participation by all potential solutions. The Army has a milestone decision date for acquisition of new agents and agent delivery systems for the affected vehicle systems in Fiscal Year 97.

Annual Conference on Fire Research
Gaithersburg, MD, October 28-31, 1996

Flammable Liquid Storeroom Halon Replacement Testing

Alexander Maranghides,[a, b] Ronald S. Sheinson,[b] Bruce H. Black[a]

NAVAL RESEARCH LABORATORY
Navy Technology Center for Safety and Survivability
Combustion Dynamics Section, Code 6185, Washington, DC 20375-5342, USA
(1-202) 404-8101, Fax (1-202) 767-1716
E-mail: maranghi@ccfsun.nrl.navy.mil; sheinson@ccfsun.nrl.navy.mil

The United States Navy is investigating fixed fire extinguishing systems for future use in shipboard Flammable Liquid Storerooms (FLSRs) where halon 1301 total flooding systems have been used. The test program aimed at determining the halon replacement agent of choice for shipboard FLSRs will be conducted at the Naval Research Laboratory's (NRL's) Chesapeake Bay Detachment (CBD) in two test compartments. Phase 1 tests will be conducted in a 28 m^3 (1,000 ft^3) test compartment. This test bed will be applicable to many smaller shipboard compartments. Phase 2 tests will use a 280 m^3 (10,000 ft^3) compartment, a representative size for large shipboard FLSRs.

The purpose of this paper presentation is to address the design of the Phase 1 test compartment. Phase 1 tests will serve as a learning process for designing and executing larger scale FLSR tests. The prime objectives of Phase 1 testing are:
- identify the halon replacement agent of choice and its optimum design concentration;
- determine the optimum post fire suppression hold time (time prior to venting) and reentry time;
- evaluate the option of using the Water Spray Cooling System (WSCS), an NRL innovation.

The WSCS is designed to reduce compartment temperature and acid decomposition products as well as to enhance reignition protection and expedite compartment reclamation.

WSCS results from real scale halon replacement testing aboard the *ex*-USS SHADWELL demonstrated that the Water Spray Cooling System is a viable option for rapid reduction of compartment temperature and reduction of acids generated during suppression as well as subsequent acid removal.[1] In the 370 m^3 (13,000 ft^3) test compartment, the low pressure WSCS tested provided very rapid compartment temperature reduction in 15 seconds with less than 20 gallons of water. The ability of the WSCS to run off the ship's firemain or from its own pressurized water tank make it a viable option for rapid post incident compartment reentry by the fire fighting party.

After intermediate and initial full scale testing, NRL proposed heptafluoropropane, HFP, (HFC-227ea, C_3F_7H, manufactured by Great Lakes Chemical Corporation as FM-200) as the

---

Supported by the U.S. Naval Sea Systems Command
a. GEO-CENTERS, Inc. Fort Washington, MD.
b. Authors to whom correspondence should be addressed.

clean agent of choice for U.S. Navy shipboard machinery spaces where the primary fire threat is pressurized flammable liquids.[2] FLSR Phase 1 testing will be performed primarily with HFP, with limited baseline comparison tests with Halon 1301. Other alternative and replacement technologies will also be evaluated.

This paper presentation will address the layout and instrumentation particulars of FLSR Phase 1 test compartment. Suppression agent discharge system and Water Spray Cooling System layout and instrumentation particulars will be addressed. This paper will also cover fuel selection and use, fire scenario particulars including compartment ventilation shutdown and preburn time selection, test running procedures, and the test matrix for Phase 1.

References:

1. A. Maranghides, R. S. Sheinson, B. H. Black, M. Peatross, and W.D. Smith, "The Effects of a Water Spray Cooling System (WSCS) on Real Scale Halon 1301 Replacement Testing and Post Fire Compartment Reclamation," Proceedings of the Halon Options Technical Working Conference, May 7-9, 1996, Albuquerque, NM, pp. 435-446.

2. Sheinson, R. S., Maranghides, A., Friderichs, T., Black, B. H., Smith, W., and Peatross, M.,"Recommendations for the LPD-17 Main and Auxiliary Machinery Rooms Total Flooding Fire Suppression Systems," NRL Letter Report 6180/0193.1, 24 July 1995.

The Products of Thermal Decomposition in Intermediate Scale Testing

Mark Driscoll
Chemical Engineer
Paul Rivers, P.E.
Sr. Fire Protection Engineer
St. Paul, MN USA

Previous experimentation, Brockway et al(1994), indicate a point of "diminishing returns" in both the extinguishment time and acid gas levels produced for intermediate scale(1.28 m^3) tests employing a single Class B fuel(n-heptane). It was concluded that concentrations on the order of 140% of the cup burner extinguishing concentrations were necessary for optimum extinguishment performance (shortest extinguishment time and lowest hydrofluoric acid(HF) levels) and that concentration up to 160% of the cup burner extinguishing concentration resulted in no significant reduction to extinguishment time or peak HF levels. Discharge times were maintained at "approximately" ten seconds for all discharge scenarios. Phase I experimentation was performed, for a single Class B fuel(n-heptane) and single fire scenario(3.7 kW), to investigate the effects of increased agent concentration to 200% of the cup burner value. FC-3-1-10(CEA-410) was the only agent included for this study. Data was used to verify if in fact there is a point of "diminishing returns" and/or an optimum design concentration. Discharge times, extinguishment times, and HF levels were utilized to illustrate that similar performance was attainable at 120% of the cup burner extinguishing concentration as that gained at 200% of the cup burner value.

The second phase of this study investigated the effects of extinguishment time on HF levels for intermediate scale(1.28 m^3) testing employing a single Class B fuel(heptane) and multiple fire scenarios(0.1, 0.6, 1.7, and 3.7 kw). Two discharge scenarios, 9.50 and 3.25 seconds, at a single agent design concentration, were utilized to illustrate that reductions in peak HF levels ranging from 50 to 83% were possible for the various fire scenarios.

Phase III of this study incorporated data from two previous studies, Ferreira et al(1992) and Brockway et al(1994), to illustrate trends concerning peak HF levels vs.

extinguishment time and peak HF levels vs. energy density(kW/m^3). A correlation for "anticipated" HF levels was extrapolated as a possible tool for designers in evaluating the feasibility of CEA-410 for the protection of Class B commodity. The validity of this correlation was investigated for three previous studies; small scale(0.20 m^3), intermediate scale(56.0 m^3), and full scale(526 m^3), respectively.

All experimentation(Phase I, Phase II, and Phase III) was performed in a 1.28 m^3(45 ft^3) enclosure, referred to as the "box". The box was constructed of polycarbonate sheeting and reinforced with angle iron and has two ports which provided access to its interior. The enclosure was fitted with a ventilation system, to provide preburn and post burn purging of the volume, and discharge system consisting of an agent cylinder, piping, and interchangeable discharge nozzles. The weight of agent required to achieve a given enclosure concentration was calculated employing equation (1) of NFPA 2001 "Standard on Clean Agent Fire Extinguishing Systems -1996 ed." Cylinders were super pressurized with nitrogen to 360 psig to ensure complete agent discharge and homogeneity within the enclosure. A data acquisition system was included to monitor nozzle pressure, agent cylinder pressure, and enclosure pressure. Four stainless steel pans of dimensions 1.9 cm x 1.9 cm (0.75" x 0.75"), 4.5 cm x 4.5 cm(1.75" x 1.75"), 7.0 cm x 7.0 cm(2.75" x 2.75"), and 9.5 cm x 9.5 cm(3.75" x 3.75"), were used for the four test fires. Pans were calibrated with n-heptane and a cone calorimeter and found to have heat release rates of 0.1 kW, 0.6 kW, 1.7 kW, and 3.7 kW, respectively, following a one minute preburn. Pans were given a one minute preburn prior to discharge of the agent. All experiments were documented with a video camera and used to determine pan extinguishment times to within one tenth of a second. Products of decomposition were gained at flame extinguishment, following a thirty second mix period, with the use of "grab" gas sampling tubes. Previously employed "wet chemistry" techniques, found to be within $\pm$10% accuracy, were then followed to determine the actual acid gas(HF) concentrations of the test enclosure in parts per million(PPM) by volume. This method provided a single HF data point per experiment, considered to be the peak level. A 0.20 m x 0.31 m x 0.31 m(8" x 12" x 12") steel baffle was employed to shield the pans and mitigate against "flame blow off" during agent discharge.

Clean Extinguishing Agents and Continuously Energized Circuits

Mark Driscoll
Chemical Engineer
Paul Rivers, P.E.
Sr. Fire Protection Engineer
St. Paul, MN USA

Recent testing performed through the Modular Protection Group indicates that even low energy, 48 W and 192 W, Class C fire scenarios require elevated clean agent concentrations for proper mitigation of the hazard(flame extinguishment and inertion). Agents included for that study are recognized by the NFPA 2001 standard as follows: FC-3-1-10(CEA-410), HFC-227ea(FM-200), HFC-23(FE-13), IG-541(INERGEN). Phase I of this study extended that investigation to increased energy levels (up to 1200 W) for the halocarbon agents(not including INERGEN). It was suspect that a point of decreased performance would be reached at which time the agent concentrations may become excessive(above the LOAEL). Acid gas(HF) production was quantified to illustrate whether adverse effects to sensitive equipment located within the protected enclosure should be expected.

The purpose of this testing is to demonstrate the performance capabilities of various clean agents on continuously energized fuel/energy scenarios. A sample consisted of a polymethylmethacrylate cylinder wrapped with resistance wire(nichrome). Energy levels to 1200 W were tested for this series. Performance was evaluated concerning the following issues: concentrations required for a thirty(30) minute flame inertion and levels of acid gas(HF) produced during the inertion period. Inadequate agent performance was defined as satisfying either of the following criteria:

1.) Agent concentrations required for thirty(30) minute flame inertion, at a given energy level, compare to or exceed the agents listed LOAEL, as defined per NFPA 2001,

2.) Levels of HF generated, at a given power level, compare to or exceed the minimum levels to cause adverse effects to "sensitive" equipment. Reference was made to previous studies concerning the required levels of acid gas(HF) and the minimum exposure times necessary to cause adverse effects to such equipment.

Agent concentrations were elevated, at a given energy level, until reignition of the sample did not occur within thirty(30) minutes of agent discharge. Agent discharge times were maintained at or below limits set by NFPA 2001. Tests were conducted per agent at increasingly intense energy levels(300 W, 600 W, 900 W, and 1200 W).

Phase II encompassed a modification to the cup burner apparatus included in NFPA 2001 "Standard on Clean Agent Fire Extinguishing Systems - 1996 ed.". Two outputs from a 1.2 kW DC power supply were fixed to the top of the burner and a length

of nichrome resistance wire was employed to complete the circuit. Two digital meters were incorporated within the circuit to monitor amperage and voltage. Circuit current was maintained to within $\pm$0.01 of an ampere. The data illustrated the effects of electrical energy inputted to the system. Three agents; FC-3-1-10(CEA-410), HFC-227ea(FM-200), and HFC-23(FE-13), were tested at four wire temperatures, 0°C(0°F), 427°C(800°F), 649°C(1200°F), and 871°C(1600°F) to gain trends concerning energized fire hazards. N-heptane was employed as the fuel. The performance of the agents was discussed on a relative basis.

A third phase(Phase III) of experimentation was conducted to quantify the effects of wire temperature, wire surface area, agent concentration, and hold times on the products of thermal decomposition in a continuously energized scenario. Hydrofluoric gas generation rates are expected to increase with increases in; wire surface temperature, wire surface area, or agent concentration, for a given halocarbon agent discharge scenario. Correlations concerning HF generation rates were extracted from the data sets to provide additional tools for the designers of halocarbon fire suppression systems protecting continuously energized facilities.

The objective of this test series was to investigate the effects of wire surface temperature and wire surface area on acid gas production. There was no fuel source included for these experiments. Instead, various lengths and gauges of resistance wire(nichrome) were suspended within a test enclosure in a complete circuit. The circuits were energized, allowed to reach the steady state temperature, and the agent discharged. Following discharge, acid gas levels, agent concentration, and circuit amperage were continuously monitored via an FTIR analyzer and amperage ,meter, respectively. Sampling continued for the fifteen(15) minute period following agent discharge. Trends were discussed on a relative basis, and correlations, concerning wire temperature/surface area, were extracted from the various data sets.

Phase I and Phase III experimentation was performed in a 1.28 m^3(45 ft^3) enclosure, referred to as the "box". The box was constructed of polycarbonate sheeting and reinforced with angle iron and has two ports which provided access to its interior. The enclosure was fitted with a ventilation system, to provide preburn and post burn purging of the volume, and discharge system consisting of an agent cylinder, piping, and interchangeable discharge nozzles. The weight of agent required to achieve a given enclosure concentration was calculated employing equation (1) of NFPA 2001 "Standard on Clean Agent Fire Extinguishing Systems -1996 ed." Cylinders were super pressurized with nitrogen to 360 psig to ensure complete agent discharge and homogeneity within the enclosure. A data acquisition system was included to monitor nozzle pressure, agent cylinder pressure, and enclosure pressure. Circuits were energized with a 1.2 kW DC power supply. Data acquisition was performed via Labtech Notebook version 7.3.0W software for DOS.

Flame Suppression Properties of HFC-227ea: Fundamental Studies and Suppression of Real-World Class A Hazards

Mark L. Robin, Ph.D.
Fluorine Chemicals Department
Great Lakes Chemical Corporation

ABSTRACT

During the past several decades the use of the highly efficient, clean, nontoxic fire suppression agent Halon 1301 in total flooding applications has prevented the loss of human life, and billions of dollars worth of equipment worldwide are protected by Halon 1301. However, due to its implication in the destruction of stratospheric ozone, the production of Halon 1301 was halted on January 1, 1994. As a result, intensive research efforts have been undertaken in the industrial, academic and governmental sectors with the goal of developing a replacement for Halon 1301.

One of the more widely investigated Halon 1301 replacements is HFC-227ea (CF_3CHFCF_3, FM-200®). HFC-227ea is an active fire suppressant, providing extinguishment of flames through a combination of physical and chemical mechanisms. The physical contribution to flame suppression stems mainly from the heat absorbing ability of the agent, which results in a lowering of the flame temperature and a slowing of the radical chain reactions occurring in the flame. HFC-227ea also acts chemically by removing key chemical species involved in the flame chain reactions, breaking the chain reactions responsible for flame propagation.

While numerous halon replacements have been proposed, and limited testing of some of these agents on Class B fires has been reported, very little information is available addressing the performance of these agents on those hazards most commonly protected by gaseous suppression systems, i.e., Class A materials such as those found in electronic data processing (EDP) and telecommunication facilities. We describe here the results of small and field-scale testing of HFC-227ea for the suppression of flames of Class A hazards.

The suppression of flames of typical Class A materials with HFC-227ea was investigated in two enclosures, the smaller enclosure having a total volume of 14.5 m^3, and the larger enclosure of a total volume 72.6 m^3. Each of the enclosures was fully instrumented to allow the monitoring of enclosure temperatures and pressures, agent concentration and combustion and decomposition product concentrations. Rectangular slabs of typically encountered Class A materials, vertically mounted within a metal cabinet, were ignited via an electrical resistance coil, allowed a predetermined preburn period, and extinguished with HFC-227ea. The test configuration was designed so as to produce a high degree of baffling of the flame, in order to

remove any aerodynamic contributions to flame extinguishment (i.e., "blowing out" of the flame). Materials investigated included slabs of PMMA (black and clear), polypropylene, polyethylene (low and high density), PVC and ABS; the suppression of pine crib fires was also investigated. The results of this investigation indicate that the extinguishment of typically encountered Class A materials occurs at concentrations of less than 5.8% v/v HFC-227ea.

The ultimate purpose of conducting fire suppression tests should be to ascertain whether the system design will perform as intended under the assumed challenge. In order to design meaningful large-scale fire tests, it is necessary to understand the fundamentals of fire growth and fire suppression systems, and to understand the nature of the particular real-world hazard being protected. When developing a fire test protocol it is important to have the fire occur in a way which is as realistic as possible based upon the worst-case scenario envisioned for a particular hazard. Failure to fully consider any special hazards can lead to underdesign of the suppression system, resulting in inadequate protection. Similarly, testing under conditions so far removed from the realistic worst-case that the occurrence of such conditions is of zero probability leads to unnecessary overdesign of the suppression system, and the accompanying waste of relatively expensive suppression agent.

The objectives of the second phase of this study were to quantify the amount of decomposition products formed under conditions typical of those encountered in EDP industry applications, and to assess the damage potential for electronics exposed to the post-suppression environment. Suppression testing of HFC-227ea on realistic Class A fires was conducted in the large test enclosure. For this series of tests, the enclosure was equipped with an ionization detector located 4.3 m from the fire location. The hazards investigated included fires involving PVC cables, printed circuit boards, waste paper and magnetic tape. Fire sizes ranged from approximately 4 to 35 kW at detection plus 30 seconds (following detection, a 30 second delay was allowed before commencement of agent discharge). The results of this second phase of testing will be discussed in detail.

COMPUTATIONS OF INHIBITION EFFECTIVENESS OF HALOGENATED COMPOUNDS IN PREMIXED FLAMES

V. Babushok*, T. Noto^, A. Hamins^, and W. Tsang*
* Chemical Science and Technology Laboratory, NIST
^ Building and Fire Research Laboratory, NIST

The burning velocity, S_u, is an important parameter which characterizes the inhibition efficiency of halogen-containing additives employed as flame retardants. The burning velocity decreases with increasing inhibitor concentration. Rosser et al. [1] studied experimentally the inhibition effect of different additives on methane flames and found that the burning velocity decreased linearly with increasing additive concentration for concentrations less than 0.5 % by volume. In addition, Rosser et al. [1] used the parameter Φ ($=dS_u/dC_{in}$) as a measure of inhibition efficiency. Based on the linear dependence of S_u on additive concentration, Fristrom and Sawyer [2] suggested using a dimensionless inhibition parameter Φ_{FS} for evaluation of the inhibitive efficiency of additives:

$$\Phi_{FS} = [(S_0-S_u) \cdot C_{O2}] / [S_0 \cdot C_{in}] \qquad (1)$$

where, S_0 and S_u are the burning velocities for CH_4-air flames without and with additives, respectively, C_{in} is the additive mole fraction, C_{O2} is the initial concentration of oxygen in the mixture. Fristrom and Van Tiggelen [3] suggested that the parameter Φ_{FS} could be written as the sum of the inhibition indices ϕ_i for each atom constituting the additive molecule:

$$\Phi_{FS} = n_H\phi_H + n_C\phi_C + \sum n_x\phi_x \qquad (2)$$

Here, the subscript x indicates a halogen atom. The assumption of a linear dependence of the burning velocity on inhibitor concentration is, however, not consistent with other studies. Parks et al. [4] showed that for CF_3Br addition over a wide range of additive concentrations and mixture compositions, the flame speed of premixed methane-air and propane-air flames decreased exponentially.

In this study, flame structures were computed for stoichiometric laminar flames burning mixtures of air with methane, ethylene, ethane, and methanol at atmospheric pressure and an initial temperature of 298 K. From these computations the burning velocity was determined. The following halogenated retardants were considered: CF_3H, C_2HF_5, C_2F_6, CF_4, CF_3Br and CF_3I. The PREMIX code was employed [5] with the data base for the C/H/O system based on existing kinetic models. A comprehensive set of elementary reactions for fluorine-containing C_1-C_2 species and the kinetic sub-models for bromine and iodine containing species were the same as that in our earlier work.

Calculations showed that for the halogenated additives CF_3Br, CF_3I, CF_3H, C_2HF_5, C_2F_6 and CF_4, the burning velocity of C_1 - C_2 hydrocarbons decreased exponentially with increasing additive concentration over a wide range of additive concentrations consistent with experimental results. The inhibition parameter Φ proposed by Fristrom and Sawyer [2] indicating inhibition efficiency was modified to the expression:

$$\Phi=(C_{O2}/C_{in}) \cdot \ln(S_0/S_u) \qquad (3)$$

which accounts for the nonlinear dependence of burning velocity over a wide range of additive concentrations. The inhibition indices for halogen atoms and groups were obtained for stoichiometric premixed C_1 - C_2 hydrocarbon-air flames. Calculations showed that increasing agent concentration leads to saturation of chemical effects. Subsequent additive action is due to physical influences including heat capacity and dilution effects.

Scavenging of chain carriers by a flame inhibitor is controlled by the reactions which regenerate the scavenging agent and due to the concentration of a chemically active inhibitor [6]. The superior efficiency of CF_3Br and CF_3I as flame inhibitors, as compared to CF_4 and other fluorinated hydrocarbons, is due to the regeneration cycle associated with HBr and HI, respectively. It is possible to define a regeneration coefficient which indicates the effective number of catalytic cycles involving the inhibitor during the combustion process. The regeneration coefficient (RC) is determined by the ratio of the total concentration of scavenging agent (HBr, HI) consumed (or produced) to the initial concentration of this species which formed the agent:

$$RC = [HBr]_{total} / [CF_3Br]_{initial} \quad (4)$$

The total HBr consumed is determined by integration of the rate of reactions in which HBr is consumed in extent to maximum of H atom concentration. Calculations showed that the regeneration coefficient varied from seven to five as the CF_3Br concentration in stoichiometric CH_4/air flames varied from 0.5 to 4 percent by volume. The regeneration coefficient for HI was approximately four.

References

1. Rosser, W. A., Wise, H., and Miller, J., *Seventh Symposium (International) on Combustion*, Butterworths, London, 1959, p.175.
2. Fristrom, R. M., and Sawyer, R. F., *AGARD Conference Proceedings*, 84:12-1 (1971).
3. Fristrom, R. M., and Van Tiggelen, P. J., *Seventeenth Symposium (International) on Combustion*, The Combustion Institute, Pittsburgh, 1979, p.773.
4. Parks, D. J., Alvares, N. J., and Beason, D. G., *Fire Safety J., 2*, 237, (1979/1980).
5. Kee, R. J., Grcar, J.F., Smooke, M.D., and Miller, J. A., Sandia National Laboratories Report, SAND 85-8240, 1985.
6. Dixon-Lewis, G. and Simpson, R.J., *Sixteenth Symposium (International) on Combustion*, The Combustion Institute, Pittsburgh, 1976, pp.1111-1119.

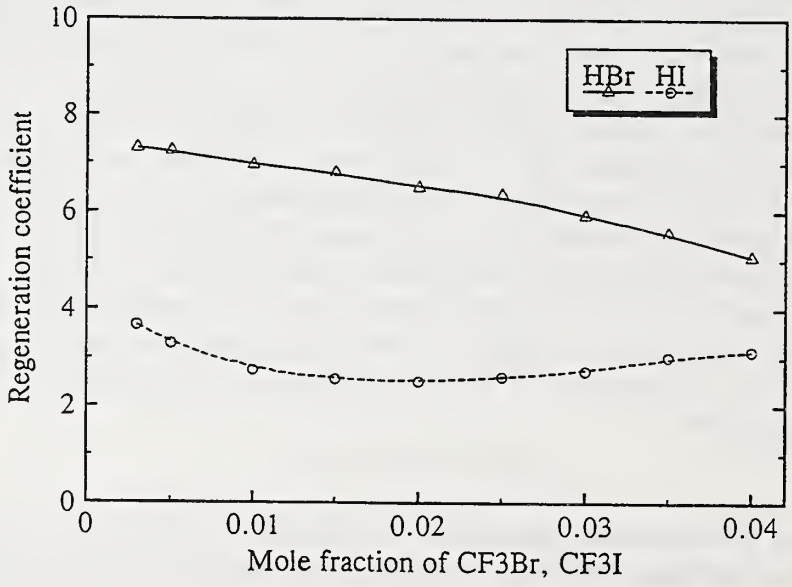

Figure 1. Regeneration coefficients of HBr and HI as a function of CF_3Br and CF_3I mole fraction in stoichiometric CH_4/air flames.

Structure of Low Pressure Premixed Methane Flames Inhibited with CHF_3 and C_3HF_7*

Drew M. L'Espérance,† Bradley A. Williams, James W. Fleming, and Ronald S. Sheinson
Navy Technology Center for Safety and Survivability
Code 6185, Chemistry Division
Naval Research Laboratory
Washington, D.C., 20375-5342

We have studied changes in flame structure of low pressure premixed methane/oxygen flames as they are inhibited by the fluorinated halon replacement agents CHF_3 and C_3HF_7 (HFC-227ea). We have measured temperature and intermediate species profiles in both inhibited and uninhibited flames. In the case of CHF_3, the measurements on flame structure are compared to calculations performed with the Sandia PREMIX code, using the kinetic mechanism recently developed at NIST for the combustion of C_1 and C_2 fluorocarbons. A primary purpose in conducting these studies is to provide experimental data for validation of these kinetic models, since comparatively few studies of the detailed flame structure of these systems have been performed to date, and many important reactions have not been thoroughly studied experimentally.

Experiments were performed using a McKenna burner 6 cm in diameter operated with a premixed flame of methane and oxygen having an equivalence ratio of unity. The flame pressure was maintained at 10 Torr, and a co-flow of argon having an identical mass flux surrounded the premixed gases. To this base flame were added two fluorinated suppression agents: CHF_3 and C_3HF_7. Heptafluoropropane was added in quantities up to 4% of the total flow rate of methane and oxygen (in four increments), while trifluoromethane was added up to 8.8% of the total. The relative proportions of the two dopants were chosen to achieve equal loadings of F atoms. The addition of the two agents made the overall flame stoichiometry slightly fuel rich, raising ϕ to 1.07 in the case of CHF_3, and 1.09 for C_3HF_7.

Temperature profiles of both the inhibited and uninhibited flames were recorded using a type R (Pt. vs. Pt/13% Rh) thermocouple, having a wire diameter of 0.08 mm. The thermocouples were coated with alumina to avoid catalytic activity in the flame zone. The ceramic coating was reasonably stable in the fluorinated environment, surviving for several hours without noticeable decomposition. A radiation correction was determined by making comparisons with a reference flame whose temperature has been previously measured by LIF of OH. The magnitude of the correction was approximately 300K at the peak temperature region of the uninhibited flame.

Profiles of intermediate species were recorded using laser-induced fluorescence. An excimer-pumped dye laser was used to excite fluorescence, which was collected at right angles by a photomultiplier using appropriate bandpass filters. Background flame emission was also collected in the same way. Irises on the incoming laser beam and at the focal point of the collection optics gave a spatial resolution of 0.5-1 mm.

---

*This work was supported by the Naval Sea Systems Command, Code 03V2

†National Research Council Postdoctoral Associate

As the agents were added, the methane/oxygen flame became noticeably more luminous and the emission zone moved further from the burner, from about 8.5 mm in height in the uninhibited flame, to about 10.5 mm when either 8.8% CHF_3 or 4% C_3HF_7 was added. The increase in standoff distance with the addition of the agents is consistent with the expected decrease in flame speed. The amount of flame emission from both CH (recorded at 430 nm) and C_2 (recorded at 516 nm) increased by a factor of seven when 4% C_3HF_7 was added. Addition of 8.8% CHF_3 produced about half as much CH emission as 4% C_3HF_7. These observations indicate that the fluorine chemistry has a substantial effect on the reactions leading to chemi-luminescence.

Compared to the uninhibited flame, the temperature profiles of the inhibited flames have a slower rise above the burner surface, but reach a peak temperature some 100K higher. Temperature profiles of the two inhibited flames are almost identical. Since the relative loadings of the two agents were chosen to provide equal numbers of fluorine atoms, this close coincidence of the temperature profiles indicates that, for agents with a high fluorine/hydrogen ratio, the inhibition depends primarily on the number of fluorine atoms added to the flame, rather than on the structure of the agent or the initial reaction pathways.

We are currently studying LIF profiles of several species, fluorine-containing as well as those present in the uninhibited flame. The profiles of these intermediates gives a further indication of flame structure. The profile of the CH radical, for instance, moves about 3 mm further from the burner as C_3HF_7 is added up to a mole fraction of 4%. Unlike the emission from excited state CH, which increases dramatically as the agents are added, the ground state CH concentration only increases by about 20% upon the addition of 4% C_3HF_7.

To interpret the flame studies, we have performed flame structure calculations using the fluorocarbon reaction mechanism recently developed at NIST. The reaction set as it currently exists includes all fluorinated methane derivatives, but not any C_3 species such as heptafluoropropane. The calculation was performed using the measured temperature profile. The predicted location of the ground state CH peak is at 13 mm above the burner, about 4 mm higher than the location experimentally observed. In the uninhibited flame, the predicted and observed locations of the CH peak lie within 1 mm of each other. This predicted change in flame standoff distance is primarily a result of the fluorocarbon kinetics, not the altered temperature profile. Performing a calculation on the uninhibited flame, but using the temperature profile of the inhibited flame, shifts the CH location by less than 1 mm.

This disagreement in the profiles of the inhibited flame indicates that the mechanism significantly overpredicts the effect of CHF_3 on the flame speed, at least under the the current conditions of pressure and composition. Among the possible causes for the discrepancy is the behavior of COF_2, which is a relatively stable species predicted to slowly react with H atoms to form HF. Since HF formation is primarily responsible for the reduction in the number of atomic hydrogen when the agent is added, a slower removal rate for COF_2 would mean that fewer H atoms could be removed, and thus the flame speed would not be reduced as significantly. The removal reactions of COF_2 are not well investigated experimentally, and so the behavior of this species in these flames may allow the kinetics to be optimized to better predict the observed behavior of these agents.

AEROSOL AND SPGG TECHNOLOGY FIRE SUPPRESSION SCREENING METHODS

W.L. Grosshandler, J.C. Yang, and T.G. Cleary

National Institute of Standards and Technology
Gaithersburg, Maryland 20899 U.S.A.

The search for alternatives to halons for fire suppression applications has identified not only new compounds which have physical properties similar to the bromochlorofluorocarbon family, but also inert gaseous agents that are released from a solid state and condensed phase agents that may be misted or generated pyrotechnically. Industry is already investigating innovative ways that these multiple technologies can be blended or hybridized to create an optimum fire fighting agent/release mechanism for specific applications. The traditional cup burner method is unable to evaluate these not-in-kind replacement systems. Two new concepts for testing liquid aerosol and solid propellant gas generator (SPGG) fire suppression technologies are presented here. (See also ref. 1.)

The first concept is for a bench-scale suppression screen suitable to compare the ability of dispersed fluids with differing chemical and physical properties to extinguish a propane flame in a counter-flow burner based upon the design by Tsuji and Yamaoka[2]. The porous fuel tube ($\approx$ 25 mm dia.) is placed across a uniform air stream as show in Figure 1. The advantages of this arrangement are that (1) the flame is laminar, two-dimensional, and very stable in the forward stagnation region; (2) the flow field of the flame is simple, thus allowing the evaluation and modeling of experimental results; (3) the flame can be controlled quite easily over a wide range of fuel and oxidizer velocities; (4) the flame extinction limit can be observed with little ambiguity and good reproducibility; (5) the flame front can be easily accessed by intrusive or non-intrusive probing techniques, thus enabling detailed studies of flame structure; and (6) the burner has been used for powder inhibitors with very encouraging results[3].

Two different methods of generating aerosols are envisioned. For 25 μm to 250 μm diameter particles, a multiple orifice piezoelectric droplet generator[4,5] will be used. The aerosol literature will be scanned to identify candidate techniques for generating droplets in the 0.25 to 25 μm range. Aqueous and fluorocarbon aerosols can be introduced directly into the burner air stream. However, no existing technique may be suitable for some fluids such as slurries, emulsions, or chemically-generated aerosols. A separate aerosol chamber will be needed in those cases into which high concentrations of agent can be injected using whatever technique envisioned in practice. The size distribution, number density and other characteristic of the aerosol may not be independently controllable, but if the aerosol is stable in time (over at least tens of seconds), critical properties can be measured. The aerosol will be transported from the generating chamber to the burner where it can be metered into the air stream. Aerosol uniformity measurements will be made within the burner using either a PDPA or stroboscopic micro-photography, and the air and fuel flows will be precisely monitored to ensure the above effects can be separated from the physical/chemical effects of the different aerosols.

The second concept is for a facility to test SPGG-based agents and release mechanisms. Potential fire environments can be broken into forced flows and otherwise quiescent situations. In the forced flow scenario, the flow assists in the mixing and transport of agent to the fire location, but it also carries the agent away from the fire. In the quiescent environment, the mixing and transport of the agent to the fire zone depends almost entirely on the momentum of the effluent with obstacles and wall boundaries impacting the flow. Two facets separate typical SPGGs from the "clean agents" addressed in NFPA 2001[6]: the elevated temperature and the composition of the effluent. In addition, hybrids could contain solid or liquid particulates. These factors pose problems regarding the use either of the cup-burner or of an explosion flask for obtaining inerting concentration. If the only application of the SPGG or hybrid system were a quiescent total flooding scenario, a suitable test fixture could be a fire established in a small enclosure, blocked from direct impact of the discharge. Scaling based on the volume of the enclosure would provide the design criterion. However, applications such as engine nacelle protection where an air flow is always present are quite different. There is no accepted NFPA test for evaluating agent effectiveness for a fire established in a forced flow. The NIST turbulent spray burner and the Walter Kidde Aerospace baffle stabilized pool fire configuration (both described in ref. 7) are forced flow apparatuses that do provide measures of effectiveness. With these systems, the effects of flow velocity, agent concentration, and discharge duration can be explored. Of these two facilities, the baffle-stabilized pool fire is

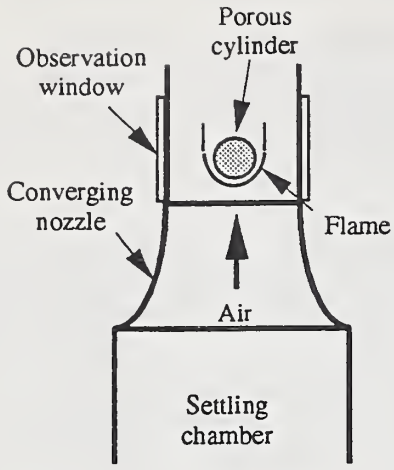

Figure 1. Schematic of Tsuji burner for aerosol suppressant screen.

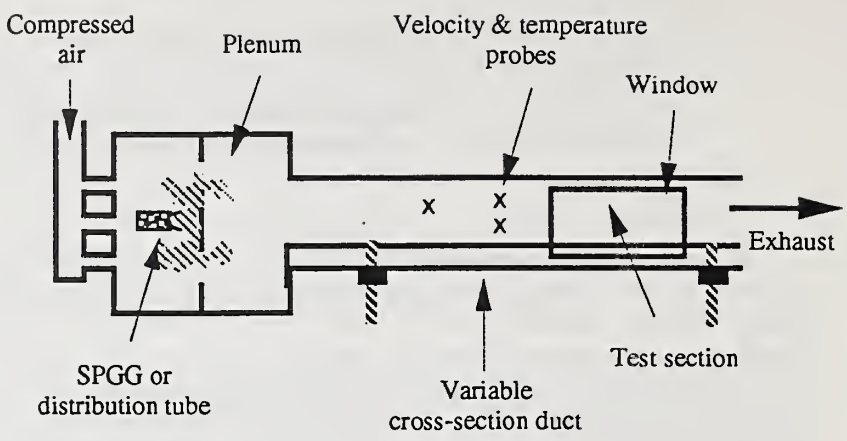

Figure 2. Schematic of SPGG suppressant screen.

more attractive because it appears to be more difficult to extinguish. The mixing time scale is longer and the minimum agent concentration is higher than for the turbulent spray flame.

A wind tunnel configuration is proposed to provide the forced flow and to facilitate the mixing of the SPGG discharge. Figure 2 is a schematic. The SPGG is discharged into a plenum and mixed with incoming air. The air will be provided from a compressed air bottle farm, or compressor at sufficient delivery pressure so that the SPGG discharge, itself, does not effect the air flow. From the plenum, the flow then moves into a duct that holds the test section. The duct will have a movable floor to control the cross sectional area which will readily change the flow velocity at the test section for a given volumetric flow. Temperature and axial velocity measurements will be made at a number of locations in the duct. The duct will have windows at the test section location for visible observation of flame extinction. The baffle-stabilized pool fire will follow the design of Hirst and Sutton[8] with some modifications. The flame is stabilized by the recirculation zone in the wake of a rearward facing step, 5 mm to 25 mm high. The pool, imbedded in an airfoil with an elliptical nose that extends the width of the duct (about 300 mm), will consist of a flat sintered metal burner about 120 mm on a side with gaseous propane fed at a specified rate. The test fixture will be put through a series of tests with inert compressed gases (such as nitrogen) with tighter flow control to probe sensitivities to the operating parameters such as fire scenario (including fuel and step height), velocity, duct cross-section, inert concentration and discharge duration. The results will be used to characterize the dynamics of the recirculation/fire zone in terms of a characteristic mixing time for flame extinction, as discussed by Hamins *et al.*[7]

Evaluations of SPGGs for directed discharge applications (as opposed to total flooding) must proceed on an *ad hoc* basis. The nature of the effluent flow is as important (or more so) than the chemical constituents. Proper discharge nozzle design, which depends on the application, in addition to sufficient agent mass flow are required for such cases. The test fixture proposed here will still be valuable in screening particular formulations for their efficacy once they reach the fire zone.

[1] Grosshandler, W., Yang, J., and Cleary, T., "Screening Methods for New Fire Suppression Technologies," *1996 Int'l Conf. on Ozone Protection Technology, Proceedings,* Washington, DC, October 21-23

[2] Tsuji, H. and Yamaoka, I., *Eleventh Symposium (International) on Combustion*, pp. 979-984, The Combustion Institute, Pittsburgh, 1967

[3] Milne, T.A., Green, C.L., and Benson, D.K., *Combust. Flame*, **15**, 255-264 (1970)

[4] Ashgriz, N. and Yao, S.C., *Rev. Sci. Instrum.*, **58** (7), 1291-1296 (1987)

[5] Dressler, J.L., U.S. Patent No. 5,248,087, 28 September, 1993

[6] National Fire Codes, *NFPA 2001 Standard on Clean Agent Fire Extinguishing Systems*, Nat'l Fire Protection Assoc., Quincy, MA, 1996

[7] Hamins, A., Cleary, T., Borthwick, P., Gorchkov, N., McGrattan, K., Forney, G., Grosshandler, W., Presser, C., and Melton, L., "Suppression of Engine Nacelle Fires," chap. 9 in *Fire Suppression System Performance of Alternative Agents in Aircraft Engine and Dry Bay Laboratory Simulations*, NIST SP 890: Vol. II, Gann, R.G. (ed.), U.S. Department of Commerce, Washington, D.C., November 1995

[8] Hirst, R. and Sutton, D., *Combust. Flame*, **5**, 319-330 (1961)

Fire Suppression Using Solid Propellant Gas Generator Technology

Gary F. Holland, Lyle D. Galbraith
Olin Aerospace Company

Solid propellant gas generator (SPGG) technology has recently evolved to become an effective, environmentally benign alternative to Halon 1301 in fire suppression applications. In one aspect of the SPGG approach, a solid propellant mixture of fuel + oxidizer is combusted to produce large volumes of a mixture of inert gases (nitrogen, carbon dioxide and water vapor – N_2, CO_2 and H_2O). This mixture of gases creates an oxygen-deficient environment which no longer supports combustion and rapidly suppresses various fire scenarios. The primary mechanism of effectiveness for this SPGG approach appears to be a combination of flame detachment that arises from the rapid generation of large volumes of gas, plus creation of an environment which is too depleted in oxygen to support hydrocarbon combustion. This rapidly evolving field has been the topic of a recent NIST workshop(1).

Some of the earliest solid propellant/fire suppression-type technology was discussed by Filter et al in 1976(2). Later, Reed et al. described a family of propellant formulations which combusted flamelessly to yield large amounts of nitrogen gas(3). More recently, several other solid propellant formulations have been described in the patent and technical literature(4, 5). The concepts described by Galbraith et al. include stoichiometrically-balanced formulations which yield large amounts of nitrogen gas together with CO_2 and water vapor(4). Suitable concentrations of the exhaust can be directed into a fire zone to effect fire suppression.

Flow rates and chemical reaction times can be addressed for solid propellants by controlling the propellant combustion process. Two important considerations in optimizing a system for fire suppression are the rate of agent delivery and the total time over which the agent is delivered. The rate of combustion for a given propellant is a function of pressure and is described by

$$\text{rate} = A * P^n$$

where the exponent n is characteristic of the propellant's pressure sensitivity. The rate of mass generation during propellant combustion, dm_{gen}/dt, is given by

$$dm_{gen}/dt = \rho_P * A_b * r,$$

where ρ_P = propellant density, A_b = burning surface area and r = rate of combustion. Larger propellant loads, with their larger mass and larger surface area, require a longer time for complete combustion. Therefore, the rate of agent generation and the total delivery time are controlled via the combustion pressure and the burning surface area.

Solid propellants provide a means for circumventing the high-pressure bottle penalty of stored gases with efficient high-density storage of N_2, CO_2 and H_2O in vessels at ambient pressures. One suitable solid propellant formulation is based upon sodium azide, NaN_3. Mixtures of NaN_3 with iron oxide, Fe_2O_3 upon combustion yield nearly pure nitrogen gas. Since N_2 is an effective physically-acting fire suppressant, typical critical concentrations are readily obtained by extrapolation from, e.g. cup burner studies. One challenge in using azide-based SPGG's is the toxicity associated with azide materials.

Another suitable solid propellant formulation avoids the toxicological shortcomings of azides, relying instead on the combustion of an energetic fuel (e.g. 5-amino-tetrazole) with an inorganic oxidizer (e.g. strontium nitrate):

$$5AT + Sr(NO_3)_2 \longrightarrow N_2 + CO_2 + H_2O + SrO.$$

Since the rate of agent generation is important, the rate of propellant combustion can be moderated with combustion modifiers such as magnesium carbonate, $MgCO_3$, which absorbs heat and decomposes to form CO_2:

$$MgCO_3 \longrightarrow CO_2 + MgO.$$

Through careful control of the propellant combustion rate, the solid residue (e.g. SrO, MgO) from propellant combustion can be restricted to the combustion reactor rather than exhausting into the protection volume.

The SPGG technologies described above can be competitive with Halon systems, particularly if their distribution in the volume-of choice is well understood. To this end, we have obtained temporally- and spatially-resolved analysis of CO_2 and O_2 concentration levels over the course of a fire suppression test event. CO_2 sensing is accomplished using optical detection of its IR absorption. Oxygen detection utilizes a zirconia electrochemical sensor similar to those used in automobile combustion manifolds. Measurements in highly turbulent conditions correlate well with cup burner measurements and indicate that when oxygen concentrations are reduced by approximately 25%, suppression is typically effective.

Besides dilution of oxygen concentration, another means for extending the chemical reaction time in a combustion zone is to reduce the frequency of effective chain propagating steps in the combustion process. The chemical activity of Halon-1301 falls under this category, where thermal dissociation of CF_3Br leads to formation of combustion-radical trapping bromine radicals, $Br^{\bullet}$. There is considerable evidence in the literature that powders and dusts also exhibit some amount of chemical reactivity and can be particularly effective in the extinction and suppression of fires. Furthermore, particle size was shown to be a significant factor in powder effectiveness, with the work of Ewing et al.(6), indicating that many powders exhibit a plateau of high reactivity for powders smaller than $< 20 - 50\ \mu m$

Solid propellant gas generator technology provides an ideal platform for the creation and distribution of reactive powders, droplets and dusts. Since solid propellants typically react in a controlled but rapid fashion at very high temperatures, condensed byproducts from their combustion reaction tend to be of small particle size. The composition and particle size distribution of these aerosols can be controlled by taking advantage of propellant composition and reaction rate. These factors can be controlled both chemically and through proper design of the generator hardware. OAC has examined this capability of chemically reactive fire suppression agents via solid propellant processes.

OAC has demonstrated the effectiveness of SPGG fire suppression technology in aircraft engine nacelles (F-18 E/F), drybays (F-18 E/F, V-22)(7) and ground vehicle engine compartments. This presentation will review and discuss the concepts of solid propellants for fire suppression applications, as well as our findings regarding their distribution and effectiveness.

This work has been sponsored by Olin Corporation, Olin Aerospace Company, the U.S. Navy (Mr. James Homan), U.S. Air Force (Mr. Mike Bennett), and the U.S. Army/TACOM (Mr. Steve McCormick).

References

1. J. C. Yang, W. L. Grosshandler, Eds., *Solid Propellant Gas Generators: Proceedings of the 1995 Workshop* (NIST, Gaithersburg, MD, 1995).
2. H. E. Filter, D. L. Stevens, U.S. Patent No. 3,972,820, 1976.
3. R. Reed, M. L. Chan, K. L. Moore, U.S. Patent No. 4,601,344, 1986.
4. L. D. Galbraith, G. F. Holland, D. R. Poole, R. M. Mitchell, U.S. Patent No. 5,423,384, 1995.
5. D. Guesto-barnak, et al., Fire Test Results for Solid Propellant Inert Gas Generators in the Walter-Kidde Aerospace Dry Bay Simulator, Halon Options Technical Working Conference Albuquerque, NM, 1996), pp. 75-87.
6. C. T. Ewing, F. R. Faith, J. B. Romans, J. T. Hughes, *J. of Fire Prot. Engr.* 4, 35-52 (1992).
7. P. Proctor, "Aviation Week & Space Technology," March 6, 1995, p. 47.

Submitted for presentation at the NIST Annual Conference on Fire Research, Gaithersburg, MD, October 1996

Extinguishment of a Diffusion Flame over a PMMA Cylinder by Depressurization in Low-gravity

Jeffrey S. Goldmeer [1*], David L. Urban[2], and James S. T'ien[1]
1. Case Western Reserve University
2. NASA Lewis Research Center

The behavior of flames in low-speed flows in low-gravity is relevant to spacecraft fire safety (Friedman and Sacksteder, 1988). Previous work (Yang, 1995; Ferkul and T'ien, 1994; Olson et al., 1988) has shown that flames in the presence of low-speed flows in low-gravity may be more flammable than in the same flow in normal gravity. Additionally, fire suppression plans for the International Space Station includes the use of venting (depressurization) as an emergency option for extinguishing fires. This procedure would induce flows in the affected compartment that could temporarily intensify the fire, as was observed in flammability tests of solids conducted on board Skylab (Kimzey, 1986). Despite a general understanding, current knowledge of the effects of reduced pressure and forced flow on a burning solid in low-gravity is inadequate for the design of a venting extinguishment system. In the current work, the extinction of a diffusion flame burning over horizontal PMMA (Polymethyl Methacrylate) cylinders during depressurization was examined experimentally and via numerical simulations.

The experiments were conducted on board the NASA Lewis Research Center's reduced-gravity aircraft that provide twenty second periods of low-gravity (±0.01 g's). The PMMA cylinders were 1.9 cm in diameter and 2.5 cm in length. The experiments examined the low-pressure extinction limit in air as a function of pressure and solid-phase centerline temperature at a constant velocity of ten cm/s. Both quenching and blow-off extinction were observed. Quenching occurred with a centerline temperature below 320 K, and blow-off with a centerline temperature above 320 K. A flammability map was created using the experimental blow-off data (Figure 1). As the solid-phase centerline temperature increases, the extinction pressure decreases, and with a centerline temperature of 525 K, the flame is sustained to a pressure of 0.1 atm before extinguishing.

The numerical simulation used in this work iteratively couples a two-dimensional quasi-steady gas-phase model (Yang, 1995) with a transient solid-phase model that includes conductive heat transfer within the solid and surface regression due to vaporization (Goldmeer, 1996). The gas-phase model includes Navier-Stokes, continuity, energy and species equations with a one-step overall chemical reaction and Arrhenius kinetics. The model uses an energy balance at the gas/solid phase interface that equates the energy conducted in the gas-phase to the gas/solid phase interface to the sum of the energy used for vaporization, surface radiation, and sensible heat within the solid. The model does not include gas-phase radiation. The ratio of the solid-phase and gas-phase conduction terms in the energy balance is defined as Φ, which can be written as:

$$\Phi = \lambda_S(\partial T/\partial r)_S / \lambda_G(\partial T/\partial r)_G = 1 - \left[(\dot{m}L + Q_{RAD})/\lambda_G(\partial T/\partial r)_G\right]$$

in which L is the heat of vaporization, $\dot{m}$ is the vaporization rate and Q_{RAD} is surface radiation. This ratio varies in time and along the circumference of the cylinder. High values of Φ (near 0.9) occur at ignition, and Φ decreases as the gas-phase heats the solid-phase.

Initial simulations examine conditions similar to the low-gravity experiments and predict low-pressure extinction limits consistent with the experimental limits (Figure 2). Additional simulations examine velocities ranging from one to twenty cm/s, increases in the solid-phase temperatures (decreases in Φ) prior to depressurization, and lower depressurization rates (longer depressurization times). The effect of velocity on the extinction limit is not monotonic (Figures 3 and 4). At values of constant Φ, flames are sustained to lower pressures at ten cm/s than at one or twenty cm/s. Increasing the solid-phase temperature (decreasing Φ) by either a longer period of burning prior to depressurization, or an increase in the depressurization time decreases the extinction pressure. The model predicts blow-off extinction at twenty cm/s and quenching at one cm/s (Figure 3). At velocities of five and ten cm/s, the simulations predict quenching will occur in cases with a cooler solid-phase (Φ at the forward stagnation point greater than 0.25), and blow-off when the solid-phase is heated (Φ at the forward stagnation point less than 0.25). Transition of the extinction mode from quenching to blow-off, as the solid-phase temperature increases (decrease in Φ) at a constant velocity, was also observed experimentally. Additionally, the simulations predict that the path taken to the extinction boundary is not critical; extinction will occur at the boundary whatever the path taken (assuming a quasi-steady gas-phase process). This information could be used to refine the International Space Station's venting specifications, which state that the affected module would be depressurized

* J. Goldmeer is currently a National Research Council Research Associate at the NASA Lewis Research Center.

from 1.0 atm to 0.3 atm within a period of ten minutes. This research suggests that an effective venting procedure would be to rapidly depressurize the affected module to a pressure of 0.1 atm, which would minimize additional heating of the solid-phase, minimize reductions in the extinction pressure, and most likely extinguish the fire.

Acknowledgments

This research was funded by the NASA Graduate Student Research Program and the Microgravity Combustion Branch at the NASA Lewis Research Center.

References

Ferkul, P., and T'ien, J., 1994, "A Model of Concurrent Flows Flame Spread Over a Thin Solid Fuel", Combustion Science and Technology, Vol. 99, pp. 345-370.

Friedman, R., and Sacksteder, K., 1988, "Fire Behavior and Risk Analysis in Spacecraft", NASA TM-100944.

Kimzey, J., 1986, "Skylab Experiment M-479: Zero-Gravity Flammability ", NASA JSC 22293.

Goldmeer, J.S.,1996, "Extinguishment of a Diffusion Flame over a PMMA Cylinder During Depressurization in Reduced-Gravity", Ph.D. Dissertation, Case Western Reserve University.

Olson et al., 1988, "Near-Limit Flame Spread Over a Thin Solid Fuel in Microgravity", Twenty-Second Symposium (International) on Combustion, The Combustion Institute, pp. 1213-1227.

Yang, C.T., 1995, "Numerical Simulation of the Combustion of a Solid Cylinder in Low Speed Flows", M.S. Thesis, Case Western Reserve University.

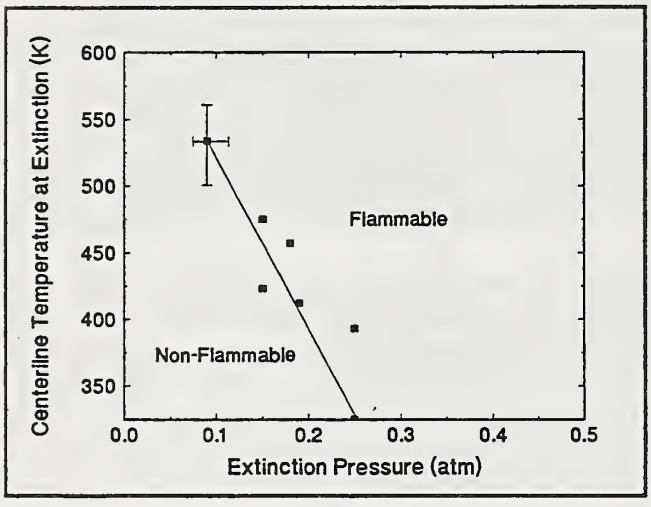

Figure 1
Experimental extinction boundary at constant velocity (10 cm/s)

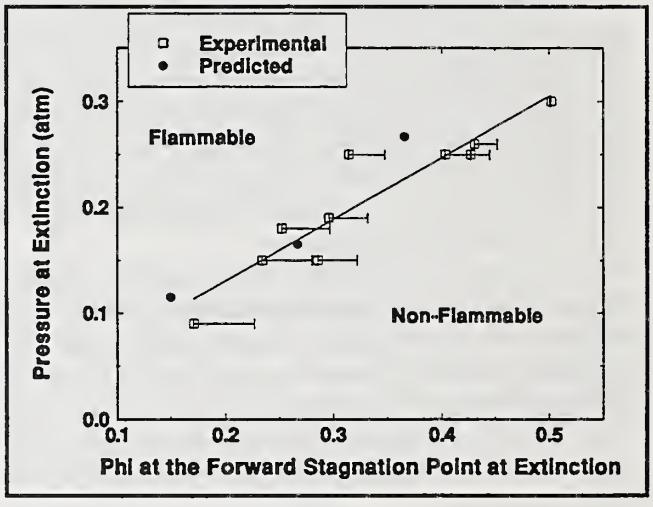

Figure 2
Comparison of Experimental and Predicted Extinction Boundaries at 10 cm/s

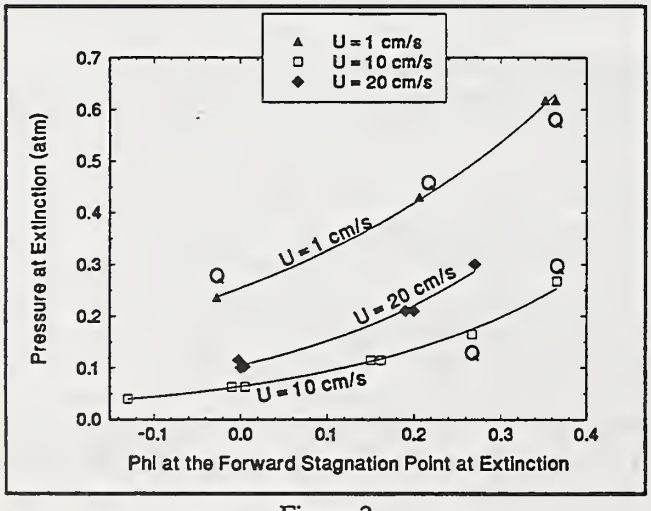

Figure 3
Predicted extinction boundaries at constant velocity (Quenching occurs at points labeled Q)

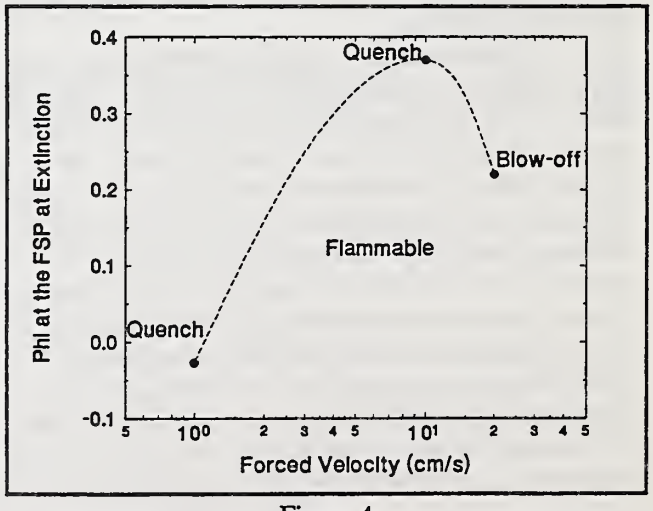

Figure 4
Predicted extinction boundary at constant pressure (P = 0.25 atm)

Smoke Plume Trajectory over Two-Dimensional Terrain

K.B. McGrattan, J. Trelles, H.R, Baum, and R.G. Rehm
National Institute of Standards and Technology, Gaithersburg, Maryland, USA

Under the sponsorship of the US Minerals Management Service and the Alaska Department of Environmental Conservation, the National Institute of Standards and Technology has conducted a series of large outdoor burns of crude oil on water to assess the feasibility of using *in situ* burning as an oil spill remediation tool. In conjunction with these experiments, a numerical (ALOFT - A Large Outdoor Fire plume Trajectory) model has been developed to predict the downwind concentration of smoke particulate and other combustion products.[1] The numerical model has been carefully compared with results from field experiments, and the results are very favorable.[2]

The range of validity of the original model was from a few fire bed diameters downwind to roughly 20 kilometers downwind of the burn, and it was limited to flat terrain. The model has now been extended to cover the burning region and to include terrain effects to the far field. The burn region is resolved with a modified version of the authors' compartment fire model[3] which is a low Mach number, high resolution Navier-Stokes solver. The results of the burn region simulation are used to initialize the windblown model which predicts the rise and dispersion of the particulate matter over distances up to 20 km downwind.

Terrain effects are accounted for by computing the steady, inviscid flow over isolated two-dimensional obstacles in a stratified atmosphere. The formulation allows for a cross-wind that is determined by initial (upstream) conditions and the two-dimensional stratified flow field. Large circulation regions, known as rotors, can form above and in the lee of these ridges. Particulate tends to flow between the rotor and the terrain, dispersing in the lee of the obstacle. Three-dimensional terrain can be handled by a different, three-dimensional, time dependent finite difference model for a Boussinesq, stratified fluid. The downwind domain can be extended until the point is reached where enough dispersion has occurred so that there is no longer a significant health threat.

The ALOFT model has also been extended to accommodate multiple plumes. In the accompanying figure, 3 plumes with flow rates varying from 2.2 to 2.6 kg/s and heat release rates varying from 500 to 700 MW are convected in the first domain by a 6 m/s wind. The total flow rate is 7.2 kg/s and the net heat release rate is 1.8 GW. The atmosphere is linearly stratified at -5°C/km. 10,000 Lagrangian particles are used to track the particulate's path through the plumes. The two grayscale values shown are for 50 and 150 $\mu g/m^3$. Once the complex plume merging dynamics have subsided such that the plume's trajectory is governed by atmospheric forces (5 km in the example), the two-dimensional terrain model can be applied. For this example, the atmosphere contains two crosswind shear periods with extrema of -4 and 4 m/s. The initial crosswind is zero at the ground and above 3 km. The terrain is a 350 m high, bell-curve-shaped peak centered 2.5 km into the second domain with a base width of 3 km. The stronger wind fluctuations found over land disperse the plume more than out at sea. The crosswind further separates the particulate. The multiple plumes have a wider initial angle of separation than a single plume with a flow rae of 7.2 kg/s and a heat release rate of 1.8 GW. Efforts are underway to allow the 2-D terrain model to handle semi-infinite ridges, such as cliffs, which are characteristic of many seashores.

---

1. Baum, H.R., McGrattan, K.B., and Rehm, R.G., "Simulation of Smoke Plumes from Large Pool Fires" in *Twenty-fifth International Symposium on Combustion*, 1463 - 1469, 1995.
2. McGrattan, K.B., et al., "Smoke Trajectory from *In Situ* Burning of Crude Oil in Alaska: Field Experiments," NIST Internal Report No. NISTIR 5764, US Dept. of Commerce, Washington, DC, Nov., 1994.
3. Baum, H.R., McGrattan, K.B., and Rehm, R.G., "Large Eddy Simulations of Smoke Movements in Three Dimensions" in *Interflam '96*, 189 - 198, 1996.

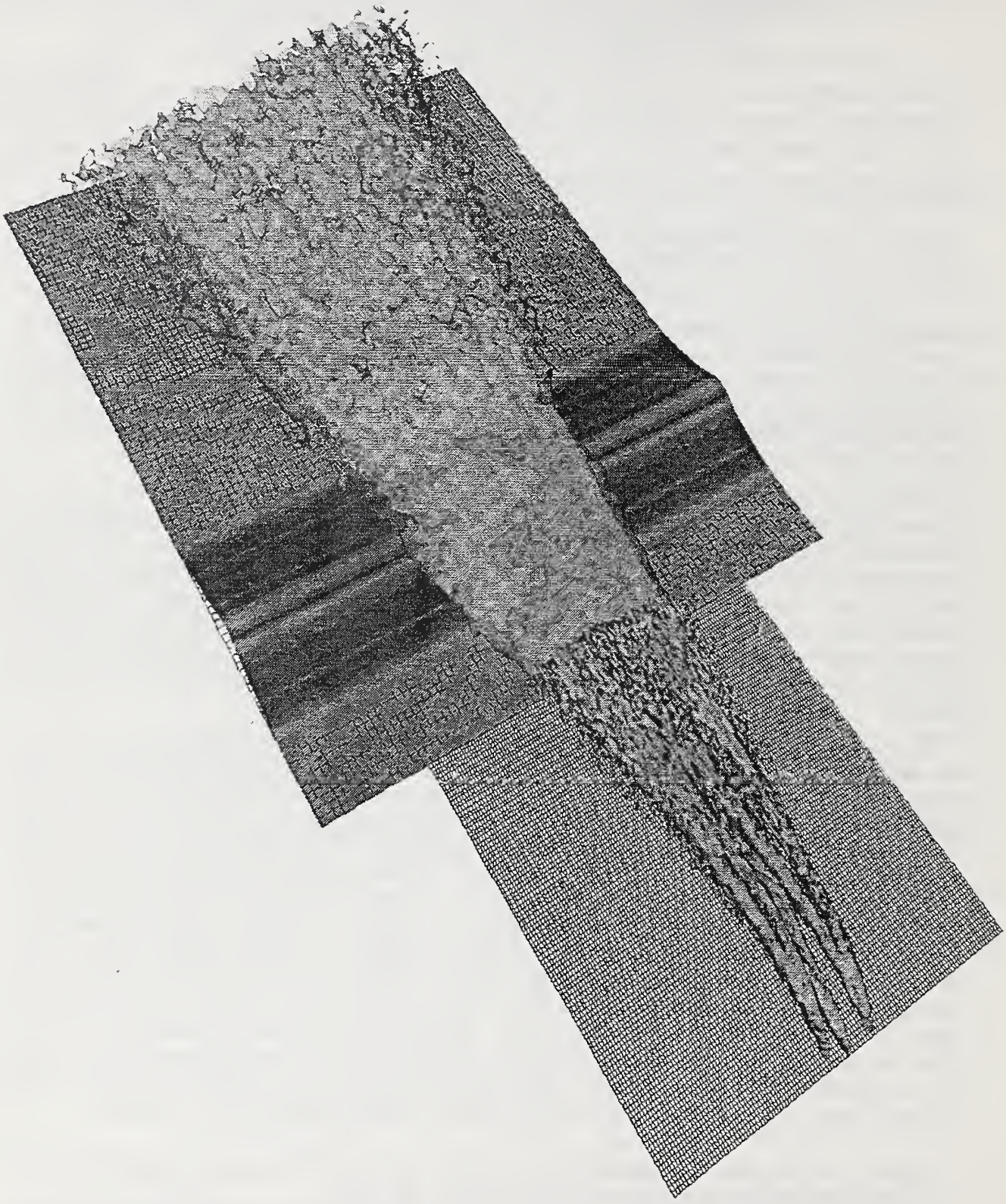

Figure 1: The cell dimensions are finer in the lofting than in the terrain transport domain. This resolution difference accounts for the change in isosurface appearance between the two regions.

Brand Lofting in Large Fire Plumes

J.P. Woycheese and P.J. Pagni
Mechanical Engineering Department, University of California, Berkeley, CA 94720-1740

Urban/wildland intermix conflagrations occur when dry vegetative fuels of the wild areas combine with structural fuels from houses to produce a combustible environment that, once ignited, easily becomes uncontrollable. The dominant mechanism for propagation of these fires is the copious fire brands these fuels produce. This research is a first step in the development of a modular model for fire growth in the urban/wildland intermix. The goal is to predict the area that is at risk from brand-induced fire spread during a large conflagration. Our work expands that performed by Tarifa, et al.[2,3], substituting a more realistic plume velocity field based on the Baum and McCaffrey plume model[4] for the constant plume velocity assumed there.

The problem of fire spread by brands consists of two major parts: lofting above and propagation downwind of the fire. The emphasis here is on lofting. The height to which a firebrand will ascend is a function of two forces: the drag induced by the gas velocity relative to the brand, and gravity. A preliminary assumption is that during the lofting process the brand does not change size, shape, or mass. This allows us to focus on the dynamics of the problem; e.g. finding the maximum height to which a firebrand will ascend before the drag and gravity forces balance, as well as calculate the particle velocity, with respect to ground, as a function of height. The latter is determined by numerical integration of the dimensionless vertical force balance on the particle.

$$V^* (dV^*/dz^*) = (3BC_d/4d^*)(U^*_{bm} - V^*)^2 - 1 \qquad (1)$$

where the symbols are defined in the notation and B is a weighted air-to-particle density ratio, $B = (\rho_a/\rho_s)(z_c U_c/\nu)$. C_d(Re) is given in Fig. 1 for spherical brands[5] in the range of Reynolds numbers relevant to fire plumes with $Re = d^*(U^* - V^*)$ since the normalizing diameter is defined as $d_c = \nu/U_c$. From Baum and McCaffrey [4], the dimensionless centerline plume velocity is

$$U^*_{bm} = \begin{cases} 2.13\, z^{*0.5} & z^* \le 1.32 \quad (2a) \\ 2.45 & 1.32 \le z^* \le 3.3 \quad (2b) \\ 3.64\, z^{*-0.33} & z^* \ge 3.3 \quad (2c) \end{cases}$$

This double-valued velocity, shown in Fig. 3, dictates the existence of both a maximum height to which a brand of a given dimensionless diameter can be lofted and a minimum height below which the plume velocity is not sufficient to lift the brand. At both of these extremes, the plume is moving past the brand at its terminal velocity (i.e., the brand velocity relative to the ground is zero). Setting $V^*=0$ and using Eq (2c) in Eq (1) gives $z^*_{max} = 31.3(BC_d/d^*)^{1.5}$. Similarly, using Eq (2a), we obtain $z^*_{min} = 0.294 d^*/BC_d$. These limits are shown in Fig. 2 as functions of dimensionless diameter and parameterized in B. The implication of Fig. 2 that the smallest brands achieve the greatest loft in the plume is misleading; the smallest brands will burn up before they reach z^*_{max}.

To determine the time each brand takes to reach its maximum height, we need to solve Eq (1) for $V^*(z^*)$, as shown by the solid lines in Figs. 3 and 4. Fig. 3 has been parameterized in d* for B=7600, typical of pine brands in a plume from a 50 MW house fire. Fig. 4 has d*= 5000 and a range of B that is pertinent to brands in urban/wildland intermix fires. The dotted lines in both figures indicate the local relative velocity past the brand, $U^*_{bm} - V^*$. The initial condition required by Eq (1) is $V^*(z^*_{min}) = 0$. From Figs. 3 or 4 the brand height can be easily found as a function of time. The next step is to introduce brand consumption as $d^*(t^*)$, e.g., from Tarifa's data[6]. The net effect will be to eliminate the smallest diameters in Fig. 2 and to produce an extremum in z^*_{max} near d^* of order one.

Notation

d^*	dimensionless brand diameter, $d/(\nu/U_c)$	z^*	dimensionless brand height, z/z_c
g	9.8 m/s^2	U_c	characteristic velocity, $(g^2\dot{Q}_o/(\rho c T)_\infty)^{0.2}$
$\dot{Q}_o$	fire heat release rate in Watts	ν	kinematic viscosity
V^*	dimensionless brand velocity, V/U_c	z_c	characteristic height, $(\dot{Q}_o/(\rho c T)_\infty g^{0.5})^{0.4}$
U^*_{bm}	dimensionless centerline plume velocity, U_{bm}/U_c	ρ	density of air

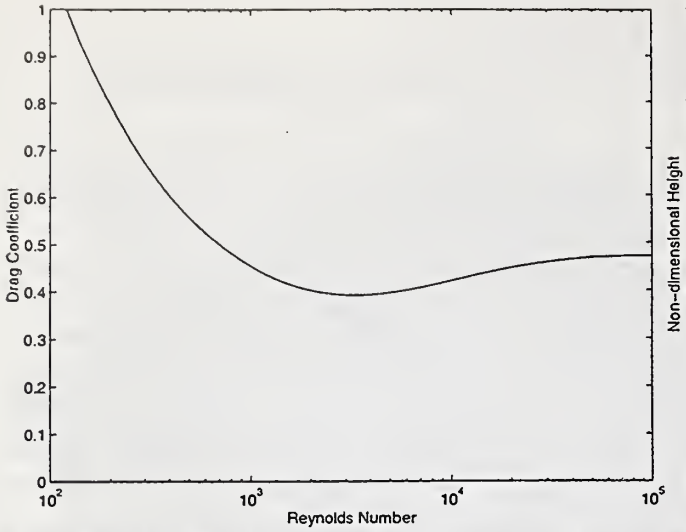

Fig. 1 Drag coefficient for an assumed spherical brand as a function of Reynolds number, Haider and Levenspiel. All variables in these four figures are dimensionless.

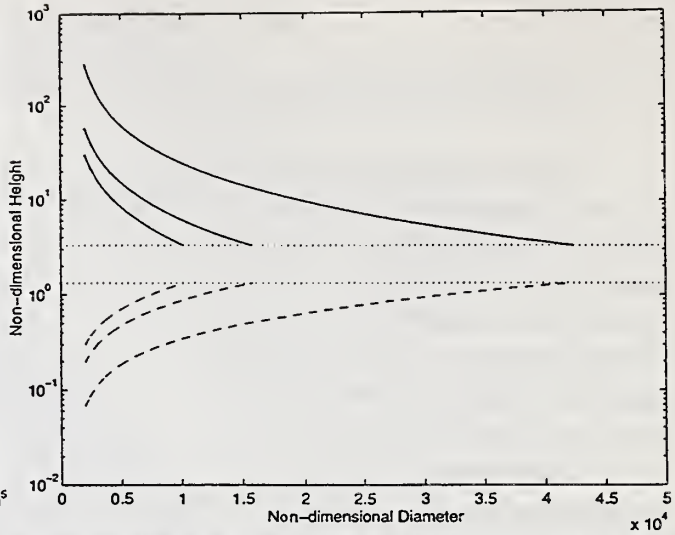

Fig. 2 Solid lines indicate the maximum height to which a spherical brand can ascend along the centerline in an axisymmetric, steady-state, Baum and McCaffrey plume as a function of diameter and the weighted density ratio, B. B = 5000, 7600, and 20000 from left to right. Dashed lines indicate the minimum height required for a brand to move, with the same parameterization. Dotted lines show the limits of the intermittent-flame region in the Baum and McCaffrey plume.

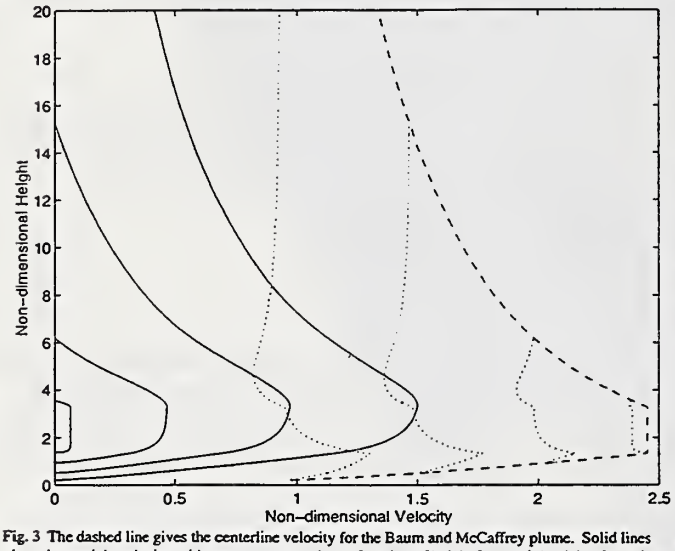

Fig. 3 The dashed line gives the centerline velocity for the Baum and McCaffrey plume. Solid lines show the particle velocity, with respect to ground, as a function of height for a weighted density ratio, B = 7600; d* = 2000, 5000, 10000, and 15000, from right to left. Dotted lines indicate the relative velocity as seen by the particle for the same values of B and d*, which increases from left to right.

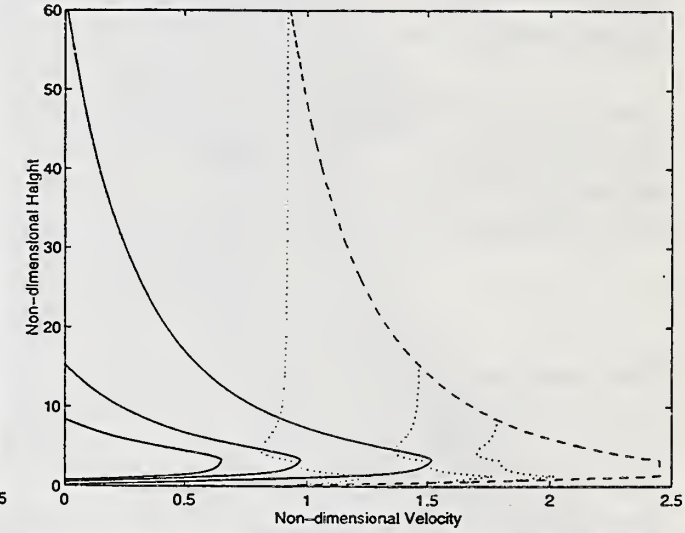

Fig. 4 The dashed line gives the centerline velocity for the Baum and McCaffrey plume. Solid lines show the particle velocity as a function of height for a diameter of 5000; B = 5000, 7600, and 20000 from left to right. Dotted lines indicate the relative velocity as seen by the particle for the same values of B and d*; B increases from right to left.

References

1. Pagni, P.J., "Causes of the 20 October 1991 Oakland Hills Conflagration," *Fire Safety J.*, 21, 331 - 339, 1993.
2. Tarifa, C.S., del Notario, P.P., and Moreno, F.G., "On the Flight Paths and Lifetimes of Burning Particles of Wood," *10th Symposium (Int'l) on Comb.*, 1021 - 1037, The Comb. Inst., 1965.
3. Tarifa, C.S., del Notario, P.P., Moreno, F.G., and Villa, A.R., *Final Report on Grants FG-SP-114 and FG-SP-146*, Forest Service,U.S.D.A., Madrid, Spain, 1967.
4. Baum, H.R. and McCaffrey, B.J., "Fire-Induced Flow Field – Theory and Experiment," *Fire Safety Science -- Proc. of the 2nd Int'l Symp.*, 129-148, Hemisphere, N.Y., 1989.
5. Haider, A. and Levenspiel, O., "Drag Coefficient and Terminal Velocity of Spherical and Nonspherical Particles," *Powder Tech.*, 58, 63 - 70, 1989.
6. Lee, S.-L and Hellman, J.M., "Firebrand Trajectory Study Using an Empirical Velocity-Dependent Burning Law," *Comb. and Flame*, 15, 265 -274, 1970.

Acknowledgments

This work was partially supported by NIST BFRL Grant 60NANB3D1438 and by the SFPE.

Buoyant Flows in Shafts

Lakshman Benedict and Edward Zukoski
California Institute of Technology

Introduction

The motions of buoyant flows contained within vertical shafts are being investigated in an experimental program that will lead to a prediction of the transport of heat and toxic materials within shafts due to buoyancy controlled mixing and the stack effect when the influence of heat transfer to the walls of the shaft can not be neglected. This work is based in part in part on the earlier experiments of Cannon, J. B. and Zukoski, E. E. (1975).

In this program, the basic flow under investigation is the motion of hot air within a vertical shaft and the subsequent heat transfer when the shaft is completely closed except at the bottom. The shaft and a mixture of air and carbon dioxide within it are initially at room temperature; the flow of interest is started when the bottom of the shaft is suddenly opened and is exposed to a reservoir filled with hot gas that is held at a constant temperature. The penetration of the hot air into the shaft in a vertical direction and the subsequent development of gas temperature, heat transfer to the walls from the hot gas, and removal of the carbon dioxide are then measured as a function of time. Configurations with windows that allow the stack effect to become the dominant flow are also being studied.

Experiments are carried out in an aluminum walled shaft 0.25 m square and 2.54 m high, and the bottom of the shaft can be suddenly exposed to air at temperatures up to 140° C. Heat transfer gages and thermocouples are used to determine heat transfer and the gas and wall temperature, and the transport of carbon dioxide within the shaft is studied to determine the transport processes within the gas column.

The flow can be divided into a relatively short *transient regime* or initial flow, some 10's of seconds, during which the hot gas front reaches the top of the shaft, and a *steady state regime* in which the time averaged gas temperature and heat transfer rates become constant. In the latter regime, fluctuations of up to 20 % about the time averaged values are observed. A quasi-steady state is reached because the walls of the duct have a very large heat capacity. The slow rise in surface temperature produced by the heat transfer is accompanied by a corresponding slow rise in the gas temperature for periods of 20 m.

The aim of this work is to develop models for predicting the motion of the initial front in the shaft, and the gas temperature field within the shaft, the rate of heat transfer to the walls, and the rate of transport of gas species within the shaft.

Closed Shaft Experiments

When the shaft is only open at the bottom, the transport of species and energy occurs because of a turbulent mixing process that is driven by the positive density gradient in the vertical direction. This produces a gravitational unstable configuration that feeds energy into a turbulent motion in the gas within the shaft. The instability is also driven by the heat transfer to the walls of the shaft which also produces an unstable density gradient in the gas near the wall.

The transport of species within the shaft is much slower and the transient period lasts for much longer periods. Models for both heat and species transfer rates are being developed.

The Nusselt number $Nu \equiv \frac{h_c W}{k}$, based on the shaft width W, and thermal conductivity of the gas k, and the heat transfer coefficient h_c, were about 60 for a wide range of conditions used for these closed shaft experiments and a correlation for the data is being sought. The dependence on the Grashof numbers, shown below for the stack

effect cases, does not fit the closed shaft data very well although the values for the Nusselt numbers were almost equal.

Stack Effect Experiments

The stack effect is present when an opening in the shaft allows the gas within the shaft to communicate with the outside pressure field. Consider a shaft open at the bottom and filled with a gas with an average density $\overline{\rho}$ when the density outside the shaft is ρ_∞ . If the bottom of the shaft is at the local ambient pressure, the pressure difference produced at a window that is H above the bottom of the shaft will be $(\rho_\infty - \overline{\rho})gH$ and the mass flux per unit area of the window will be given by

$\left[(\rho_{window})\sqrt{2\left(\frac{(\rho_\infty - \overline{\rho})}{\rho_{window}}\right)gH}\right]$. In our experiments, fluid is withdraw the shaft through the window and passed through a metering system so that a known flow can be established. Both the *transient* and *state regimes* are again established in the shaft. The influence of the mass withdrawal rate on the heat transfer and species transport within the shaft have been measured for flow rates that are 100, 50, and 25% of that given above. The window is at the top of the shaft and the area is 16% of the shaft area.

The turbulent mixing process still dominates this flow and correlations of the data for a wide range of conditions can be correlated by the simple relationship for the heat transfer coefficient:

$$Nu \equiv \frac{h_c Z}{k} = 0.13(Gr_Z\, Pr)^{\frac{1}{3}} \quad when \quad Gr_Z\, Pr = \left(\frac{g\beta\Delta T\, Z^3}{\upsilon^2}\right)\left(\frac{Cp\,\mu}{k}\right)$$

Grashof numbers, based on the height above the bottom of the shaft, Z, are between $8x10^8$ and $3x10^{10}$.

Our experimental data fits this correlation, based on data obtained with flows inside circular cylinders, to within 20%. Modeling will be simplified because the length scale drops out of the correlation since Z is linear on both sides and consequently the heat transfer coefficient becomes independent of the vertical scale; however, the dependence of heat transfer on the temperature of the gas and wall is strong. The range of conditions for both sets of experiments are being extended so that better models for these types of flow can be developed.

The transport of gas species vertically in the shaft are also being studied with the aim of producing a correlation.

References:

Cannon, J. B. and Zukoski, E. E. (1975) *Turbulent Mixing in Vertical Shafts Under Conditions Applicable to Fires in High Rise Buildings,* Technical Fire Report No. 1 to the National Science Foundation, California Institute of Technology, Pasadena, California.

Acknowledgments

This work has been supported by grants from the Building and Fire Research Laboratory, NIST, the Department of Commerce, under the guidance of Dr. Walter Jones of the Building and Fire Research Laboratory, NIST.

Need for the Development of Advanced Computational Methods to Determine Smoke Movement in Large Buildings

Rizwan-uddin
Department of Mechanical, Aerospace and Nuclear Engineering
University of Virginia
Charlottesville, VA 22903-2442

ABSTRACT

A relatively large proportion of deaths in fires result due to the inhalation of combustion products, away from the combustion sites. Generation rate of harmful gases critically depends upon the temperature reached. Hence, accurate prediction of maximum temperature reached, faithful modeling of the generation rate of harmful gases [1], and accurate determination of smoke movement away from the fire source through rooms, corridors, and stairways are essential for accurate fire safety assessment and codes.

Zone models have traditionally been used to characterize smoke movement in enclosed areas. Considerable number of assumptions and simplifications are necessary in the development and analysis of zone models. Though recent developments in computer hardware and numerical methods now permit increasing use of *field models*—which are based on local conservation of mass, momentum, energy and species, expressed in the form of partial differential equations—such applications are still somewhat limited to small computational regions due to the large number of grid points (and hence large computing resources) required by conventional numerical schemes. New computational techniques that will permit the solution of field equations over large volumes—such as those in typical buildings—are hence, very desirable. These methods will allow accurate solution of field equations to determine smoke movement over complex geometry in large buildings, and hence will help in the establishment of accurate fire safety codes.

Development of nodal methods and their applications over the last two decades to various branches of science and engineering has clearly shown that these methods are superior to more conventional numerical techniques, and lead to far more accurate results for given mesh size; or for specified accuracy, need far fewer "grid points" than conventional schemes, such as upwind-difference scheme. These methods have been applied to solve among other problems, the particle transport equation, neutron diffusion equation, Fokker-Planck equation, Navier-Stokes equations, Navier-Stokes-Boussinesq equations, and the convection-diffusion equation. In all cases the results have been exceptionally encouraging.

The main idea behind the nodal integral methods (NIM) is to not blindly subject the entire set of field equations to discretization, but rather to attempt *to solve as much of these equations analytically as possible*. This does require *some* approximations, and a certain amount of one time pre-processing, which pays off handsomely at the numerical calculation stage. Reference 2 outlines a typical application of the nodal integral method to solve the convection-diffusion equation. To show the superiority of the NIM, results obtained for a standard benchmark problem, solved using the NIM and using the upwind-difference scheme, are presented here. The rectangular computational domain, $-1 \leq x \leq +1$, $0 \leq y \leq 1$, is shown in Fig. 1. The flow is recirculating, where the velocity field is given analytically as $u = 2y\,(1-x^2)$ and $v = -2x\,(1-y^2)$. Constant Dirichlet boundary conditions are specified at the top, and the left and right walls of the domain. A specific temperature profile, $T(x,y=0) = 1 + \tanh(10(2x+1))$, is given at the domain flow inlet ($-1 \leq x \leq 0$), and a no-conduction boundary condition is given at the domain flow outlet ($0 < x \leq 1$, $y = 0$). The standard convection-diffusion equation is solved using a convergence criterion of 10^{-14} for both the upwind-difference scheme (UWDS) and the NIM. Table 1 shows that, for $Pe = 10^3$, the NIM solution obtained on a 60 x 30 mesh with a percent relative average L_1 error of 0.1406, is more accurate than that obtained by the UWDS on a 700 x 350 mesh which has a corresponding error of 0.7262. NIM, even with five times smaller error, is faster than the UWDS by about 950 times. Clearly, the analytical pre-processing in the development of the NIMs, leads to a scheme that can yield very accurate results on rather coarse

mesh size. This property of the NIM will be very beneficial in solving the smoke movement problem in large size buildings.

Field equations—mass, momentum, energy and species conservation equations—to be solved to determine smoke movement are similar to those to which NIM has already been successfully applied [3]. Hence, no conceptual difficulty is foreseen in developing a NIM for this problem. As far as turbulence is concerned, either a standard k-ϵ type turbulence model can be incorporated in the NIM development, or a nodal method can be developed to directly solve the inviscid equations of conservation in the Boussinesq approximation. Though the problem described above is steady-state, extension to time-dependent problems, though non-trivial, is straight forward. Nodal integral methods have already been developed to solve time-dependent problems. A recently developed *modified* nodal integral method when applied to (time-dependent) Burgers equation shows results that are even better than those obtained using conventional nodal integral method [4].

Clearly, the problem of the transport of combustion products from fires, due to rather large computational domain involved, can take advantage of these advanced computational methods, making it possible to solve the smoke generation and movement problem in large size buildings.

References

[1] E.L. Johnson et al., "Fire-Induced Mass Flow Into a Reduced-Scale Enclosure," in Annual Conf. on Fire Research, S.B. Smith, Editor, NISTIR 5499, National Institute of Standards and Technology (1994).

[2] E.P.E. Michael et al., "Third-Order Nodal Integral Method for the Convection-Diffusion Equation," Trans. Am. Nucl. Soc., 71, 195 (1994).

[3] H.R. Baum et al., "Mathematical Modeling and Computer Simulation of Fire Phenomena," Theoret. Comput. Fluid Dyn., 6, 125-139 (1994).

[4] Rizwan-uddin, "A Modified Nodal Integral Method for Partial Differential Equations," submitted for publication in Numerical Methods for Partial Differential Equations.

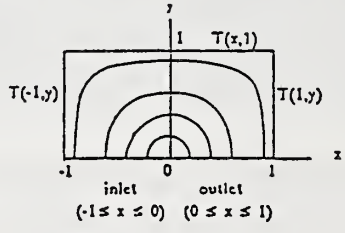

Fig. 1.

Table 1: Percent relative average L-1 errors of NIM vs. UWDS for a recirculating flow problem which has a sudden rise in inlet temperature profile and Pe = 10^3.

Mesh	% Relative Average L-1 Errors		CPU (sec)	
	UWD*	NIM**	UWD	NIM
20 x 10	1.40061E+01	1.53124E+00	0.06	0.12
60 x 30	6.53091E+00	1.40663E-01	0.45	1.60
100 x 50	4.37948E+00	4.85390E-02	3.27	12.29
140 x 70	3.31469E+00	2.42280E-02	10.10	51.38
180 x 90	2.67006E+00	1.44600E-02	24.91	139.68
220 x 110	2.23504E+00	9.59382E-03	52.54	312.84
260 x 130	1.92061E+00	6.82725E-03	101.86	618.13
300 x 150	1.68223E+00	5.10653E-03	175.65	1100.92
340 x 170	1.49505E+00	3.96427E-03	281.73	1867.65
700 x 350	7.26169E-01	9.35244E-04	1546.98	13695.41

MODELING HOT LAYER DEVELOPMENT IN STRUCTURAL FIRES[1]

G. M. Poole, E.J. Weckman and A.B. Strong
Department of Mechanical Engineering, University of Waterloo
Waterloo, ON, Canada N2L 3G1

Structural fires result in significant capital loss and multiple deaths each year. These losses are decreasing with advances in fire protection engineering but further refinements require improved understanding and quantification of the conditions within a building during an interior structural fire, particularly the development of the hot ceiling gas layer. Modeling hot layer development in fires is very complex. Due to limited availability of real structures for full scale experimentation, as well as the costs involved, existing models of hot layer development generally have been tested using data from relatively well-controlled tests in enclosures with simple geometries. More comprehensive development and testing of such models requires data collected from controlled fires in real structures in order to describe real fire effects (leakage, ambient wind, failure of windows and doors, etc.), to determine the processes and boundary conditions important in realistic simulations of hot layer development and to identify limitations in existing models vis-à-vis prediction of hot layer growth during real structural fires.

This paper reports data obtained from five full scale fire tests in two residential structures, which were instrumented with twenty, 24 gauge, Type K thermocouples placed near the ceiling or at elevations of 1 m above the floor to monitor the development of temperature with time throughout the structures. The data, taken at approximately 2 s intervals throughout each test, is compared to predictions from three different models of hot layer development: 1) a correlation based model [1], 2) the ASET-BX model in FPETool [2] and 3) the CFAST model [3]. Limitations in the models are identified and recommendations made for potential improvements in their prediction of real fire scenarios.

Experimental data and model predictions for tests in two multi-room residential structures are plotted in Figures 1 through 4. Results from the correlation [1] and ASET-BX [2] models were for the room of fire origin only, while those from CFAST [3] were based on 5 and 8 room simulations of the structures. In Figure 1, the hot layer temperatures measured by T1 and T3 on the ceiling was overpredicted by all models, probably due to insufficient account for leakage of hot gases to the exterior of the structure. Inclusion of leakage factors in the correlations [1] and ASET-BX [2] only slightly improved the results, since no account could be taken of flow between internal compartments of the building. In contrast, lower layer temperatures (T2, T14) were well predicted by CFAST [3] until the hot layer descended below the thermocouple positions.

Figure 2 illustrates typical data compared to 5 and 8 room CFAST predictions [3] for hot layer development in a room on the upper floor of the structure. Hot layer temperatures were overpredicted, with significantly lower temperatures predicted in the 8 room simulation. This suggests excess enthalpy transport from the fire room through the structure, demonstrating a limitation in accounting for mass movement between compartments in a real fire scenario. Such overprediction may arise from the plume correlation used to model entrainment (which for real fires is often applied outside its range of validity) and/or from difficulties in modeling mass flow through ventilation openings from one section of the structure to another.

In Figure 3, although hot layer temperatures were initially overpredicted by all models, there was generally better agreement between the data and the predictions, probably due to the direct dependence of the fuel heat release rate correlation on measured values of hot layer temperature. Through this dependence, the shape of the measured hot layer temperature-time curve was mirrored in the heat release rate curve, and thereby reflected in predictions of hot layer temperature. In adjoining rooms, Figure 4, upper layer temperatures were slightly overpredicted, but trends were reasonable. In upper floor rooms,

[1] Research supported through individual NSERC operating grants to E. Weckman and A. Strong

the predicted upper layer temperatures were in good agreement with the data, but lower layer temperatures were underpredicted. Again, refinements in the modeling of mass flux between compartments would be required to improve the predictions further.

Prediction of hot layer development in enclosure fires is very dependent on the accuracy of the submodels used for heat release rate of the fuel, for mass flow between compartments and for direct mass flow or leakage mass flow to the exterior of the structure. Limitations in these model elements are identified as major factors limiting application of current models of hot layer development to real fire scenarios; however, comparison of model predictions with real fire data suggests that these models can be improved to more accurately represent real fire conditions and thereby allow improved prediction of hot layer development during fires in multi-room structures.

1. McCaffrey, B.J., Quintiere, and M. Harkleroad, Fire Technology, 17, (2), 1981, p. 98.
2. Nelson, H. E., FPETool, Center for Fire Research, NIST, Gaithersburg, MD, 1991.
3. Jones, W. and G. Forney, NIST Technical Note 1283, Center for Fire Research, NIST, Gaithersburg, MD, 1990.

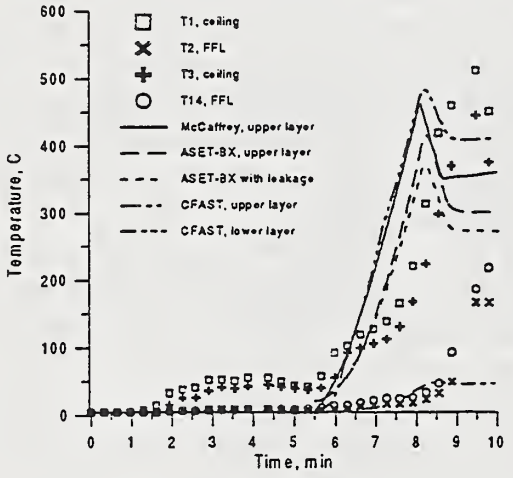

Figure 1: Upper and lower layer temperatures in fire room in multi-room fires in structure 1.

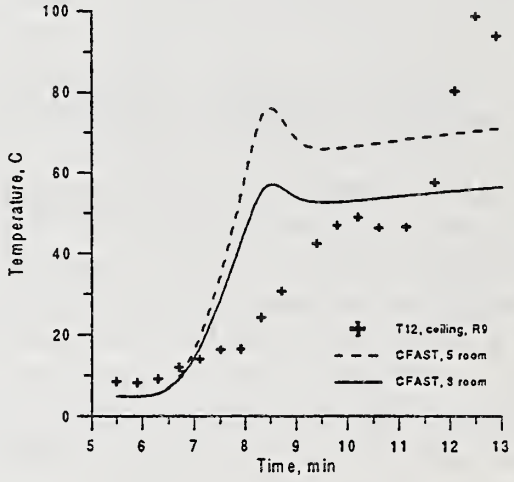

Figure 2: Upper layer temperatures in Room 9 on upper floor of structure 1.

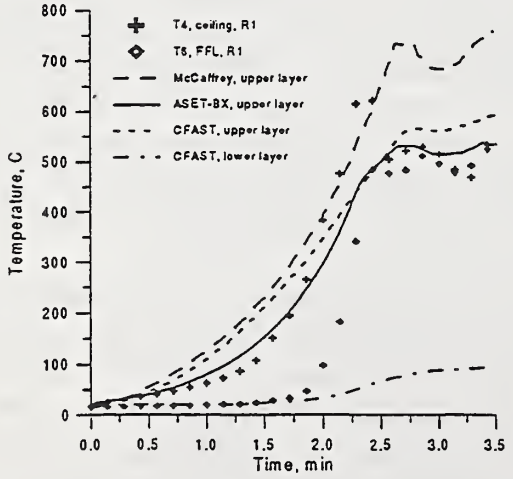

Figure 3: Upper and lower layer temperatures in fire room in multi-room fires in structure 2.

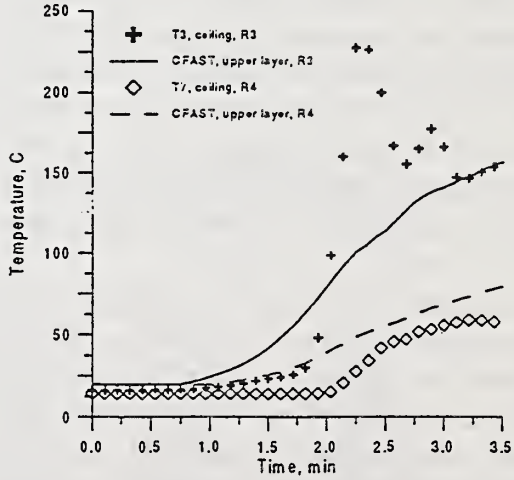

Figure 4: Upper layer temperatures in rooms adjoining fire room in structure 2.

Comparison of Fire Model Predictions with Experiments Conducted in a Hangar with a ceiling Height of 14.9 m

W. D. Davis, K. A. Notarianni, and K. B. McGrattan
Building and Fire Research Laboratory
National Institute of Standards and Technology, USA

The purpose of this study is to examine the predictive capabilities of fire models using the results of two fire experiments conducted in an aircraft hangar with a ceiling height of 14.9 m (49 ft). The fire experiments were conducted at Barbers Point, Hawaii by NIST in conjunction with the United States Navy [1]. This study is designed to investigate fire model applicability at a ceiling height where only a limited amount of experimental data is available. Some earlier efforts to compare computer fire models with experimental data at heights above 14 m include Walton [2], Duong [3] and Notarianni and Davis [4]. Model predictions compared with the experiments include: plume centerline temperature at the ceiling, temperature variation of the ceiling jet both radially from fire center and in depth beneath the ceiling, ceiling jet velocity, draft curtain filling and spilling times, temperature variation across the draft curtain and smoke detector activation. The fire models included in the study are the plume correlations of Heskestad [5] and McCaffrey [6], the ceiling jet correlation of Alpert [7], the zone models CFAST [8], FPEtool [9], and LAVENT [10], and the computational fluid dynamics models (CFD) CFX [11] and LES [12].

The fire experiments conducted in a Navy hangar at Barbers Point were designed to test a number of fire detection devices which could be used to detect fires in large spaces. The fires experiments consisted of eleven JP-5 pan fires with and without a draft curtain. The fire experiments were located at the floor of the hangar and were positioned 12.2 m from the center of the hangar where the ceiling height was 14.9 m. The roof consisted of built-up tar and gravel over a corrugated metal deck and exhibited only a 3 degree slope. The metal deck was directly supported by 0.25 m I beams which run the width of the hangar and are spaced 4.1 m on center.

There were no permanent draft curtains in the hangar. A temporary draft curtain made of fire retardant canvas was constructed for the fire experiments modeled here. The draft curtain area measured 24.4 m in length, 18.3 m in width and 3.7 m in depth.

Instrumentation included a load cell to measure the fuel burning rate, thermocouples to measure the gas temperature near the ceiling at radial distances of 0.0 m, 1.5 m, 3.0 m, 6.1 m, 8.5 m, 9.1 m and 11.6 m from the geometric center of the fire and 0.3 m beneath the ceiling, thermocouples to measure the temperature profile at 6.1 m and 9.1 m radially from fire center and at distances of 0.15 m, 0.30 m, 0.46 m, 0.61 m and 0.76 m beneath the ceiling, gas velocity measurements 6.1 m radially from fire center and 0.3 m beneath the ceiling, and smoke detectors which activated at a sensitivity of 8.2 % per meter. Details of the experimental configuration are available in reference 1. Two of the eleven experiments were chosen for modeling comparisons based on the excellent load cell data and plume behavior experienced during the tests. These tests consisted of a 0.6 m by 0.6 m square pan fire and a 1.5 m diameter pan fire which reached heat release rate values of 500 kW and 2.7 MW respectively. Both tests were conducted with the draft curtain in place.

The results of the analysis indicated that no single fire model could match the experimental measurements within a 25 % accuracy in all categories investigated. The models performed best in the comparison of centerline temperature predictions at the ceiling where most of the models predicted the experimentally measured temperature rise to within 50 % of the measured value. The poorest performance involved the comparison of the radial temperature variation from fire center along the ceiling where only three of the models could predict the measured variation within 50 %. Smoke detector activation predictions were also poor as none of the models which had a smoke detector algorithm predicted the detector activation time within 50 %. Other comparisons where several of the models provided predictions to within 50 % of the measured values included draft curtain filling time, temperature variation beneath the ceiling and ceiling jet velocity.

1 Notarianni, K. A., Gott, J., Lowe, D., Davis, W. D., and Laramee, S., Analysis of High Bay Hangar Facilities for Detector Sensitivity and Placement. National Institute of Standards and Technology, Special Report, 1996.

2 Walton, W. D., and Notarianni, K. A., A Comparison of Ceiling Jet Temperatures Measured in an Aircraft Hangar Test Fire with Temperatures Predicted by the DETACT-QS and LAVENT Computer Models, NISTIR 4947, National Institute of Standards and Technology, Gaithersburg, MD, 1992.

3 Duong, Duy A., The Accuracy of Computer Fire Models: Some Comparisons with Experimental Data from Australia, Fire Safety Journal 16, 415(1990).

4 Notarianni, K. A. And Davis, W. D.,The Use of Computer Models to Predict Temperature and Smoke Movement in High Bay Spaces, NISTIR 5304, National Institute of Standards and Technology, 1993.

5 Heskestad, G., Engineering Relations for Fire Plumes, Fire Safety Journal, 7, 25 (1984).

6 McCaffrey, B. J., Purely Buoyant Diffusion Flames: Some Experimental Results, NBSIR 79-1910, National Institute of Standards and Technology, 1979.

7 Alpert, R. L., Calculation of Response Time of Ceiling-Mounted Fire Detectors, Fire Technology, 8, 181 (1972).

8 Peacock, R. D., Forney, G. P,, Reneke, P., Portier, R., and Jones, W. W., CFAST, The Consolidated Model of Fire Growth and Smoke Transport, NIST Technical Note 1299, 1993.

9 Deal, Scot, Technical Reference Guide for FPEtool, Version 3.2, NISTIR 5486-1, National Institute of Standards and Technology, 1995.

10 Davis, W. D., and Cooper, L. Y., Estimating the Environment and the Response of Sprinkler Links in Compartment Fires with Draft Curtains and Fusible Link-Actuated Ceiling Vents - Part II: User Guide for the Computer Code LAVENT, NISTIR 89-4122, National Institute of Standards and Technology, 1989.

11 HARWELL FLOW3D, Release 3.2: User Manual, CFD Department, AEA Industrial Technology, Harwell Laboratory, Oxfordshire, United Kingdom, 1992.

12 McGrattan, K. B., Rehm, R. G., and Baum, H. R., Fire Driven Flows in Enclosures, Journal of Computational Physics, 110, 285 (1994).

Measurements and Prediction of Fire Induced Flow Field

Xian Chuan Zhou and Jay P. Gore
Thermal Sciences and Propulsion Center
School of Mechanical Engineering
Purdue University
W. Lafayette, IN 47907-1003
and
Howard R. Baum
Center for Fire Research
Building and Fire Research Laboratory
National Institute of Standards and Technology
Gaithersburg, MD 20899

Motivated by the various application of entrainment rate correlations in fire research and the large uncertainty in the efficacy of existing correlations and experimental data, the first Particle Imaging Velocimetry (PIV) based measurements of fire induced flow field around pool fires burning methanol, heptane and toluene were obtained. Air entrainment rates for 15 cm and 30 cm pool fires burning the three different fuels were calculated based on the mean velocity field. The entrainment data for the six fires could be correlated well using the fire Froude number, defined in Ref. [1] as the nondimensional parameter. A kinematic approach for the prediction of the fire induced flow field , following Ref. [2], was extended to the present fires. The driving processes for the entrainment flow, namely the volumetric heat release and the baroclinic vorticity generation, were evaluated based on correlations of buoyant diffusion flame structure in the literature [2, 3]. The predicted entrainment velocities were substantially higher than the measurements but were in qualitative agreement with the data. Based on this, the heat release rate and vorticity correlations used in the analysis were corrected by using a smaller radius for the 1/e point in the velocity profile. The modified predictions were in better agreement with the experimental data. Therefore, further evaluation of the kinematic approach with proper heat release rate and vorticity distributions is warranted.

The upper half of Fig. 1 represents the measured mean entrainment flow field around the 30 cm toluene pool fire. The vectors represent the mean convection velocities. Also shown in the figure is an instantaneous visible flame boundary. Large vertical velocity components at the elevation of the fuel surface, at radii larger than that of the pool edge, show that considerable air is entrained from regions below the elevation of the fuel surface. At a given height, both axial and radial velocities increase with smaller radial distance from the flame, and at a given radial location, the velocity only changes slightly with the axial distance. At the farthest radial location (r = 27 cm) the vertical velocity component is comparable to the radial velocity component.

The past correlations for heat release rate and vorticity distributions require that the radius of the 1/e point in the velocity profile be approximately 17.5 cm as shown in the bottom half of Fig. 1. With these correlations, a substantial overprediction of both the radial and axial velocity components was observed. Since the vorticity and heat release rate data for the present fire are not available, a reduction in the radius of the 1/e point in the velocity profile to 9.5 cm was utilized. The resulting predictions of velocity vectors are shown in the bottom half of Fig. 1. These are in reasonable qualitative and quantitative agreement with the measurements. The discrepancies between the measurements and predictions in Fig.1 are mainly in the vertical velocity component. To resolve these differences, the volumetric heat release rate distribution and the vorticity distribution need to be measured for conditions representative of the present fires.

References

[1] Delichatsios, M. A., *Combust. Flame* 70:33-46 (1987).
[2] Baum, H. R., and McCaffrey, B. J., *Fire Safety Science - Proceedings of the Second International Symposium*, Tokyo, Japan.
[3] McCaffrey, B. J., National Bureau of Standards (currently NIST) Report No. NBSIR 82-2473, 1982.

Acknowledgments

The research was supported by the Center for Fire Research, Building and Fire Research Laboratory, National Institute of Standards and Technology under Grant No. 60NANB2D1291 with Drs. Anthony Hamins and Takashi Kashiwagi serving as NIST Scientific Officers.

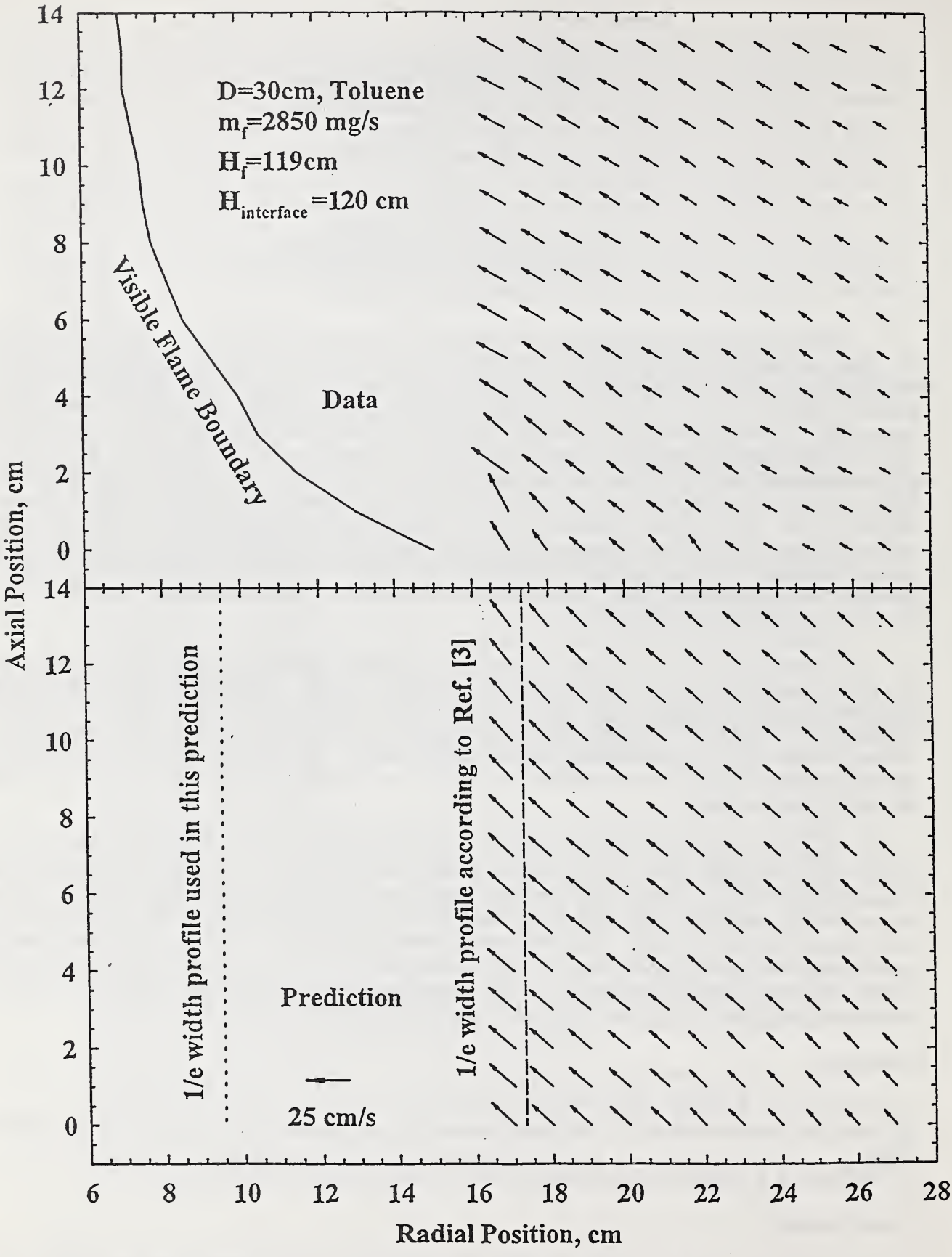

Figure 1: Measurements and Predictions of Fire Induced Flow Field around a 30 cm Toluene Pool Fire

A PHENOMENOLOGICAL MODEL OF NEAR-FIELD FIRE ENTRAINMENT

Baki M. Cetegen
Mechanical Engineering Department
University of Connecticut, Storrs, CT 06269-3139

Periodically shed large scale toroidal vortices in pool fires are believed to strongly affect the entrainment process in the flaming regions near the flame base. Entrainment data obtained in the near burner regions of pool fires suggest an approximately linear increase of plume mass flowrate with height above the burner surface, although the data scatter preclude extracting an precise dependence on height. In this presentation we propose a simple phenomenological model which accounts for the effects of the large scale vortical structures on entrainment in the near field. The model assumes that the intermittent engulfment by large scale toroidal vortices is responsible for the major portion of entrainment into the fire plume (neglecting the diffusive transport of air towards the wrinkled flame sheet). If the strength of vorticity (or vortex circulation) is determined as a function of height and source diameter, the entrained volume flux induced by the vortex can be computed as:

$$Q_{ent} = \frac{D}{2} \int_{x_{min}}^{x_{max}} \left[\int_{0}^{(x_c - x_o)} V_{vortex}\, dx \right] \frac{dx_c}{u_c}$$

where D is burner diameter, V_{vortex} is the induced entrainment velocity by the vortex between its location and the burner surface, and u_c is the vortex convection velocity. This expression determines the volume flux entrained per one cycle of vortex passage. Vortex velocity can be expressed outside its core region as $V_{vortex} = \Gamma(x_c)/[2\pi(x_c-x)]$ where x_c is the position of the vortex ring as shown in Fig. 1. Evaluation of the integral can be performed once the vortex strength $\Gamma(x_c)$ is determined experimentally. Our preliminary results for a 60 kW propane pool fire on a 20 cm. diameter circular sand burner suggest that vortex circulation increases with downstream distance as $\Gamma = \Gamma_0\, x_c^{2/5}$ shown in Fig. 2. We are currently making more measurements to determine the dependence of Γ on burner diameter as well. The entrained volume per cycle is determined by substituting this variation into the above expression., The mass entrainment rate is found by multiplying the entrainment volume per cycle with the ambient air density and the frequency of vortex shedding.

$$\dot{m}_{ent} = \rho_\infty Q_{ent}\, f \quad \text{where } f = CD^{-1/2} \;;\; \dot{m}_{ent} \propto x^{0.9} D^{0.5}$$

This expression suggests that entrainment is practically a linear function of distance from the burner surface, x and has a diameter dependence of $D^{1/2}$. The dependence on downstream distance, x is consistent with experimental data of Cetegen et al[1] and Toner et al[2]. The diameter dependence from this expression appears to be somewhat smaller than the one obtained from limited experimental data[1] on diameter variation (D = 0.1 to 0.5 m.) which scale as $m \propto D^{0.7}$. However, our model does not yet include the effect of D on Γ which we are currently studying. In summary, the dependence of entrainment rates in lower flaming regions of pool fires are obtained through a phenomenological model which accounts for the major effect of vortex induced entrainment. The preliminary results are in good agreement with experimental data. This model also provides a basis for scaling entrainment measurements in the near field.

References:

1. B. M. Cetegen, E. E. Zukoski and T. Kubota, Entrainment in the Near and Far Field of Fire Plumes, Combust. Sci. & Tech., Vol. 39, 305-331 (1984)

2. S. J. Toner, E. E. Zukoski and T. Kubota, Entrainment, Chemistry and Structure of Fire Plumes, Report to NIST, Caltech, September 1986

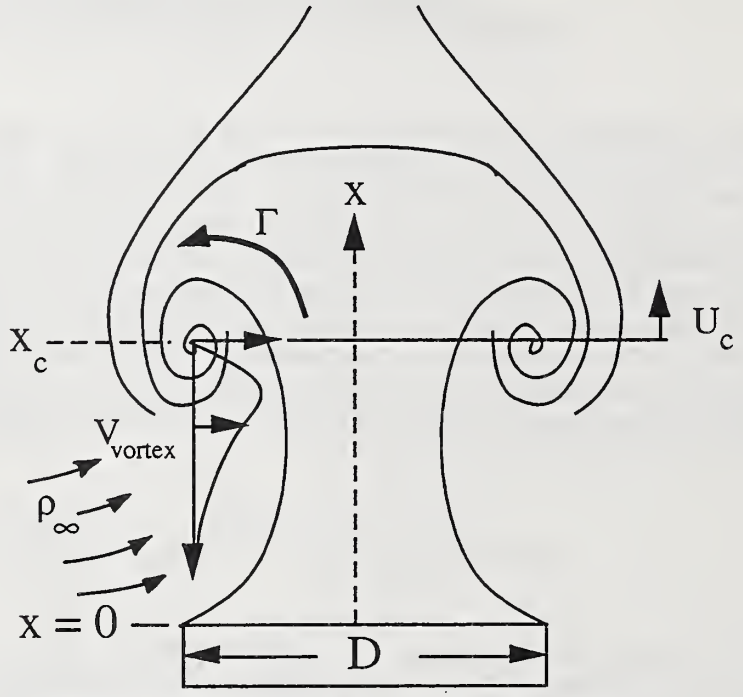

Figure1. Schematic of fire plume entrainment

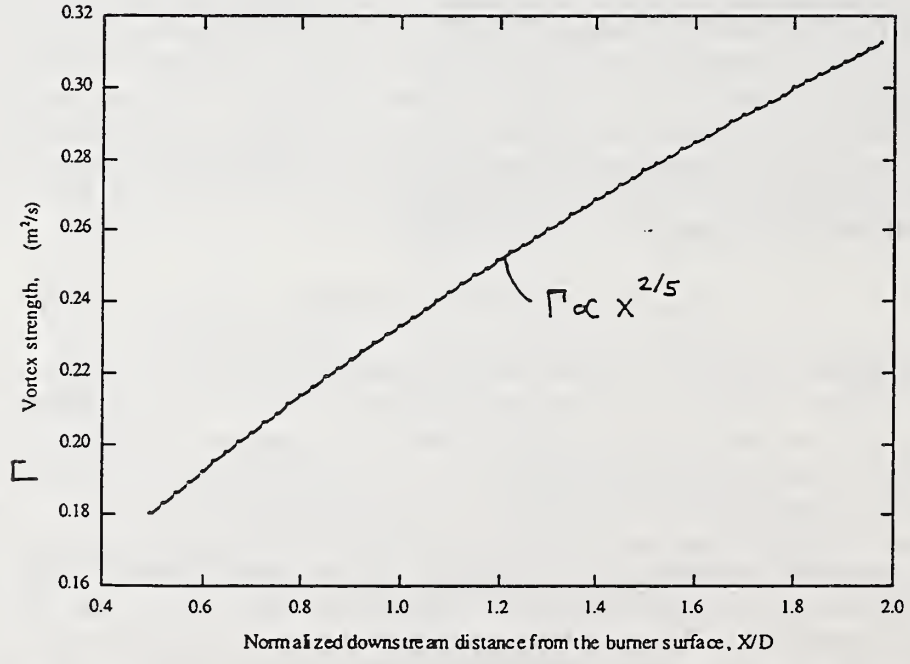

Figure 2.Vortex circulation as a function of downstream distance from burner surface

BEHAVIOR OF PERIODICALLY FORCED BUOYANT PLUMES

Baki M. Cetegen and Jennifer McTeague
Mechanical Engineering Department
University of Connecticut, Storrs, CT 06269-3139

This presentation reports on experiments concerning the behavior of periodically forced plumes of helium which naturally exhibit oscillations of the type observed in pool fires. Detailed characterization of non-reacting oscillating buoyant plumes has been recently reported[1,2]. The naturally occurring plume instability results from buoyant acceleration of the light plume gas in stagnant surroundings forming a toroidal vortex which exerts its influence on the unstable density stratification to lock the shedding frequency to a value described by the expression $S= fD/V = 0.8\ Ri^{0.38}$ for $Ri = (\rho_\infty - \rho_p)gD/\rho_\infty V^2 \leq 500$ and $S = 2.1\ Ri^{0.28}$ for $Ri > 500$. In this effort, we are exploring the receptivity of this natural instability to externally imposed periodic oscillations. Figure 1 shows the schematic of the experimental facility which consists of a 10 cm diameter nozzle attached to a loudspeaker, a wave form generator and an amplifier to provide the excitation, two pressure transducers, one in the cavity and another located at a height of one half burner diameter downstream along the centerline of the nozzle to detect the excitation and plume pulsation wave forms. The low frequency pressure transducer signals are first amplified and subsequently analyzed by a spectrum analyzer. For a helium plume originating from a 10 cm. diameter nozzle, the natural oscillation frequency is between 4.5 to 5.0 Hz. Our initial experiments involved excitation of this plume at single frequencies of 1 to 10 Hz . The excitation amplitude was kept to a low level providing a perturbation to the nozzle exit velocity. Later on, we conducted dual frequency excitation tests where a fundamental and a sub harmonic of the same amplitude were superimposed as the excitation wave form. Figure 2 shows a series of plume oscillation spectra with excitation frequencies in the range of 2 to 6 Hz. The natural oscillation frequency of this plume lies at 4.5 Hz. When excited at 2 Hz, the frequencies detected in the plume are those of the excitation and its harmonics. The highest amplitude occurs at 2 Hz. At 3 Hz, the amplitudes are all small and only the excitation frequency and its harmonics appear. Results at 4 Hz are similar to those at 2 Hz with similar pressure perturbation amplitudes. At 4.5 Hz excitation, the only identifiable frequency is at 4.5 Hz with no other significant peaks in the spectrum. The 5 Hz excitation also exhibits a single peak at the fundamental frequency. Finally at 6 Hz, spectrum is devoid of any significant peaks indicating that the coherence of the pulsations is destroyed to a large extent at this frequency. This result is also similar to that obtained at 3 Hz excitation. There also appear some frequency peaks which result from the interaction of the excitation frequency with the natural plume frequency. In general, these preliminary experiments show that the buoyant plume instability is highly receptive to the externally imposed frequencies and does not seem to have a preferential range of frequencies which undergo amplification. These results along with dual frequency excitation results and motion images of these plumes will be further analyzed and presented at this meeting.

References:

1. K. D. Kasper and B. M. Cetegen, Experiments on the Oscillatory Behavior of Buoyant Plumes of Helium and Helium-Air Mixtures, to appear in *Physics of Fluids*, 1996

2. A. Hamins, J. C. Yang and T. Kashiwagi, An Experimental Investigation of the Pulsation Frequencies of Flames, *Proceed. of the 24th Int'l Symp. on Comb.*, p. 1695 (1992)

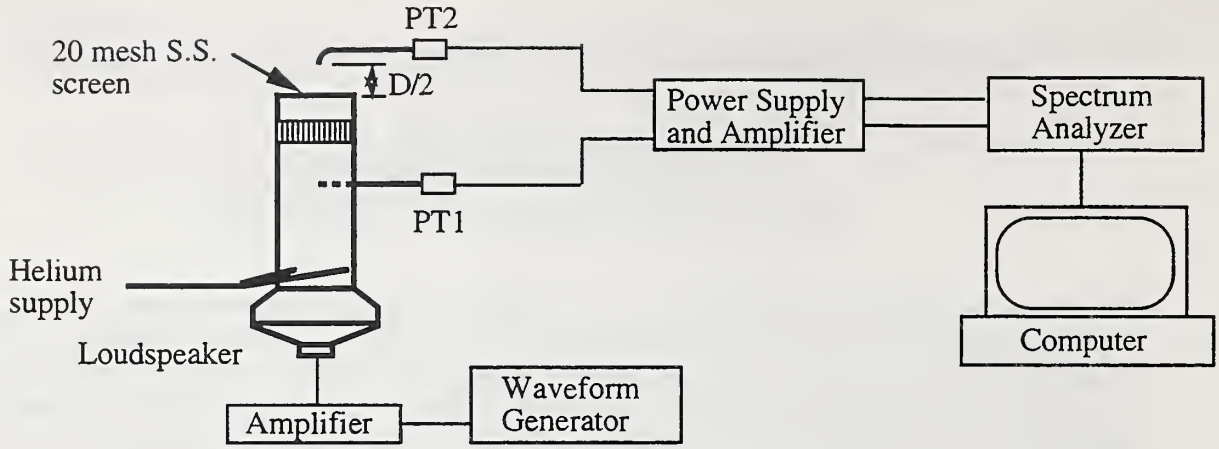

Figure 1. Experimental Set-up

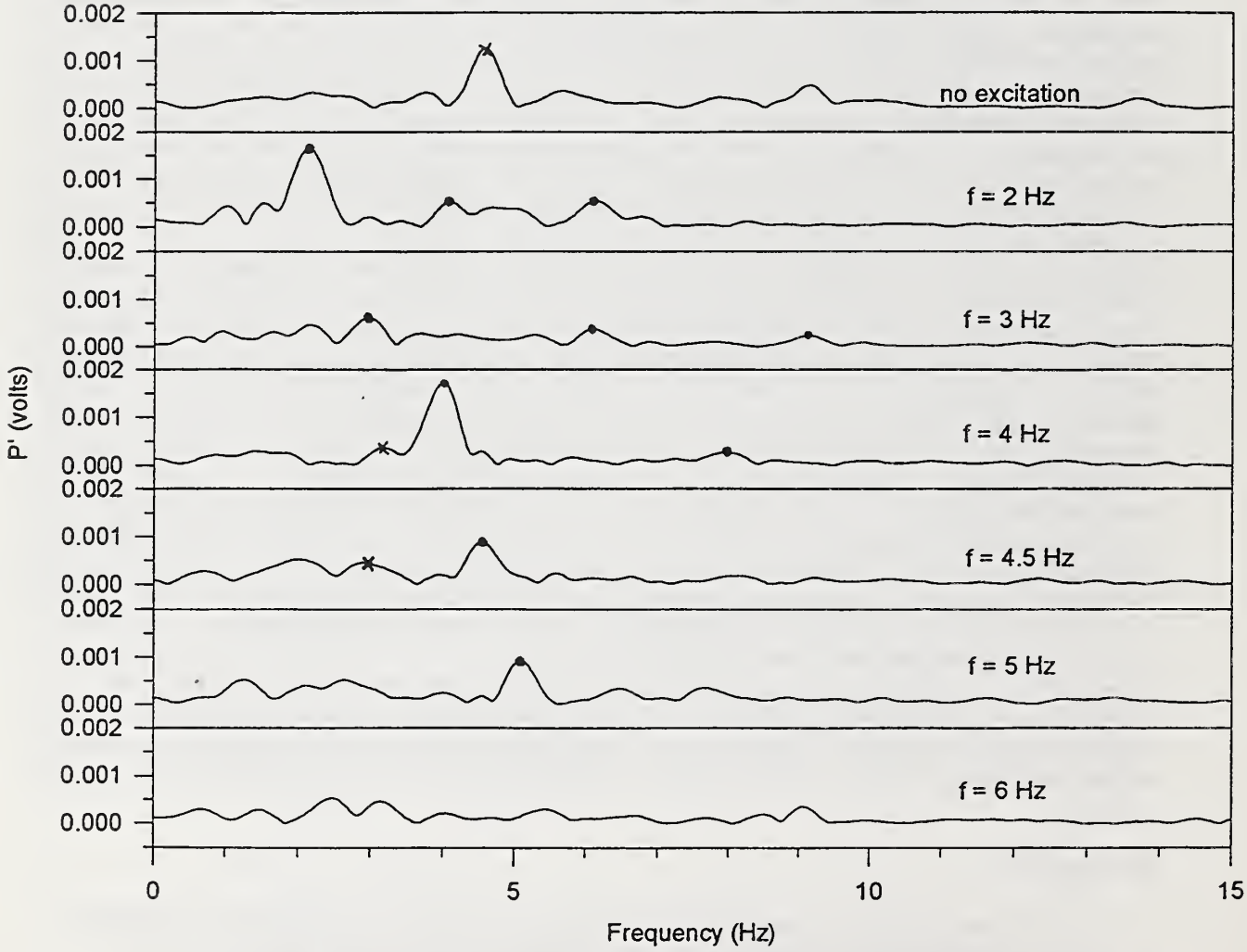

Figure 2. Frequency spectra of a helium plume at different excitation frequencies. Dots indicate excitation frequency and its harmonic peaks.

Numerical Investigation of the Effects of Buoyancy Production Terms in Predicting the Lateral Spread of a Propane Flame[1]

M. Ashrafizaadeh,E. Weckman and A. B. Strong
Dept. of Mechanical Engineering
University of Waterloo
Waterloo, Ontario, Canada, N2L 3G1

An elliptic fire model [1] has been developed and used to numerically investigate the validity of the commonly used $k-\varepsilon$ turbulence model and its modified variations in simulating buoyancy dominated diffusion flames. The present model consists of 2D time averaged conservation equations for mass, momentum and energy. Turbulence is modeled using the $k-\varepsilon$ turbulence model and the Eddy Dissipation Concept is used for combustion. Flame radiation is also accounted for by a constant fraction assumption. The governing equations are solved using a pressure based control volume method on a collocated variable arrangement.

This model is used to simulate the 2D rectangular propane flame of Annarumma et al. [2]. Details of the numerical setup used in the present simulations (e.g. boundary conditions, grid size, etc.) can be found in [1]. Figure (1) shows the predicted velocity and temperature fields. Although centerline values of the vertical velocity and temperature are predicted reasonably well, the lateral spread of the fire is clearly underpredicted (as reported by other authors as well, e.g. [2, 3]).

The analysis of a detailed set of data obtained from medium scale methanol pool fires [4] shows that the buoyancy production term, $g\overline{v'\rho'}$, in the turbulent kinetic energy equation has a positive contribution in the vicinity of the fire base. However, the widely used gradient hypothesis gives a modeled form for the buoyancy production term which is proportional to $\partial\rho/\partial z$. The density gradient is negative in the region adjacent to the fire base where temperature is rising. This causes the buoyancy production term to become negative and suppress turbulence in that region. The latter may partially explain the underprediction of the fire spread.

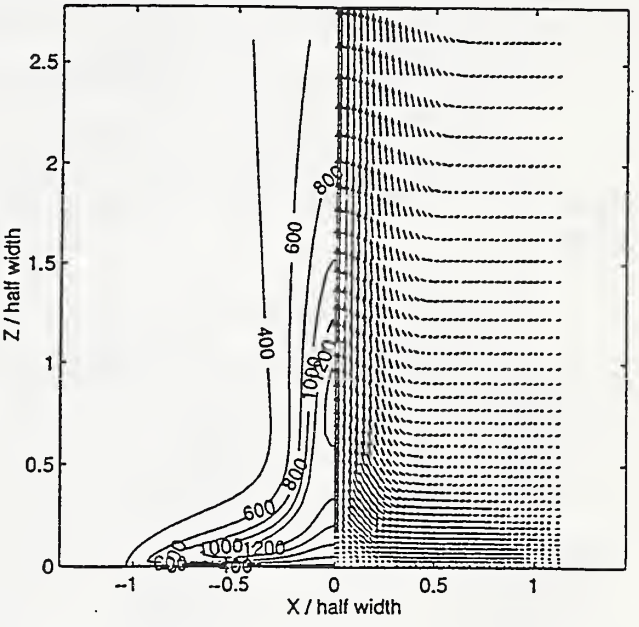

Figure 1: Temperature contours and velocity vectors

To investigate the effects of the buoyancy production term in the k equation, the results obtained from a case where all values of $\partial\rho/\partial z$ are accounted for *(case I)* are compared with the results obtained from another case where only positive values of $\partial\rho/\partial z$ are considered *(case II)*. Results show that turbulent Reynolds numbers for *case II* are much higher than those for *case I* . In fact, the values of Re_t for *case I* near the fire base are so low that the validity of using any turbulent fire model is questionable.

The lateral profiles of vertical velocity and temperature at different heights above the burner are shown in Figures (2) and (3) and compared against experimental data. As evident in these figures, considering only positive values of buoyancy production in the k equation improves the lateral spread of the fire at the cost of lowering the centerline values. Therefore, it appears necessary to model the buoyancy production term such that a positive contribution is ensured. For improved overall accuracy of the numerical results a more accurate chemistry and radiation models will also be required.

[1]research supported through individual NSERC Operating Grants to E. Weckman and A. Strong

References

[1] M. Ashrafizaadeh, A. B. Strong, and E. Weckman. In *Proceedings of The Combustion Institute, Canadian Section, Spring Technical Meeting*, 1996.

[2] M. O. Annarumma, J. M. Most, and P. Joulain. *Combustion and Flame*, 85:403–415, 1991.

[3] K. C. Adiga, D. E. Ramaker, P. A. Tatem, and F. W. Williams. *Fire Safety Journal*, 16:443–458, 1990.

[4] E. J. Weckman and A. B. Strong. *Combustion and Flame*, 105(3):245–266, May 1996.

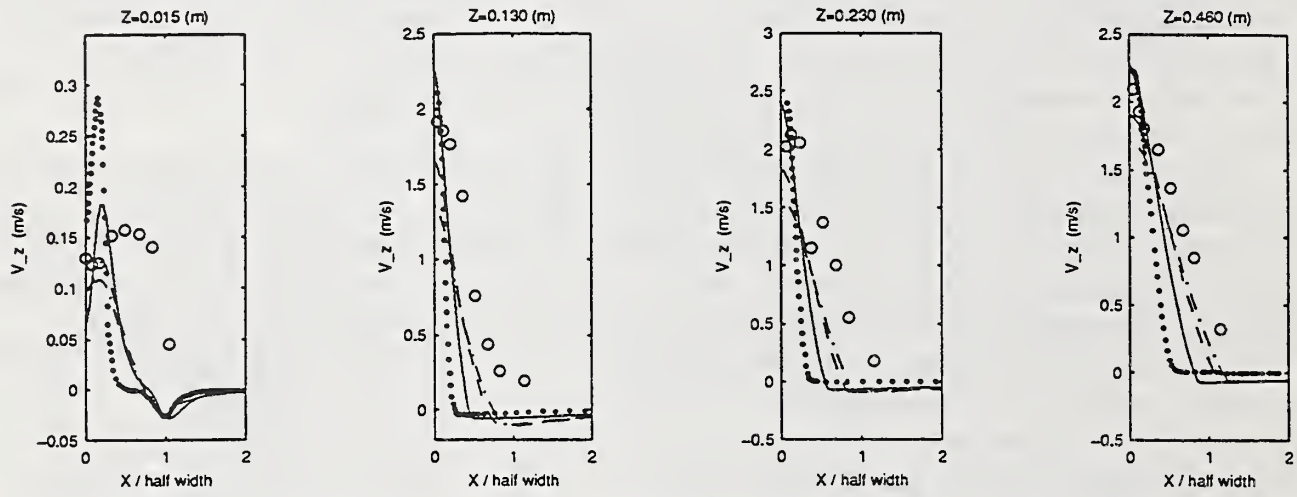

Figure 2: Cross-wise velocity distributions at different heights, see the caption of Fig. (3) for the legend.

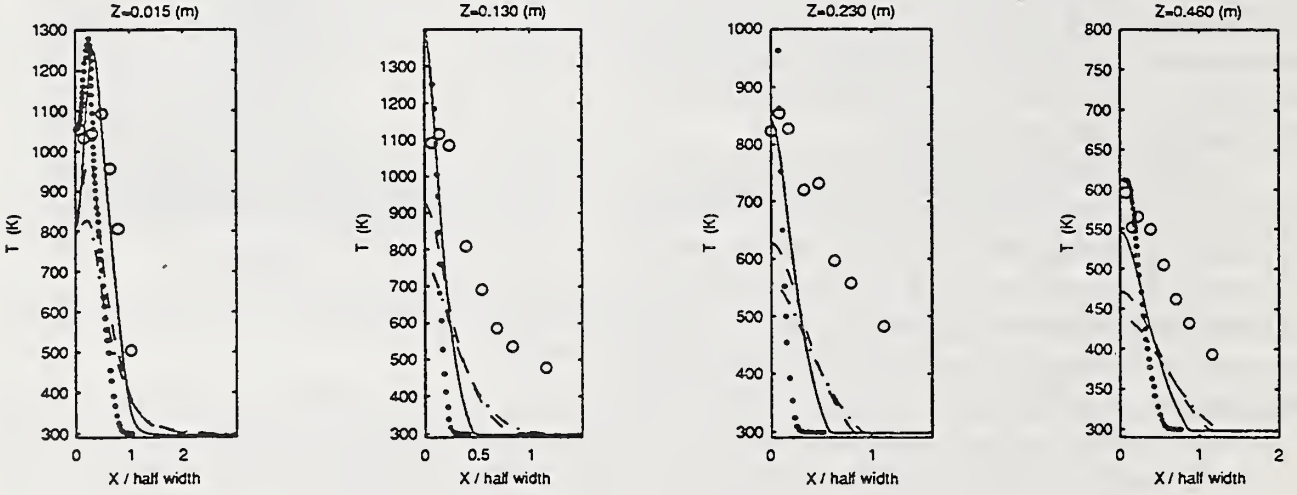

Figure 3: Cross-wise temerature distributions at different heights, ∘ data [2], — *case I* with 20% radiation, ··· Annarumma's model [2], – – *case II* with 10% radiation, –. *case II* with 20% radiation

LAGRANGIAN SIMULATION OF LARGE FIRE PLUMES

Ahmed F. Ghoniem and Issam Lakkis

Department of Mechanical Engineering
Massachusetts Institute of Technology
Cambridge, MA 02139

The numerical simulation of large fire plumes poses an uncommon challenge due to (1) the multiplicity of the physical processes which contribute to the outcome of burning a pool of fuel in a windy environment, (2) the multiplicity of scales which arise as the flow, transport and chemical reactions interact requiring numerical resolution in time and space which exceed 10^6 in each dimension, and (3) the enormous demand on the computational power as one tries to accommodate such resolution. Large fires are controlled by buoyancy dynamics, heat and mass transport which includes a major contribution from radiation, and combustion chemistry in which soot formation and destruction plays an important role. The evolution of a turbulent flow within the bulk of a fire is nearly unavoidable no matter how small the fuelpool is, and as such leads to all the known complexity of turbulence, turbulence-combustion interactions, and turbulence-radiation interactions. Developing a predictive tool which can be used to study the impact and footprint of a large fire is clearly a daunting task.

We have initiated an effort to develop a flexible and efficient framework for numerical fire simulation which takes advantage of (1) the current understanding of the physics of turbulence, combustion and radiation to simplify the model used to incorporate each component, (2) a powerful set of Lagrangian, grid-free numerical schemes which optimize the effort by concentrating the computational elements where they are most needed, and (3) the most advanced class of parallel, scalable computers. At the heart of the approach is the integration of the unsteady Navier-Stokes equations, cast in their vorticity transport form, using the transport element method in which the vortex elements are tracked along their trajectories while their circulation is being updated due to the action of the pressure gradient and the gravity field. Moreover, the gradients of the species concentrations, density and temperature are also computed along the same trajectories to efficiently solve for the mixing and combustion field.

The combustion model used at this stage assumes fast chemistry and considers the combustion process to be diffusion limited. To the extent that one is interested in fuel consumption, this is a reasonable approximation. This simplification reduces the species and energy equations into a set of conserved scalar equations which can be readily solved in terms of a mixture fraction as the different scalars are properly normalized. The dynamic effects of combustion, the primary source of energy in a fire, is represented in two mechanisms: the generation of vorticity along the combustion front and the

volumetric expansion associated with the heat release. In our first attempt to model the fire plume we accounted only for the first mechanism and showed that the observed intermittency in fire plumes, known as puffing, is due to an intrinsic instability of the vorticity layer which forms along the rising column of hot mixture, forming primarily from hot fuel and products [1]. The simulations were used to gain a better understanding of the similarities and differences between nonreacting and reacting buoyant plumes in an effort to explain some of the reported experimental data and explore the possibility of simplifying the overall model [2]. We showed that using a hot nonreacting pool of gases one can produce a plume whose dynamics are qualitatively and under some conditions quantitatively similar to those observed in the fire plume. Baroclinic vorticity generation, being the mechanism by which the potential energy of the plume is converted into kinetic energy, is very similar in both cases since even in the fire plume the density gradient acts essentially in the radial direction (fuel heating by the flame produces a hot column resembling that of an isothermal plume).

In this paper, we focus on the effect of volumetric expansion on the dynamics, mixing and combustion within the fire plume. We should mention that in the current model the effective enthalpy of reaction is reduced by about 30% to account approximately for the effect of radiation which has not been modeled comprehensively in our simulation [3]. As such, and given the overall fuel lean environment of a fire, one might expect that the volumetric expansion in the fire zone is not significant. This is indeed borne out of the simulations. We find that most of the predictions of the zero expansion model are close to those obtained in the finite expansion model in as far as the observable dynamics, e.g. puffing frequency and its dependence on the pool diameter, the average flame height and overall shape of the quasi periodic plume. We find, however, that the finite expansion model leads to reduced entrainment into the large structures and as such reduced overall fuel burning rate. The entrainment is still sufficient to reduce the temperature within the burning zone and inside the plume such that the overall field maintains the approximate distribution of a nearly isothermal plume. The paper will include detailed comparisons between the two models and a discussion of the implications of the impact of volumetric expansion on the fire evolution.

REFERENCES

1. Ghoniem, A.F., Lakkis, I. and Soteriou, M., 26th Symposium on Combustion, Naples, Italy, July 28-Aug,1996.
2. Hamins, A., Yang, J.C., Kashiwagi, J., 24th Symposium on Combustion, pp. 1695-1702, The Combustion Institute, 1988.
3. Zukoski, E.E., Chap. III in *Combustion Fundamentals of fires*, pp. 101-219, ed. by G. Cox, Academic Press, 1995.

A SIMPLE MODEL OF THE ISO 9705 IGNITION SOURCE

Marc L. Janssens, Southwest Research Institute

ISO 9705 Room Test Standard--In 1993, the International Organization for Standardization published ISO 9705, "Full-Scale Room Test." The apparatus described in this standard consists of a room (3.6 m deep by 2.4 m wide by 2.4 m high), with a single ventilation opening (0.8 m wide by 2 m high) in the front narrow wall. Several walls or the ceiling or both are covered with a combustible lining material that is exposed to a (gas burner) ignition source. The primary measurements are temperature and total heat flux at various locations inside the room, heat and smoke release rate from the fire, and time to flashover. Two ignition burners are described in the standard: the Nordic burner developed in Sweden, and the ASTM burner commonly used in North America. The former is 0.17 m wide, the latter is 0.3 m wide. Both have a square surface that is 0.3 m above the floor of the room. The Nordic burner is operated at a heat release rate of 100 kW for 10 minutes, followed by 300 kW for another 10 minutes. The ASTM burner is operated at 40 kW for 5 minutes, followed by 160 kW for 10 minutes.

Modeling of the ISO 9705 Room Test--The rather high cost of full-scale fire experiments triggered the development of simple computer models that can be used as an alternative to the test. The most complete model was developed by Quintiere.[1] This model assumes that the ignition burner flame exposes a rectangular area of the back and side walls in contact with the burner to a uniform heat flux, $\dot{q}''_{ig}$. The width of the area $x_{p,0}$ (m), is equal to the burner width W_b (m). The height of the area $y_{p,0}$ (m), is closely related to the burner flame height L_f (m). For the model calculations reported by Quintiere et al.,[1,2,3] values for $y_{p,0}$ and $\dot{q}''_{ig}$ were chosen in qualitative agreement with some experimental data. The objective of this paper is to develop a systematic procedure for calculating the burner geometry and heat flux characteristics.

Geometry--As far as the geometry of the heated area is concerned, the suggested approach is to determine $y_{p,0}$ so that the surface area of the rectangle on the right in Figure 1 is equal to that of a more realistic shape of the heated region, as shown on the left in Figure 1. The latter is characterized by the flame height, L_f, and by the width of the flame at half-height, $W_{½}$. Janssens and Tran obtained the following correlation for L_f based on measurements for the ASTM burner[4]

$$L_f = 2.9D(\dot{Q}^*)^{2/3}$$

In order to determine $W_{½}$, a criterion is needed to define the flame boundary. Janssens and Tran published Gaussian temperature profiles at various heights for the ASTM burner[4]. Their data indicate that 600°C is a suitable temperature to describe the flame boundary. Therefore, $W_{½}$ is estimated as the lateral distance from the corner at half the flame height where the temperature is equal to 600°C. Temperature profiles measured by Kokkala are used to determine $W_{½}$ for the Nordic burner.[5] Finally, the equivalent area approach is used to determine $y_{p,0}$ as follows

$$A_f = \frac{W_{½}L_f}{2} + \frac{W_b L_f}{4} \equiv W_b y_{p,0}$$

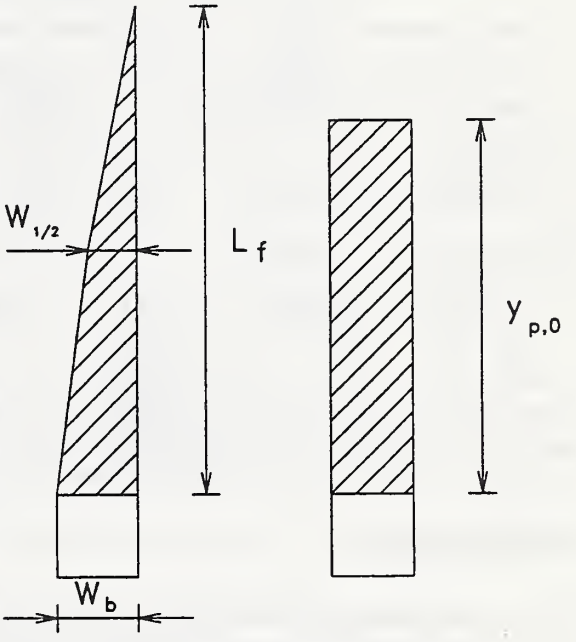

Figure 1. Equivalent heated area

The results of the calculated equivalent geometry are shown in Table 1.

Flame Heat Flux--The second step is to estimate the heat flux from the burner flame. The flux consists of a radiative and a convective part:

$$\dot{q}''_{ig,net} = \dot{q}''_{ig,r} - \epsilon\sigma T_s^4 + h_c(T_f - T_s)$$

Quintiere's model calculates T_s using Duhamel's superposition integral. To determine the incident radiative heat flux, it is assumed that a certain fraction, χ_r, of $\dot{Q}_{ig}$ is lost by radiation. McCaffrey measured χ_r for propane as a function of the Froude number, Fr.[6] His data indicate that for the range of Fr corresponding to the Nordic and ASTM burner, χ_r varies between 0.31 and 0.33. Tewarson gives χ=0.95 for the combustion efficiency of propane.[7] Assuming that half of the radiation strikes the walls, the radiative burner flame flux follows from

$$\dot{q}''_{ig,r} = \frac{\chi \chi_r \dot{Q}_{ig}}{4 y_{p,0} W_b}.$$

Estimating the convective part is more difficult because it depends on the bulk temperature and velocity of the fluid, and surface temperature of the wall. The average flame temperature over the full width at half the flame height, based on the measurements by Janssens and Tran, is equal to T_f=754 °C. Velocity distributions measured by Janssens and Tran are used to determine an average value of the upward velocity at half the flame height. Hasemi and Tokunaga found that the centerline velocity for diffusion gas burners is proportional to the square root of the product of the centerline temperature rise above ambient and the height above the burner surface.[8] This relationship is used to determine velocities for the Nordic burner. Finally, assuming a constant wall temperature of 55 °C (typical temperature for cooling water of heat flux meters), property data for air and the standard convective heat transfer correlations for forced flow over a flat plate are used to estimate convective heat transfer. The calculated values for the convection coefficient are given in Table 1. The resulting values for the total flame flux based on a 55 °C wall temperature are in the range of 30-47 kW/m^2. This is significantly lower than the value of 60 kW/m^2 used by Quintiere.

Table 1. ISO 9705 Ignition Source Geometry and Heat Transfer Characteristics

Burner type	W_b (m)	$\dot{Q}_{ig}$ (kW)	L_f (m)	$W_{½}$ (m)	$y_{p,0}$ (m)	$\dot{q}''_{ig,r}$ (kW/m^2)	h_c (W/m^{2}K)
Nordic	0.17	100	1.96	0.14	3.73	35	14
Nordic	0.17	300	4.00	0.23	1.29	36	16
ASTM	0.30	40	0.70	0.14	0.45	22	11
ASTM	0.30	160	1.79	0.18	1.37	30	13

Validation--Predictions for six materials and two ISO 9705 room test scenarios, one involving the ASTM burner and one with the Nordic ignition source, were presented earlier.[9] Calculated flashover times are in reasonable agreement with the measurements, indicating that the simple model for the ignition source is probably acceptable for engineering analyses. Additional comparisons are needed to confirm this conclusion.

REFERENCES

1. J. Quintiere, *Fire Safety Journal*, Vol 20, 1993, pp. 313-339.
2. J. Quintiere, G. Haynes & B. Rhodes, *Journal of Fire Protection Engineering*, Vol 7, 1993, pp. 1-13.
3. J. Quintiere, M. Hopkins & D. Hopkins, *ICFRE*, SFPE, Boston, MA, 1995, pp. 272-277.
4. H. Tran & M. Janssens, *Journal of Fire Protection Engineering*, Vol 5, 1993, pp. 53-66.
5. M. Kokkala, *Interflam '93*, Interscience Communications, London, UK, 1993, pp. 13-24.
6. B. McCaffrey, Combustion Institute, Western States Section, Paper No. 81-15, 1979.
7. A. Tewarson, *SFPE Handbook of Fire Protection Engineering*, SFPE, Boston, MA, 1995, pp. 3-53 to 3-115.
8. Y. Hasemi & T. Tokunaga, *Combustion Science & Technology*, Vol 40, 1984, pp. 1-17.
9. M. Janssens et al., *Fourth Fire & Materials Conference*, Interscience Communications, London, UK, 1995.

A MICROSCALE COMBUSTION CALORIMETER FOR DETERMINING FLAMMABILITY PARAMETERS OF MATERIALS

*Richard E. Lyon and Richard N. Walters**
Fire Research Section AAR-423
Federal Aviation Administration
William J. Hughes Technical Center
Atlantic City International Airport
New Jersey 08405

**Galaxy Scientific Corporation*
Egg Harbor Township, NJ

A microscale flow calorimetric method has been developed to measure flammability parameters of milligram samples under conditions which approximate flaming combustion. The present work seeks to improve upon a previously published thermogravimetric technique for determining flammability characteristics of polymeric materials [1, 2] by better reproducing the solid and gas phase processes associated with the flaming combustion of solid materials. The new microscale calorimeter accomplishes these objectives by rapid (>200 K/min) heating of milligram samples to a constant, calibrated heat flux in a thermogravimetric analyzer under an inert atmosphere followed by high temperature combustion of the pyrolyzate stream in excess oxygen. These processes correspond to the anaerobic thermolysis which occurs under non-oxidizing/reducing conditions to generate gaseous fuel and char in the pyrolysis zone of a burning solid and subsequent oxidative combustion in a diffusion flame.

Figure 1 is a schematic diagram of the microscale flow calorimeter. Mass loss is continuously monitored during the test in a thermogravimetric analyzer and volatile thermal decomposition products in the inert (nitrogen) purge gas stream are swept from the pyrolysis chamber through a heated transfer line and combined with oxygen in a heated manifold at the entrance to a coiled tubular combustion chamber maintained at several hundred degrees Centigrade. Complete oxidative combustion of the gaseous pyrolyzate occurs in the tubular reactor analogous to the combustion process in a well ventilated diffusion flame. The fuel/oxygen ratio and residence time in the combustor are simply controlled in the microscale flow calorimetric method through purge gas and oxygen flow rate adjustments so that incomplete combustion of the pyrolyzate stream is also possible. Complete and incomplete combustion products are scrubbed from the gas stream as it exits the tubular combustor. Heat release rate is calculated from oxygen consumption and mass flow rate measurements of the scrubbed gas stream as it exits the polarographic oxygen analyzer. Total heat released is obtained by numerical integration of the heat release rate and char yield is determined from the residual mass. Effective heat of combustion is calculated as the total heat divided by the mass loss, and the combustion efficiency from the effective heat of combustion divided by the chemical heat of complete combustion from an oxygen bomb calorimeter.

Figure 2 is a composite plot of the heat release rate data for some polymers tested in the microscale heat release rate device during 200 K/min heating to 50 kW/m^2 incident heat flux under nitrogen in the TGA furnace. The microscale heat release rate data are expressed as kilowatts per gram of original material in order to normalize the curves since the surface area of the sample varies between tests depending on the physical form of the material (e.g., powder, film, etc.). The polymers tested show a two order of magnitude range in peak heat release rate in the microscale device between the highest and lowest values.

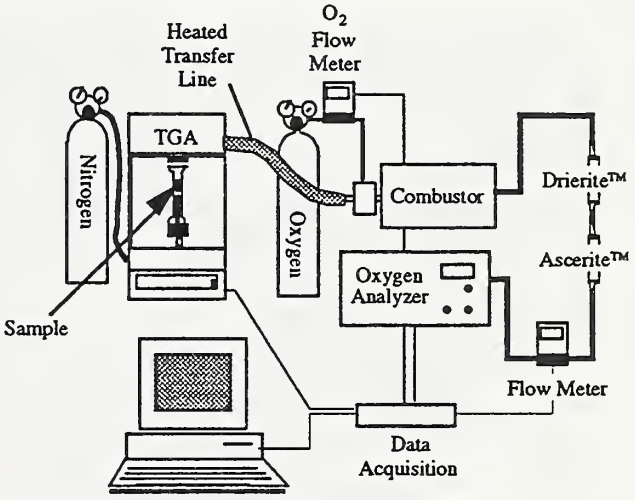

Figure 1. Schematic diagram of microscale calorimeter

Figure 3 compares the peak heat release rate data from the microscale heat release device to average heat release rate data from large (decagram) samples measured in a conventional cone calorimeter at 50 kW/m^2 incident heat flux for polymers where these data were available [3-7]. The cone calorimeter heat release rate values plotted in Figure 3 are steady-state or average values obtained by dividing the reported effective heat of combustion per unit area by the time of flaming combustion. Average heat release rate in the cone calorimeter is the bench scale fire parameter which should correlate with microscale calorimetric heat release rate if the steady-state heat release of thermally-thick specimens is simply a superposition

along the time axis of the isothermal heat release rate of the constant thickness, constant temperature pyrolysis zone as it moves through the sample during solid flaming combustion [8].

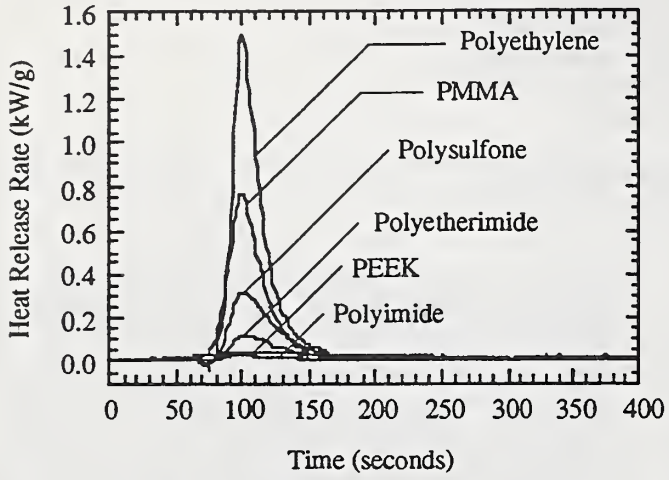

Figure 2. Heat release rate curves for various polymers at 50 kW/m^2 incident heat flux in the mini calorimeter.

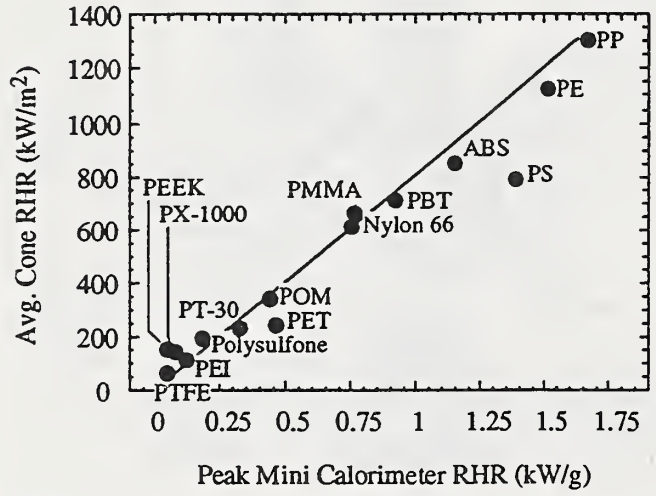

Figure 3. Correlation between polymer peak heat release rate in microscale device and cone calorimeter at 50 kW/m^2 incident heat flux.

Figure 3 indicates a good correlation between the peak heat release rates measured in the microscale device and the steady-state values measured in the bench scale cone calorimeter. As cone calorimeter heat release rate data appears to correlate well with full scale fire tests [9,10] microcalorimetric heat release rate should also be a good predictor of full scale fire performance.

Separating the thermochemical and thermophysical phenomena of flaming solid combustion in the microscale calorimetric method will more accurately reproduce the local fire environment at the surface of a burning solid and should allow direct correlation with bench- and full-scale fire calorimetry tests. Decoupling of the intrinsic, time-dependent chemical processes of material combustion from transient effects associated with thermal diffusion in large samples. It is hoped that the new microscale combustion flow calorimeter will accelerate the development of new fire resistant materials by providing flammability parameters which are physically meaningful for use in fire hazard evaluation and will help relate material properties to full-scale fire performance.

REFERENCES

1. T.D. Gracik and G.L. Long, "Heat Release and Flammability of a Small Specimen using Thermoanalytical Techniques," in *Fire Calorimetry*. Proceedings from the 50th Calorimetry Conference, R.E. Lyon and M.M. Hirschler Eds. Gaithersburg, MD. DOT/FAA/CT-95/46 (1995).
2. T.D. Gracik, G.L. Long, U.A.K. Sorathia, and H.E. Douglas, "A Novel Thermogravimetric Technique for Determining Flammability Characteristics of Polymeric Materials," in *Fire Calorimetry*. Proceedings from the 50th Calorimetry Conference, R.E. Lyon and M.M. Hirschler Eds. Gaithersburg, MD. DOT/FAA/CT-95/46 (1995)
3. Fire Calorimetry, R.E. Lyon and M.M. Hirschler, Eds. Proceedings from the 50th Calorimetry Conference, Gaithersburg, MD. DOT/FAA/CT-95/46 (1995).
4. M.J. Scudamore, P.J. Briggs, and F.H. Prager, "Cone Calorimetry–A Review of Tests Carried out on Plastics for the Association of Plastic Manufacturers in Europe," Fire and Materials, 15, 65-84 (1991)
5. T. Kashiwagi and T.G. Cleary, "Effects of Sample Mounting on Flammability Properties of Intumescent Polymers," Fire Safety Journal, 20, 203-225 (1993)
6. M.M. Hirschler in Heat Release in Fires , V. Babrauskas and S. Grayson, Eds., Elsevier Applied Science, New York, (1992).
7. A. Grand, SBIR Phase I Final Report, DTRS-57-94-C-00172
8. R.E. Lyon, "Material Properties and Flammability of Polymers," Proceedings of the 41st International SAMPE Symposium and Exhibition, Anaheim, CA, March 24-28, 1996
9. C.P. Sarkos and R.G. Hill, "Evaluation of Aircraft Interior Panels Under Full Scale Cabin Fire Conditions, Proceedings of the AIAA 23rd Aerospace Sciences Meeting, Reno, NV Jan. 14-17, 1985
10. J.G. Quintiere,V. Babrauskas, L. Cooper, M. Harkelroad, K. Steckler, and A. Tewarson, "The Role of Aircraft Panel Materials in Cabin Fires and Their Properties," DOT/FAA/CT-84/30 (June 1985)

FIRE PERFORMANCE OF PHTHALONITRILE RESINS/COMPOSITES

Satya B. Sastri, James P. Armistead, Teddy M. Keller

Materials Chemistry Branch
Naval Research Laboratory, Code 6127
Washington D. C. 20375-5320

and

Usman Sorathia

Carderock Division
Naval Surface Warfare Center
Bethesda, MD. 20084-5000

ABSTRACT

Phthalonitrile composites, under development at the Naval Research Laboratory (NRL), offer promise as high performance, high temperature composites for aerospace and advanced marine applications. Phthalonitrile polymers are thermosets derived from bis-phthalonitrile monomers and a variety of curing additives. The structures of the monomer and the curing additive used in this investigation are shown in Figure 1. The advantages and versatility of the phthalonitrile polymers may be realized in terms of processability and superior properties. For instance, the cure reaction is not accompanied by evolution of volatile byproducts, therefore, void-free components can be fabricated easily. Additionally, a prepolymer (B-staged) resin may be prepared and stored with an indefinite shelf life under ambient conditions. The polymerization rate is also easily controllable as a function of curing additive and processing temperature. This enables conventional autoclave curing as well as short time reaction injection molding (RIM) processes. As far as the thermal properties are concerned, the cured resins do not show a glass transition temperature (T_g) up to 450°C and exhibit good property retention at elevated temperatures. In addition, they retain about 65-70% char upon pyrolysis to 1000°C under inert conditions.

Phthalonitrile composites with carbon and glass reinforcements have been investigated for fire performance characteristics. High performance composites that meet the Navy's flammability requirements of MIL-STD-2031 have not been available to date. When compared to other high performance composites, phthalonitrile-based composites are the only materials that satisfy the Navy's fire performance acceptance criteria for using lightweight polymeric composites for submarine applications. For instance, the time to ignition (T_{IG}) and peak heat release (PHR) values at 100 kW/m^2 heat flux for phthalonitrile/carbon composite are 75 sec. and 118 kW/m^2,

respectively, and those of phthalonitrile/glass fabric composite are 60 sec. and 106 kW/m^2. The corresponding values for vinyl ester/glass marine composite are 24 sec. and 187 kW/m^2. The superior fire performance of phthalonitrile composites may be attributed to the highly aromatic polymer backbone that confers high thermal stability as well as the ability to form a char on burning. Smoke and combustion gas analyses reveal that the properties of phthalonitrile/glass panels are far superior to vinyl ester/glass composites. The optical density as well as the relative concentrations of toxic gases such as CO, HCN and HCl are significantly lower for phthalonitrile/glass composites. The water uptake when immersed under ambient conditions for 100 days is less than 1%. All these attributes render phthalonitrile-based composites useful as fire barriers in advanced marine applications.

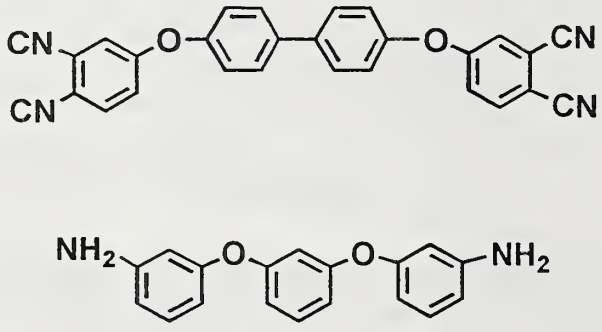

Figure 1: Structures of phthalonitrile monomer (top) and curing additive (bottom)

ACKNOWLEDGEMENTS

The authors are thankful to the Office of Naval Research for support of this program.

STRUCTURAL PERFORMANCE OF COMPOSITES AT ELEVATED TEMPERATURES DUE TO SHIPBOARD FIRES

U. Sorathia, C. Beck
Carderock Division, Naval Surface Warfare Center
Annapolis, MD 21402

The use of composites inside Naval submarines is now covered by MIL-STD-2031 (SH), Fire and Toxicity Test Methods and Qualification Procedure for Composite Material Systems Used in Hull, Machinery, and Structural Applications [1]. Two guiding criteria [2] were established for the use of composite systems aboard Navy vessels. The composite system will not be the fire source, i.e., it will be sufficiently fire resistant not to be a source of spontaneous combustion. Also secondary ignition of the composite system will be delayed until the crew can respond to the primary fire source, i.e., the composite system will not result in rapid spreading of the fire. The Navy currently has no specific standard for surface ships. The flammability requirements for surface ships are different than submarines. Instead of survivability measured in minutes, as it is in submarine fires, the critical issue in surface ship fires is the residual strength of structures at elevated temperatures for a period of 30-60 minutes.

CDNSWC has initiated a comprehensive effort focused on the issue of residual structural strength of composites during fire. This is intended to result in mathematical models that can be used by naval architects to design full scale fire-tolerant composite structures. This methodology includes determination of basic composite characteristics at elevated temperatures, determination of isothermal material characteristics for use in the computer model, determination of heat transfer characteristics of composite materials exposed to fire, construction of mathematical models using ABAQUS finite element analysis, and experimental validation of these models.

Composites retain most of their load bearing characteristics below a certain "critical" temperature. Above this critical temperature, composites begin to lose their mechanical properties rapidly and, in some cases, catastrophically [3]. To determine the limits of composite structural performance at elevated temperatures, dynamic mechanical thermal analysis (DMTA) was performed on glass reinforced vinyl ester composite panels at various temperatures under isothermal conditions. .

Dynamic mechanical thermal analyzers produce quantitative information on the viscoelastic and rheological properties of a material by measuring the mechanical response of a sample as it is deformed under periodic stress. This method has great sensitivity in detecting changes in internal molecular mobility, determination of the glass transition temperature (Tg), and determination of effects of these changes on load bearing characteristics. The property measured by DMTA that is of interest in determining the load bearing capabilities is the flexural storage modulus, E', which agrees closely with the flexural modulus as measured by ASTM D790 [4]. For dynamic heating scans, E' is a function of temperature. Also important is the ratio of storage modulus to loss modulus, E", as a material passes through the glass transition point. This ratio, Tan δ, indicates the balance between the elastic phase and the viscous phase in a polymer.

P236 PC, a quasi isotropic glass reinforced vinyl ester panel, was exposed to isothermal dynamic

testing at room temperature, 150, 200, 250, 300, 350, 400, 450, 500, 550, and 600^{0}F. All samples were exposed to these different temperatures for a period of 8 hours. In this study, all tests were carried out in a single cantilever bending mode at a constant frequency of 10Hz. Results indicate that the modulus drops at subsequently increasing temperatures. Significant drop takes place between 200 and 250^{0}F. Catastrophic drop takes place between 250 and 300^{0}F.

After the isothermal testing for a period of 8 hours, samples were cooled to room temperature. The samples were retested for dynamic testing to determine the retention of load bearing properties and assess the damage caused to the panels by exposure to the elevated temperatures. If the material retains the viscoelastic behavior, and recovers the load bearing properties, then the damage caused by the thermal exposure is termed as reversible damage. It is important to identify the temperature or thermal aging where the given transition between reversible or irreversible damage occurs. This can be observed in tan δ curves from DMTA scans. Figure 1 shows the results from dynamic testing of glass/vinyl ester panels previously exposed to isothermal conditions at elevated temperatures for 8 hrs. At isothermal aging temperatures up to 450^{0}F, the composite panels exhibit reversible thermal damage. The 500^{0}F DMTA scan shows chemical breakdown of vinyl ester moeity of composite panel and the resin loses characteristic viscoelastic behavior even after the panel has been cooled to room temperature. This resin is no longer capable of transferring the load to the fiber. This is the threshold temperature for irreversible damage.

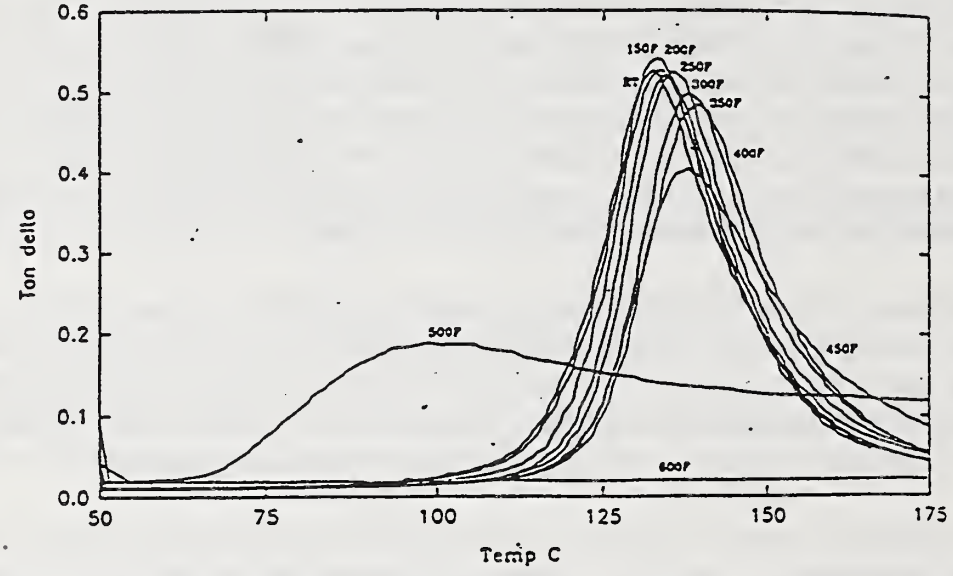

Fig. 1: DMTA scan (Tan δ) for previously isothermally exposed glass/vinyl ester panels.

REFERENCES:

1. MIL-STD-2031(SH), "Fire and Toxicity Test Methods And Qualification Procedure For Composite Material Systems....Inside Naval Submarines", February 1991.
2. DeMarco, Ronald A.; "Composite Application at Sea: Fire Related Issues", 36th International SAMPE Symposium, April 15-18, 1991.
3. Sorathia, U., C. Beck, and T. Dapp; "Residual Strength of Composites during and after Fire Exposure"; Journal of Fire Sciences, Volume 11, No. 3, May/June 1993 (ISSN0734-9041).
4. Sepe, M.P.; "Dynamic Mechanical Analysis", Advanced Materials Processes, April 1992.

ROOM/CORNER TESTS OF WALL LININGS WITH 100/300 kW BURNER

Mark A. Dietenberger, USDA, FS, Forest Products Laboratory, Madison, WI
Robert H. White, USDA, FS, Forest Products Laboratory, Madison, WI
Ondrej Grexa, State Forest Products Research Institute, Bratislava, Slovakia
Marc Janssens formerly with American Forest & Paper Assoc., Washington, DC

The primary objective of our joint U.S.-Slovak project is to develop an alternative system to assess reaction to fire of materials. The severity of an 100/300 kW program with materials on both walls and ceiling results in short and fairly close values in the times to flashover for building products with normal reaction to fire. In contrast, an 40/160 kW program with materials on wall only is insufficient to result in flashover for some materials. Some melting materials may only melt and shrink away from the flames during the 40 kW and leave insufficient material near the burner after the change to 160 kW to cause flashover. The test series conducted in this study indicate that more useful results are obtained by combining the two test protocols. The resulting protocol calls for the 100/300 kW burner program, but the test samples on walls only.

Twelve room/corner tests of common wall linings were conducted with gypsum-lined ceiling and exposure to a propane ignition burner at 100 kW for ten minutes (0 to 600 s) followed by 300 kW for ten minutes (600 to 1200 s). This burner program and Nordic burner is used in the Nordic countries (Kokkala 1993, Ostman 1993) and is in the ISO room test standard (ISO 9705). The burner was located in one of the rear corners. The enclosure is 2.44 m wide, 3.66 m deep, and 2.44 m high with a doorway (0.8 m wide and 2 m high) in the front wall. All products of combustion emerging through the doorway are collected in a hood and extracted via an exhaust duct. Heat and smoke release rate are measured continuously in the duct. The principal performance criterion is time to flashover.

All materials but the gypsum and fire-retardant-treated (FRT) polyurethane foam were wood products (Table 1). Materials used in tests 50, 53, 54 and 55 were left over from the ASTM Institute for Standards Research round robin (Beitel 1994). In that project, the 40 for five minutes/160 kW for ten minutes program and an ASTM burner were used with the materials on the walls only. Materials used in tests 51 and 52 were obtained from Forintek Canada Corp. which has a similar project with the National Research Council of Canada (NRCC). In the Forintek/NRCC project, all four possible combinations of the two burner programs and two test specimen configuration (three walls only, three walls and ceiling) are being evaluated (Sumathipala and others 1994). Materials for tests 56 to 62 are from a wood industry material bank for fire research. Some of these materials were tested previously using the 40 kW for five minutes (0 to 300 s), 160 kW for five minutes (300 to 600 s) burner program (Tran and Janssens 1991). The 40/160 kW data (Table 1) based on the 20 kW to the floor criterion are from the ISR round robin and the previous tests at the Forest Products Laboratory. Results based on different criteria for flashover are fairly consistent. Plans are to test six additional wood products between now and the spring of 1997.

In addition to the room tests, the project includes cone calorimeter tests and the development of fire growth models. Results for the first year (tests 50 to 55) are discussed in more details in as series of three papers presented at the 1995 Fire and Materials Conference (Dietenberger and others 1995, Grexa and others 1995, Janssens and others 1995). Funds for this "Room/Corner Test and Reaction to Fire of Wood and other Building Materials" project is being provided by the Slovak-U.S. Science Technology Program under project number 94072.

By using wall linings with gypsum-lined ceiling exposed to propane burning at 100 kW for ten minutes followed by 300 kW for 10 minutes, the room/corner tests of common materials indicate an effective differentiation of fire performance for the materials tested. Time to flashover of untreated plywood was less than 10 minutes, whereas that of FRT materials was greater than 10 minutes. Gypsum board did not flashover (NFO). Ranking of the untreated wood products was consistent with expectations.

Table 1. - Flashover times for tested materials.

Materials	Test No.	Density (kg/m_2)	Thickness (mm)	Flashover times for 100/300 kW exposure (s)		Flashover times for 40/160 kW exposure (20 kW to floor) (s)
				Flames out door	1000 kW	
Gypsum	49, 55	755	16	NFO[1]	NFO	NFO
FRT Plywood "F"	52	600	12	499	561	-
FRT Plywood "A"	50	560	12	870	909	NFO
FRT Polyurethane foam	57	29	23	630	630	358
Douglas-fir plywood "M"	57	515	12	521	561	378
Redwood lumber	62	420	19	499	522	378
Douglas-fir plywood "A"	53	540	12	465	477	391
Southern pine plywood	58	605	16	320	330	348
Particleboard	59	790	13	242	282	391
Hardboard	61	1025	6	225	255	-
Oriented strand board	60	645	11	196	219	270
Oak veneer plywood	51	480	13	173	180	-

References

Beitel, Jesse. 1994. Interlaboratory test program-Proposed ASTM standard method for room fire test of wall and ceiling materials and assemblies. Project Report PCN:33-000012-31. Philadelphia: ASTM Institute for Standards Research.

Dietenberger, M. A.; Grexa, O.; White, R. H.; Sweet, M.; Janssens, M. 1995. Room/corner tests of wall linings with 100/300 kW burner. Fourth Fire and Materials Conference, London: Interscience Communications. pp. 53-62.

Grexa, O.; Janssens, M.; White, R. 1995. Analysis of cone calorimeter data for modeling of the room/corner test on wall linings. Fourth Fire and Materials Conference, London: Interscience Communications. pp. 63-71.

Janssens, M.; Grexa, O.; Dietenberger, M.; White, R. 1995. Predictions of ISO 9705 room/corner test using a simple model. Fourth Fire and Materials 4th International Conference, London: Interscience Communications. pp. 73-83.

Kokkala, M.A. 1993. Sensitivity of the room/corner test to variations in the test system and product properties. Fire and Materials. 17:217-224.

Ostman, Birgit. 1993. Results of Scandinavian tests and research on reaction to fire. Tratek Rapport 9307037. Stockholm: Tratek.

Sumathipala, K.; Kim, A.; Lougheed, G. 1994. Configuration sensitivity of full-scale room fire tests. Third Fire and Materials Conference, London: Interscience Communications. pp.

Tran, H.C.; Janssens, M.L. 1991. Wall and corner fire tests on selected wood products. J. of Fire Science, 9:106-124.

FULL-SCALE TEST EVALUATION OF AIRCRAFT FUEL FIRE BURNTHROUGH RESISTANCE IMPROVEMENTS

Timothy R. Marker, Constantine P. Sarkos, Richard G. Hill
Federal Aviation Administration

Fuselage burnthrough refers to the penetration of an external jet fuel fire into the interior of an aircraft during a postcrash fire. The time to burnthrough is critical because in a majority of survivable aircraft accidents accompanied by fire, ignition of the interior of the aircraft is caused by burning jet fuel external to the aircraft. Therefore, the integrity of the aircraft and its ability to provide a barrier against fuel fire penetration is an important factor related to the survival of aircraft occupants. Fuselage burnthrough resistance becomes particularly important when the fuselage remains intact following a crash, which occurs frequently in survivable accidents. The best example of an accident with large loss of life where fuselage burnthrough was determined to be critical to the outcome was the 737 accident in Manchester, England in 1985. In this accident, the investigators concluded that burnthrough occurred within 60 seconds and did not allow sufficient time for all occupants to escape (55 people died from the effects of the fire).

Fuselage burnthrough resistance may be simplistically viewed as the time interval for a fuel fire to penetrate three fuselage shell members: aluminum skin, thermal acoustical insulation, and sidewall; panel/cabin flooring. Flame penetration may occur in other areas as well, such as windows, air return grilles, and seams/joints. The burnthrough resistance of the aluminum skin is well known. It takes only about 20 to 60 seconds for the skin to melt, depending on its thickness. The thermal acoustical insulation is the next impediment to burnthrough following the melting of the aluminum skin. In past FAA outdoor fuel fire burn tests on surplus fuselages, it was determined that the fiberglass insulation provided an additional 1 to 2 minutes of protection, if it completely covered the fire area and remained in place. Thus, the method of securing the insulation to the fuselage structural members is important. The sidewall panels/flooring offer the final barrier to fire penetration. Sandwich panels comprised of honeycomb cores and fiberglass facings are effective barriers; however, full-scale fire tests also show that the fire can penetrate into the cabin through the air return grilles, seams/joints or window reveals. Moreover, some airplanes utilize aluminum sidewall panels which offer minimal burnthrough resistance. FAA researchers are focusing on the thermal acoustical insulation as the most potentially effective and practical means of achieving a burnthrough barrier.

A full-scale test article shown in figure 1 is utilized, to evaluate improved materials/concepts when installed realistically inside a fuselage and subjected to an external fuel fire. The test article is a 20-foot-long barrel section, constructed of steel framing members, inserted in the aft end of a 707 fuselage. A 10-foot-long by 8-foot-wide fuel pan subjects the test article to an intense fuel fire. The steel framing members assure reuse of the test article. Edge effects are avoided by making the test section longer than the fuel pan. Aluminum sheet is riveted to the steel framing in a thickness typical of fuselage skin construction.

Aircraft thermal acoustical insulation bating is typically comprised of lightweight fiberglass encapsulated in a thin film moisture barrier, usually polyester or polyvinyl fluoride. Several materials have been tested which exhibit marked burnthrough resistance compared to the baseline thermal acoustical batting. The effective materials include a heat stabilized oxidized polyacrylonitrile fiber (OPF) as a replacement for the fiberglass, a lightweight ceramic fiber matt used in conjunction with the

present fiberglass, and a polymide film as a replacement for the polyester or polyvinyl fluoride films. A comparison of full-scale test temperature readings taken at the inside of the insulation and near the ceiling illustrate the burnthrough protection provided by the OPF insulation, shown in figure 2. Both the OPF and fiberglass insulation materials were securely attached to the framing members. It takes about 1.5 to 2 minutes for the fuel fire flames to penetrate the aluminum skin and fiberglass batting, whereas the OPF insulation did not burn when subjected to a fuel fire for over 5 minutes. Although the OPF insulation clearly prevented flame penetration and did not visibly burn, low concentrations of toxic gases measured within the test article indicate that the OPF may have thermally decomposed slightly.

Although test results are very promising, there is additional work underway, or planned, as follows:

1) Evaluation of additional potentially effective materials/concepts (e.g., polyimide foam, intumescent paint, etc.).

2) Determination of the effect of steel framing members employed to secure insulation batting samples in the test article on the time to burnthrough (commercial transport aircraft primarily utilize aluminum alloy structural members).

3) Determination of the benefit of burnthrough resistant thermal acoustical insulation in terms of additional survival time, when the test article is fully furnished with cabin materials.

4) Development of a small-scale performance fire test method for aircraft fuselage burnthrough resistance.

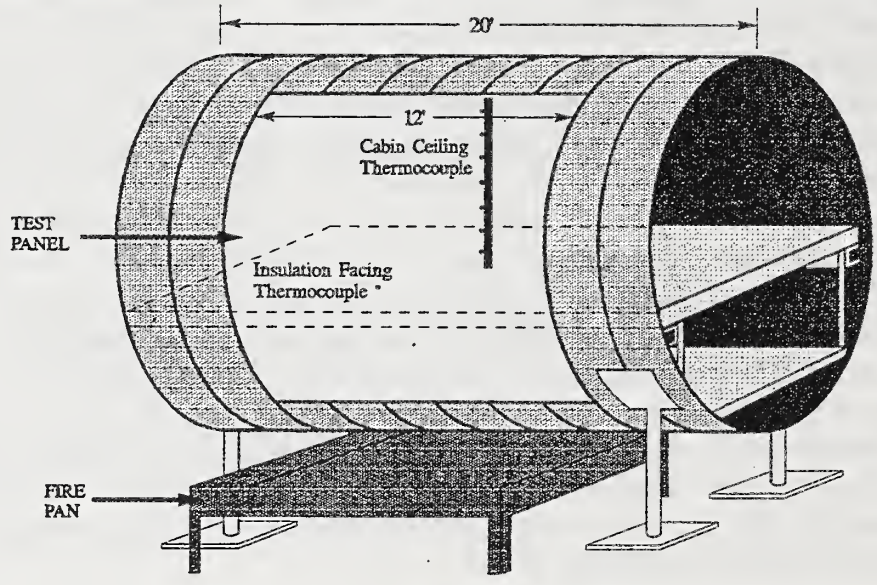

Figure 1

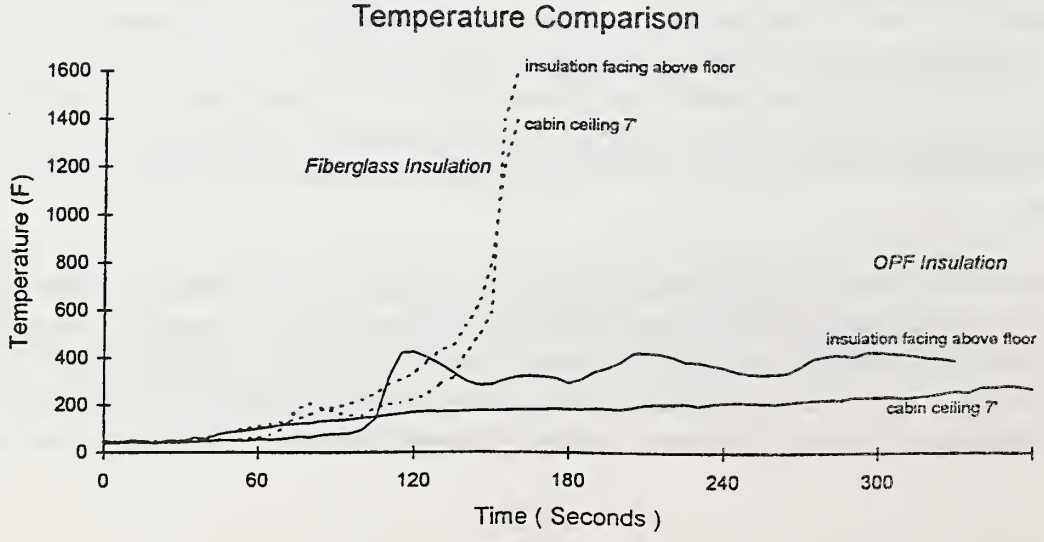

Figure 2

Ignitor and Thickness Effects on Upward Flame Spread

Cheol H. Lee* and J.Q. Quintiere
Department of Fire Protection Engineering
University of Maryland at College Park, MD 20742

Several studies,e.g. [1-5], have developed upward flame spread models which use somewhat different features. However, the models have not explicitly considered the effects of the ignitor and the thickness of material on spread. These factors have been found to be very significant in determining the potential for spread and its rate. Although theoretical results are only presented here, examples can be found in practice.

Using the flame spread model developed by Saito, Quintiere and Williams[1], the flame height(x_f) and flame spread velocity can be expressed respectively as follows:

$$x_f(t) = k_f\left[(\dot{Q}'_{ig}) + \dot{Q}'\right]^n , \tag{1}$$

where $\dot{Q}'_{ig}$ is the energy release rate per unit width of the ignitor and $\dot{Q}'$ is the corresponding value for the material

$$\dot{Q}' = \Delta H_c \left\{ \dot{m}''(t)x_{po} + \int_0^t \dot{m}''(t-t_p)V_p(t_p)\, dt_p \right\} \tag{2}$$

with $\dot{m}''$,the specific burning rate; and

$$V_p(t) = \frac{1}{\tau} \left\{ x_f - \left[x_{po} + \int_0^t V_p(t_p)dt_p \right] \right\} , \tag{3}$$

where $\tau = \frac{\pi}{4} k\rho c \left\{ \frac{T_{ig} - T_\infty}{\dot{q}''_f} \right\}^2$. This gives an integral equation for V_p. The value x_{po} represents the ignitor flame height and the initial height of material ignited in the model. The $\dot{Q}'_{ig}$ has a fixed duration time(Δt_{ig}) following ignition(t_{ig}), and its effect is only relevant in Eq.(3) as long as the burnout time(t_b) of position x_{po} is not exceeded. In terms of step functions,η,

$$\dot{Q}'_{ig} = \eta\,(t_b(x_{po}) - t) \cdot \eta\,\{(t_{ig}+\Delta t_{ig}) - t\} \cdot \dot{Q}'_{ig} . \tag{4}$$

From previous work[6,7], we have an implicit formula for transient burning rate ,$\dot{m}''(t)$, representative of a thermoplastic-like material,

$$\dot{m}''(\theta)\Delta H_v = \dot{q}''_f - \sigma T_{ig}^{\,4} - \frac{2k}{\delta}(T_{ig} - T_\infty), \tag{5a}$$

where

$$\theta = t - t_p(x) = \frac{\delta_s^2}{6\alpha}\frac{\Delta H_v}{L}\left[\frac{\delta_{ig} - \delta}{\delta_s} - \ln\left(\frac{\delta_s - \delta}{\delta_s - \delta_{ig}} \right) \right] , \tag{5b}$$

$$\delta_s = \frac{2kL}{c(\dot{q}''_f - \sigma T_{ig}^{\,4})} , \tag{5c}$$

and

$$\delta_{ig}(x) = \sqrt{6\alpha(t_p(x) - t_f(x))} \text{ ,where } t_f \text{ is time when the flame tip is at } x. \tag{5d}$$

The properties include k, c, ΔH_v, and $L = \Delta H_v + c(T_{ig} - T_\infty)$. For thickness, $\ell : \rho\,\ell = \int_0^{t_b(x)} \dot{m}''(t)\, dt$

A computer program was developed to solve the integral equation(3) for this thermoplastic model. From this program, we can obtain the pyrolysis zone(x_p), the flame height(x_f), the burnout position(x_b), the burnout time(t_b), the total energy release rate($\dot{Q}'$), and flame velocity(V_p) of a material at specific time(t).

As an illustration of results, properties representation of PMMA were used : $k=0.346*10^{-3}$ kW/mK, $\rho=1180$ kg/m^3, and c=2.5 kJ/kgK, L=2.7 kJ/g, ΔH_c=25 kJ/g, T_{ig}=636 K, and T_∞=300 K. The flame heat flux, $\dot{q}''_f$, was selected as 30kW/m^2. Experimental results for thick PMMA[3] serve as a benchmark for accuracy as shown in Figure 1. Adjustments in the properties could improve the agreement, but we stuck to the test properties available.

A study on the effect of thickness and the ignitor included variations of thickness (mm): 0.1, 0.5, 1, 3; ignitor duration (s) : 30, 60, 120, 480; $\dot{Q}'_{ig}$ (kW/m) : 10, 25, 50 or correspondingly x_{po} (m) : 0.2 , 0.5, 1.0. Figure 2 shows for the very thin material and low durations of the ignitor, the flame will never reach 5 m. But as these parameters are increased, propagation occurs and at faster speeds. Figure 3 shows the critical values of the parameters on propagation to 5 m. It is clear that all of these factors play a critical role in propagation. Recently, New York city had a real problem of fire spread in painted stairwells having up to 16 coats of paint. This presents a real problem relevant to the effect of material thickness, and ignitor characteristics on flame spread. Prescriptions for flame spread tests must also consider these factors.

* Attending W.P.I., Worcester, MA(Fall 1996)

1. K. Saito, J. Quintiere and F.A. Williams, "Upward Turbulent Flame Spread", Fire Safety Science-Proceedings of The First International Symposium, pp. 75-86.
2. F. Williams, C. Beyler, S. Hunt, and N. Iqbal, "Upward Flame Spread on Vertical Surface", NRL Ltr Ser 6180/0065.1, January, 1996.
3. L. Orloff, J. de Ris, and G. H. Marksten, "Upward Turbulent Fire Spread and Burning of Fuel Surface", The Fifteenth International Combustion Symposium, pp. 183-192, 1975.
4. H. E. Mitler and K. D. Steckler, "A Model of Flame Spread on Vertical Surface", National Institute of Standards and Technology, NIST 5619, April, 1995.
5. M.M. Delichatsios, M.K. Mathews, and M.A. Delichatsios, "Upward Fire Spread Simulation Code: Version I: Noncharring Fuels", Factory Mutal Research Corporation, FMRC J.I. OROJ2.BU., November 1990.
6. J. Quintiere and B. Rhodes, "Fire Growth Models for Materials", National Institute of Standards and Technology, NIST-GCR-94-647, June, 1994.
7. D. Hopkins, Jr, "Predicting the Ignition Time and Burning Rate of Thermoplastics in the Cone Calorimeter", National Institute of Standards and Technology, NIST-GCR-95-677, September, 1995.
8. C. H. Lee, "Investigation of a Model for Upward Flame Spread : Transient Ignitor and Burning Rate Effects", Master's Thesis, Department of Fire Protection Engineering, University of Maryland at College Park, May 1996.

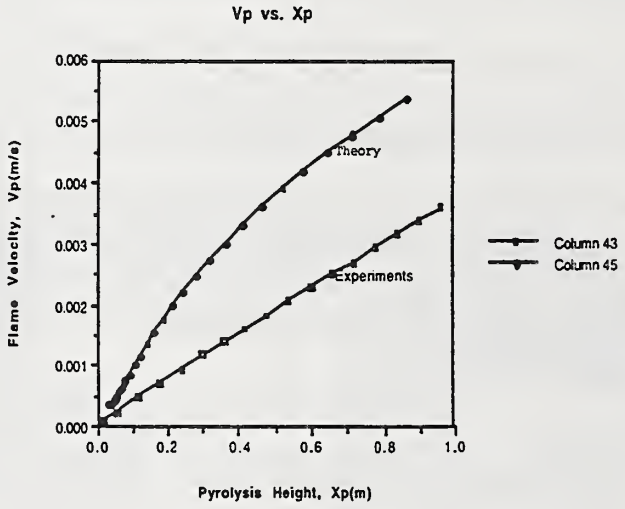

Figure 1. Comparison of Theory with experiment of Orloff et al. [3].

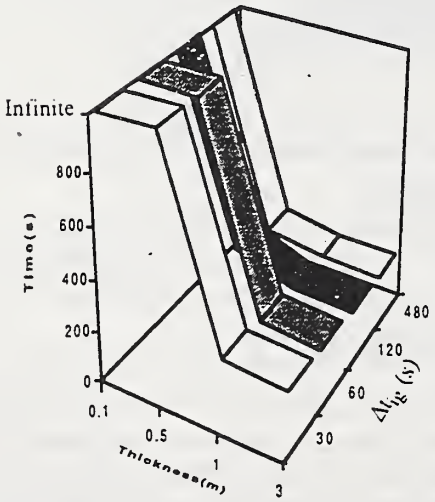

Figure 2. Time to reach 5 m as a function of material thickness and ignitor duration at 25 kW/m for the ignitor.

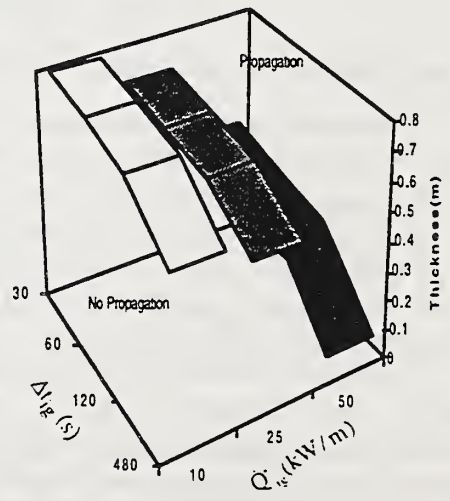

Figure 3. Estimated critical values for propagation to 5 m.

Experimental Measurements and Numerical Predictions of the Gasification of Finite Thickness Polymers

S.J. Ritchie and T. Kashiwagi
National Institute of Standards and Technology
Gaithersburg, MD 20899

During polymer combustion, there are two general processes that influence the burning rate of the material; the flame zone heat feedback to the polymer surface and the corresponding gasification rate of the polymer. The two processes are directly coupled. This study focuses on the condensed-phase processes which affect the gasification rate. Presented are the results of an experimental and numerical study into the influence of sample thickness and back surface boundary condition on the gasification rate of thermoplastic polymer materials under non-flaming conditions. Typically, the influence of thickness is ignored in theoretical developments because of the simplicity or convenience in assuming a semi-infinite material (ie. [1], [2]). However, in real applications of polymers, a semi-infinite analysis may be inappropriate.

Gasification experiments were carried out in a nitrogen gas environment with samples of polypropylene (PP) and polymethylmethacrylate (PMMA). The samples were 10.2 cm in dia and varied in thickness from 3 mm to 25.4 mm. Samples were subjected to incident fluxes of 30 and 50 kW/m^2 and the exposed and backside temperatures were measured with thermocouples. The samples were placed in a 10.2 cm dia. x (sample thickness + 6.4 mm) deep cavity which was cut into a 5.1 cm thk. x 12.7 cm dia. brick of foamglas insulation.

Numerical predictions were made using a one-dimensional model based on the classical Stefan problem for ablation that compensates for finite sample thickness and conductive losses to a backing substrate (also of finite thickness). The calculations required the solution of the heat equation in both the sample and the backing insulation. The two solutions were coupled at the interface using an energy balance and the continuity of temperature. The back boundary of the substrate was assumed to be adiabatic. The model has terms to compensate for the indepth absorption of the incident radiant energy and indepth degradation of the polymer material. The degradation is controlled by a finite rate chemical equation. The Arrhenius constants and reaction order were obtained using differential thermogravimetric analysis measurements at various heating rates [3]. Products generated indepth were assumed to be liberated from the sample immediately. The heat of vaporization was experimentally determined using a differential scanning calorimeter.

From a parametric study with the numerical model, the influence of the backing material on the gasification rate is clearly a function of the sample thickness. The predictions show that as sample thickness is increased, the gasification rate tends towards a semi-infinite solution. As the amount of material is reduced by the gasification process, the backside boundary condition eventually starts to influence the temperature gradient, which in turn alters the gasification rate. The exact nature of the change to the gasification rate depends on many factors which include: the relative material properties of the polymer and the backing material, the thickness of the backing material and the value of the externally applied flux. In the experiments, the conductivity of the backing material was much lower than that of the sample. Therefore the gasification rate rises very dramatically when the sample becomes thermally thin as shown in Figure 1 for the PMMA. For the 3.2 mm and 6.4 mm thick samples this influence is observed immediately,

precluding any evaluation of material characteristics independent of the apparatus. For the thicker samples, such as 25.4 mm, the back boundary condition does not alter the results noticeably until the sample is very thin near the end of the gasification experiment. The quasi-steady portion of the gasification rate curve is a better measure of the materials response to heating because it is independent of the backing material (ie. apparatus independent). The numerical model predicts the observed experimental trends extremely well. Small differences in the absolute values between the model predictions and the experimental measurements can be attributed to processes that have not been fully considered in the numerical prediction such as: a conductive heat transfer contact resistance between the sample and the backing material, the transport of indepth degradation products through the polymer melt, and the variation of material properties with temperature and material characteristics. For example, when bubbles are trapped within a liquid melt layer the conductive and radiative heat transfer through the sample could be dramatically altered.

The results of this study impact the evaluation of cone calorimeter data and the application of polymer materials in many realistic applications. Often cone calorimeter data is presented in terms of a maximum heat release rate per unit area of burning material. However, this value is dependent upon the material used as a backing substrate and does not represent an independent material property. A more appropriate measure would be of the quasi-steady state value achieved using samples of much larger thicknesses ($>$ 12 mm). Additionally, the gasification process of materials subjected to fire conditions in realistic applications will be influenced strongly by both the thickness of the material and the boundary conditions imposed.

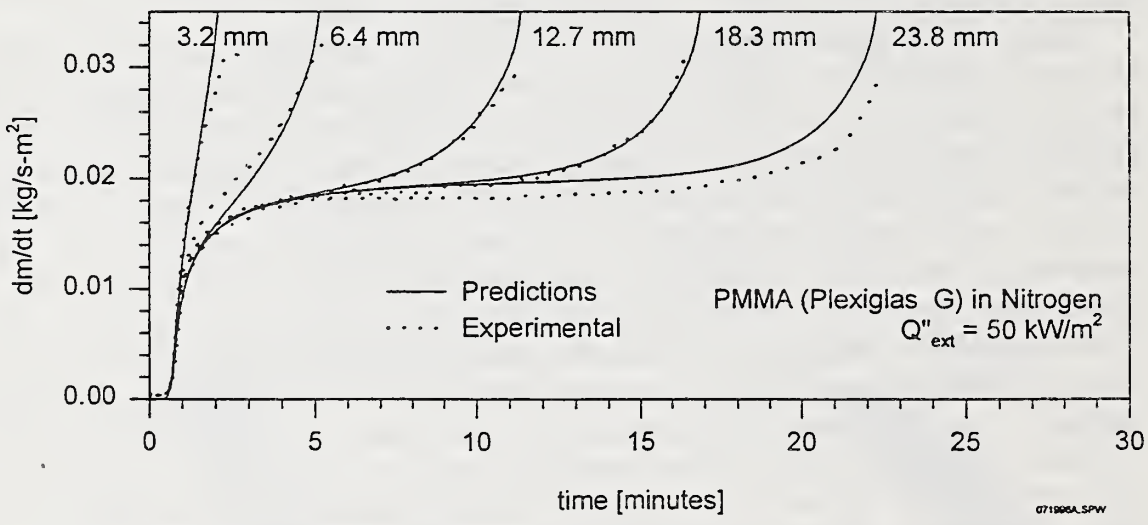

Figure 1. Gasification rate comparison of experimental measurements with numerical predictions for PMMA at various thicknesses when subjected to 50 kW/m^2 of external energy.

[1] Steckler, K.D., Kashiwagi, T., Baum, H.R. and Kanemaru, K., *Proc. 3rd Int. Symp. on Fire Safety Sci.*, 895-904, (1992).

[2] Quintiere, J. and Iqbal, N., *Fire and Matls.*, 18:89-98 (1994).

[3] Kissinger, H.E., *Analytical Chemistry*, 29:1702-1706, (1957).

AN ANALYTICAL MODEL OF PYROLYSIS FOR A FINITE THICKNESS SAMPLE ON A SEMI-INFINITE BASE

Kathryn M. Butler
Building and Fire Research Laboratory
National Institute of Standards and Technology
Gaithersburg, Maryland 20899

Introduction To test the flammability of materials, a sample is placed on a substrate and exposed to a uniform heat flux. Measurements include sample mass and upper and lower surface temperatures as functions of time. Several analytical models[1,2,3] have been developed in an attempt to fully understand the relationship between properties of the tested materials and test results. Most of these models have assumed a semi-infinite sample, although the finite thickness of the sample is known to have a significant effect on pyrolysis behavior. An analytic solution that includes *finite sample thickness* and the material properties of the base is introduced in this abstract.

Model A sample of initial thickness L, thermal conductivity k_s, density ρ_s, and specific heat c_s is placed on a base of semi-infinite extent with thermal properties k_b, ρ_b, and c_b. The interface is located at $z = 0$, and the temperature is initially uniform at T_0. At time $t = 0$, a constant heat flux $\dot{q}''$ is applied to the upper surface of the sample. When the surface temperature has reached a critical temperature T_p, the material at the surface begins to pyrolyze at a rate that depends on the heat of vaporization ΔH_v. The moving boundary is located at $z = Z(t)$ and the mass loss rate is $dm''/dt = \rho_s dZ/dt$. In-depth pyrolysis is ignored, so the temperatures within each material satisfy the diffusion equation for heat transfer.

In solving this problem, the nondimensionalized temperature is defined as $\theta = (T - T_0)/T_0$ and the nondimensionalized time as $\tau = \int_0^t (\alpha_s/Z(t)^2)\, dt$. The fixed coordinate system z is changed into a system that moves with the boundaries by defining $y = z/Z(t)$. This change of variables introduces a convective term into the heat transfer equation. A separate coordinate system for the base, $y_b = y\sqrt{\alpha_s/\alpha_b}$, matches the time coordinate in the base with that of the sample.

Other assumptions for this model are:

- Thermal properties independent of temperature
- Perfect thermal contact between sample and base, so that temperature and heat flux are continuous at the interface
- Surface temperature steady at T_p throughout pyrolysis
- Convective term in sample assumes the surface temperature gradient throughout the sample

Using these assumptions, analytic expressions can be found for temperature profiles in the sample and base during both preheating and pyrolysis stages. The nondimensional parameters that affect the temperatures in (y, y_b, τ) space are $\eta = \sqrt{k_s\rho_s c_s/k_b\rho_b c_b}$, the ratio of thermal inertias for the sample and base materials, $\beta = \dot{q}''L/k_sT_0$, a nondimensional parameter describing the incident heat flux, and $\gamma = (\Delta H_v/c_sT_0)$, which describes the heat loss due to vaporization. The parameter η appears in the solution in the form $\delta = (\eta - 1)/(\eta + 1)$, which ranges between -1 and 1 and orders the sets of infinite series that appear in the solution. For $\delta = 0$, properties of sample and base are identical, and the solution reduces to that for a semi-infinite sample. Pyrolysis begins when the temperature at the sample surface reaches the critical temperature $\theta_p = (T_p - T_0)/T_0$. To first order in δ, this occurs at time $\tau_p = \pi\theta_p^2/4\beta^2$.

Results An example demonstrates the characteristics of this model. In this problem, the sample is a material with thickness $L = 0.003175$ m, thermal properties $k_s = 16.9 \times 10^{-5}$ kW/m-°K, $\rho_s = 1190$ kg/m^3, and $c_s = 2.6$ kJ/kg-°K, pyrolysis temperature $T_p = 635$°K, and heat of vaporization $\Delta H_v = 850$ kJ/kg. The thermal properties of the base are $k_b = 7.8 \times 10^{-5}$ kW/m-°K, $\rho_b = 128.0$ kg/m^3, and $c_b = 0.76$ kJ/kg-°K. Ambient temperature is $T_0 = 300$°K, and the heat flux applied to the sample is $\dot{q}'' = 50$ kW/m^2. Heat losses due to re-radiation and convection from the hot surface are not included.

Preliminary results are shown in Figures 1 through 4. Figure 1 shows the nondimensional temperature θ as a function of y, the location normalized by the sample thickness, during preheating and pyrolysis. In

Figure 2, the same information is plotted for physical values of temperature and distance. Figure 3 plots the temperature as a function of time for locations from the sample/base interface to the upper surface of the sample. Note that the interface temperature starts to decrease after two minutes, indicating that the analytic solution is not valid beyond this point. At this time less than ten percent of the sample remains, and indepth pyrolysis becomes very important. The mass loss rate, determined from the spatial gradient of temperature at the sample surface, is plotted against time in Figure 4. The trend of this curve matches experimental behavior. More complete results will be discussed in the presentation.

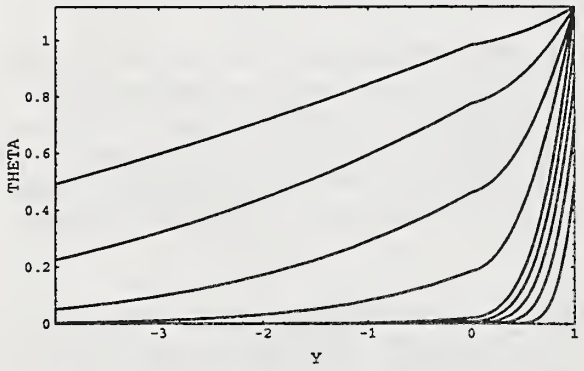

Figure 1: Nondimensional temperature (θ) vs. location (y) at times $\tau = \tau_p \times (0.2, 0.4, 0.6, 0.8, 1.0)$ during preheating and $\tau = (0.25, 0.5, 1, 2)$ during pyrolysis.

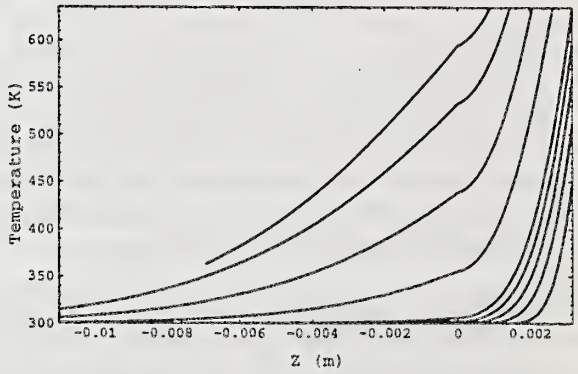

Figure 2: Same as Figure 1 but converted to physical temperature and location. Plots are at times (in seconds) t =(3.6, 7.3, 10.9, 14.6, 18.2, 41.5, 66.5, 93.9, 117.7).

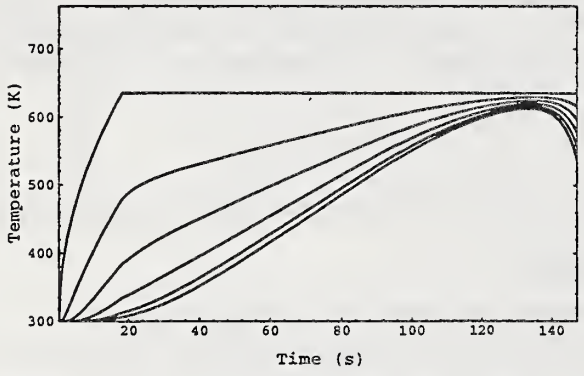

Figure 3: Temperature at evenly spaced locations between upper and lower surfaces of sample vs. time

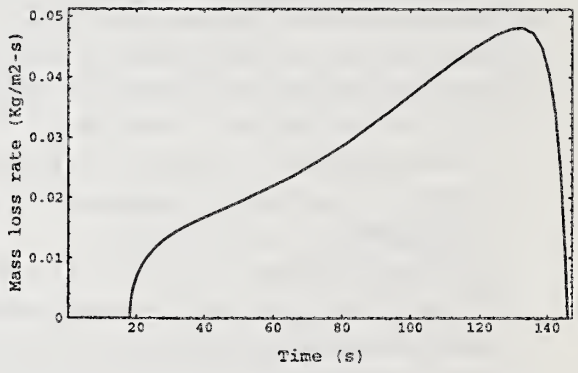

Figure 4: Mass loss rate of sample vs. time.

Conclusions An analytic solution has been determined for the pyrolysis of a sample of finite thickness resting on a substrate of a different material. Besides providing insight into pyrolysis behavior, this model may improve our capability to derive material properties from common flammability test measurements.

References

[1] Steckler, K.D., Kashiwagi, T. and Baum, H.R., "Analytical Model for Transient Gasification of Noncharring Thermoplastic Materials," *Fire Safety Sci. - Proc. of 3rd Intl. Symp.* 895–904 (1991).

[2] Chen, Y., Delichatsios, M.A., and Motevalli, V., "Material Pyrolysis Properties, Part I: An Integral Model for One-Dimensional Transient Pyrolysis of Charring and Non-Charring Materials," *Comb. Sci. and Tech.* 88:309–328 (1993).

[3] Quintiere, J. and Iqbal, N., "An Approximate Integral Model for the Burning Rate of a Thermoplastic-like Material," *Fire and Mat.* 18:89–98 (1994).

Abstract prepared for the NIST ANNUAL CONFERENCE ON FIRE RESEARCH,
Gaithersburg Hilton Hotel, Gaitersbusg, MD, October 28-31, 1996

Critical Conditions for Extinction and Transient Pyrolysis Decay in Solid Material Fires

by
Michael A. Delichatsios, FMRC, Norwood MA.02062

BACKGROUND AND INTRODUCTION

A new flame extinction condition [1] for the critical mass pyrolysis rate has been developed when extinction occurs by interaction of flames with the pyrolyzing surface of a condensed material. The extinction conditions provide both the critical mass pyrolysis rate and the corresponding convective heat flux to the surface. The extinction conditions are derived from simple analysis of combustion and heat transfer, and they are shown to be applicable for various experimental conditions such as fuel dilution by inert gas, oxygen dilution by inert gas, effects of external heat flux, material preheating, transient (charring) pyrolysis, including geometric effects which influence the critical mass pyrolysis rate through an effective heat transfer coefficient. Additional validation of the proposed extinction conditions is provided by numerical simulation reported in literature in the regime of low straining rates for a stagnation flow on a cylinder. The present approach can be used to measure critical extinction conditions in a flammability apparatus and allow them to be applied in other conditions such as in microgravity. The critical conditions can be used to apply models for the transient decay of pyrolysis when an extinguishing agent is applied until extinction or a new steady state pyrolysis/burning is reached.

TRANSIENT PYROLYSIS DECAY

We consider the following scenario which has also been reproduced experimentally. A slab of solid material (10 cm x 10 cm x 2.54 cm thick) is burning at steady state conditions in a horizontal or vertical orientation. At a given time, a suppression agent is applied so that the heat flux to the surface is decreased either by direct cooling (by water drops on the surface) or weakening of gaseous reactions (by inerting of gaseous phase). If this cooling is effective within times shorter than the thermal response of the material, pyrolysis rates will drop suddenly before recovery to a new steady state (see Fig.1a where reduction of heat flux is effected by inerting of the oxidant stream and Figure 1b where reduction of heat flux is effected by sudden decrease of the externally applied heat flux. Both experiments were conducted in FMRC flammability apparatus.} Otherwise, if cooling is not applied "fast" or uniformly, sudden drop in pyrolysis does not occur and the decay time is controlled by the solid material thermal response. This is the case for surface water application [2] as shown in Figure 2 for the correlation of times to extinction using the thermal response properties of the material (in all cases in Figure 2 the water application rates are such that extinction occurs).

References

1. Delichatsios, M. A. " Required Water Density for Fire Extinguishment or Control" Final report for NIST Grant # 60NANB4D1675, submitted for publication, 1996.

2. Magee, R. S. and Reitz, R.D. Fifteenth Symposium International on Combustion, The Combustion Institute, Pittsburgh, PA, 1975.

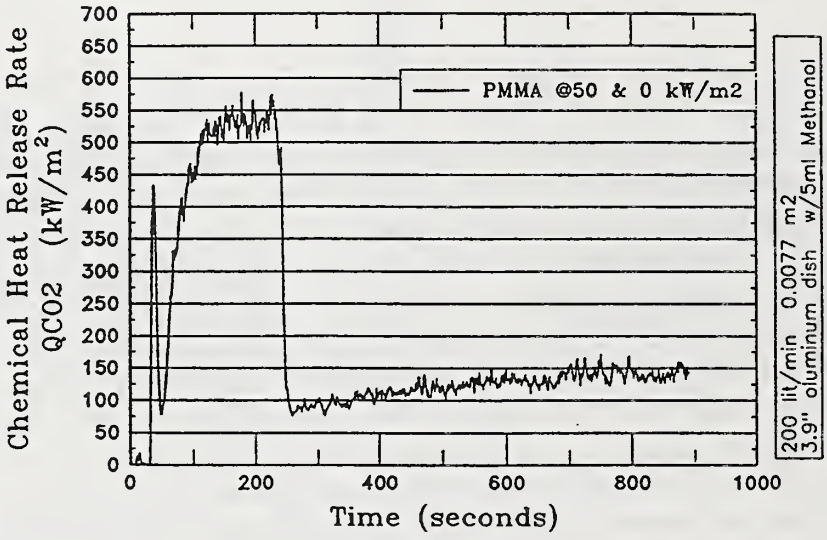

Figure 1. A similar plot as in Figure.1a but the change involves the sudden variation of external heat flux from 50 kW/m^2 to zero. The final state is supported by the flame heat flux (FMRC flammability apparatus).

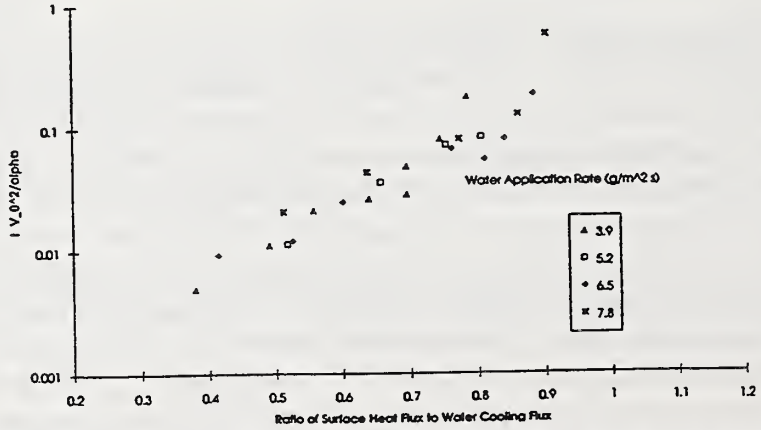

Figure 2. Correlation of time to extinction of PMMA slabs by surface water application [2]. The time is normalized by a thermal response time corresponding to the thermal profile just before water application.

MASS LOSS MODEL FOR CHAR FORMING POLYMERS

Richard E. Lyon
Fire Research Section, AAR-423
Federal Aviation Administration Technical Center
Atlantic City International Airport, N.J. 08405 USA

The basic mechanism of the pyrolysis of char forming polymers has been described as a generalized process consisting of primary and secondary thermal decomposition events. The primary decomposition step occurs through a free radical intermediate with generation of a primary gas and disproportionation to hydrogenated tar and hydrogen-deficient primary char residue. The primary char decomposes by dehydrogenation to form the secondary gas and a thermally stable char. This pyrolysis scheme accounts qualitatively for the low char yield of hydrogen-rich polymers. In the absence of hydrogen atoms, polyaromatic free radical nuclei can recombine to form crosslinks or stable, non-volatile species (char) which resist further decomposition.

A simple result for the mass loss history of a char forming polymer for use in fire models is obtained by recognizing that the important process with respect to material flammability is the fuel generation rate at or near the decomposition (≈ surface burning) temperature. With this in mind the following assumptions can be made: 1) thermolysis of primary chemical bonds in the polymer is the rate-limiting step for isothermal mass loss, 2) mass loss proceeds through an active intermediate which is a stationary state, 3) primary gas production and char formation are simultaneous processes whose magnitude and rate constants are large compared to successive products and rate processes (i.e., secondary char formation), and 4) conditions are anaerobic in the pyrolysis zone so that oxidation reactions may be neglected in the mass loss model. The above assumptions lead to a simplified kinetic scheme for polymer pyrolysis which reduces gas and char formation to a single step involving parallel decomposition reactions of the active intermediate as shown in Figure 1.

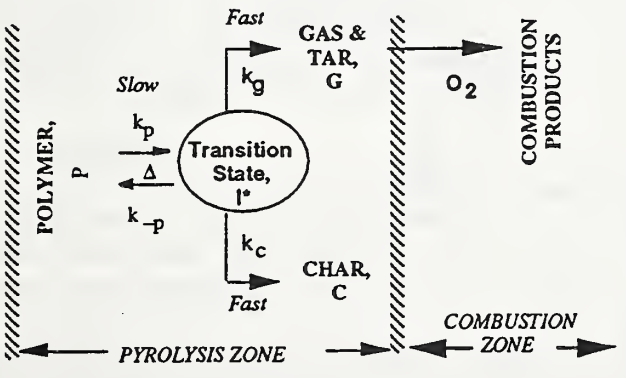

Figure 1. Kinetic mass loss model for polymer combustion

The rate equations for the instantaneous mass of polymer, P, reactive intermediate, I*, primary gas, G, and primary char, C, according to Figure 1 are

$$\frac{dP}{dt} = -k_p P + k_{-p} I^* \tag{1}$$

$$\frac{dI^*}{dt} = k_p P - \left(k_{-p} + k_g + k_c\right) I^* \tag{2}$$

$$\frac{dG}{dt} = k_g I^* \tag{3}$$

$$\frac{dC}{dt} = k_c I^* \tag{4}$$

With $I^* << P, G, C$, the total mass balance in terms of the initial mass, m_o, is

$$m_o = P + G + C + I^* \approx P + G + C \tag{5}$$

while the sensible mass of the sample (as measured for example in a TGA experiment) is

$$m = P + C + I^* \approx P + C \tag{6}$$

The solution for the mass loss history of a char forming polymer at constant temperature from Equations 1-6 and the four assumptions is

$$\frac{m}{m_o} = Y_c + (1 - Y_c)\, e^{-k_p t} \tag{7}$$

where k_p is the forward pyrolysis rate constant and $Y_c = k_c/(k_c+k_g)$ is the equilibrium char yield at a particular temperature. Equation 7 also describes the mass loss history of filled polymer systems having an inert filler loading fraction Y_c which is not temperature dependent.

Equation 7 was used to fit thermogravimetric data for anaerobic, isothermal, mass loss histories of a crosslinked phenolic triazine thermoset resin at temperatures ranging from 350–450C using k_p and Y_c as adjustable parameters. Experimental data for the isothermal mass loss histories are shown as solid symbols in Figure 2 while the solid lines are the best fit of Equation 7 to the experimental data using k_p and Y_c values listed in Table 1.

Figure 3 is an Arrhenius plot of the pyrolysis rate constants, k_p, listed in Table 1 as $\ln[k_p]$ versus $1/T$. The activation energy E_a for pyrolysis of phenolic triazine resin obtained

from the slope in Figure 3, E_a = 165 kJ/mol, is approximately half of the value obtained for these same data from n-th order kinetics while the frequency factor, A = 10^9 sec^{-1}, determined from the intercept is essentially the square root of the value determined from non-charring first-order kinetics.

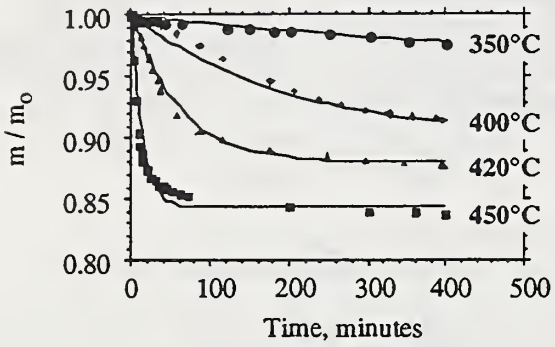

Figure 2. Mass loss history of phenolic triazine at 350, 400, 420, and 450°C. Solid lines are fit of Equation 7.

Table 1.
Best Fit k_p and Y_c Values for Isothermal Pyrolysis of Phenolic Triazine Thermoset Resin

T (°C)	k_p (sec^{-1})	Y_c
350	1.4 x 10^{-5}	0.92
400	8.5 x 10^{-5}	0.90
420	2.7 x 10^{-4}	0.88
450	1.2 x 10^{-3}	0.84

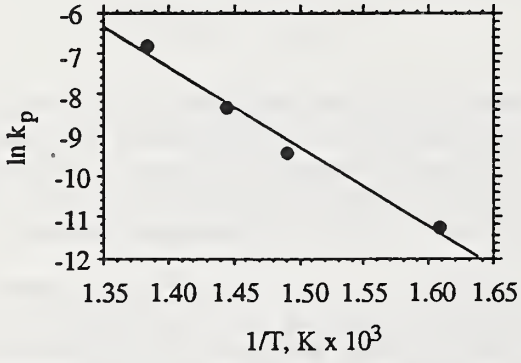

Figure 3. Plot of ln[k_p] *versus* reciprocal temperature for phenolic triazine resin.

Assuming an Arrhenius form for the gasification and charring rate constants, k_g and k_c, Equation 7 can be rearranged to give

$$\ln\left[\frac{1-Y_c}{Y}\right] = \ln\left[\frac{A_g}{A}\right] - \left[\frac{E_g - E_c}{R}\right]\frac{1}{T} \qquad (8)$$

so that a plot of $\ln[(1-Y_c)/Y_c]$ versus 1/T has a slope proportional to the difference in activation energies for gas and char formation. Figure 4 shows such a plot constructed from the isothermal char yields in Table 1. The slope gives ($E_g - E_c$) = +30 kJ/mol and the intercept, A_g/A_c = 17. This result indicates char formation is favored over volatile production by 30 kJ/mol consistent with the high char yield of this material.

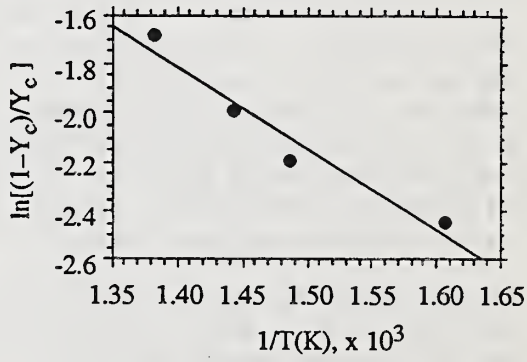

Figure 4. Plot of the natural logarithm of $(1-Y_c)/Y_c$ versus reciprocal temperature for the phenolic triazine resin.

The rate constants for phenolic triazine resin pyrolysis, char and gas formation can be substituted into Equation 7 to allow calculation of the mass loss as function of temperature at different heating rates. Results of these calculations are shown in Figure 5 as solid lines. Symbols are data from thermogravimetric experiments at constant heating rates of β =1, 5, and 20 K/min. It is seen that the predicted mass loss of the phenolic triazine resin calculated from Equation 7 is in excellent agreement with data up to the secondary mass loss event (T> 600°C) which was neglected in the present derivation. The dashed line is the calculated equilibrium char yield (β = 0) as a function of temperature.

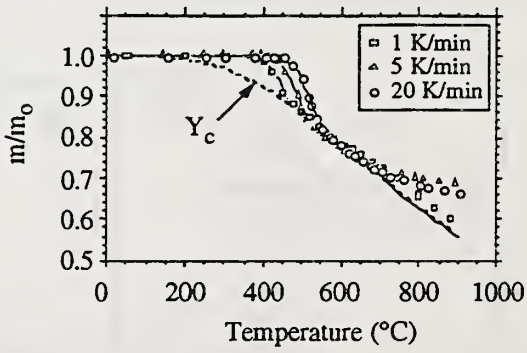

Figure 5. Measured and calculated mass loss of phenolic triazine resin in TGA at constant heating rates of β =1, 5, and 20 K/min.

Laboratory and Mine Scale Evaluation of Smoke Detectors

John C. Edwards

U.S. Department of Energy
Pittsburgh Research Center
Pittsburgh, PA 15236

Several experimental programs were conducted under the U.S. Bureau of Mines to investigate the level of mine fire detection and alarm capability currently possible using state-of-the-art technology. These programs involved comparison of the response and alarm time of optical and ionization type smoke detectors to smoldering and flaming coal combustion in a smoke chamber (1). One optical type detector operated in a diffusion mode, and a second in a pump mode. Two of the ionization type detectors operated in a pump mode, and two in a diffusion mode. CO concentration and smoke optical density were continuously measured. The coal combustion experiments conducted in the smoke chamber demonstrated that a CO concentration 5 ppm above background corresponded to an optical density of 0.022 m^{-1}. For the four smoke detectors for which a measurable continuous analog signal was available, a smoke detector alarm was defined as the average background signal plus ten times the peak-to-peak noise. This alarm criterion resulted in the association of the alarm for three of the four detectors with a smoke optical density of 0.011 m^{-1}, and 0.033 m^{-1} for the fourth smoke detector. An ionization type smoke detector which operated in a diffusion mode and had only an on-off output signal alarmed at an optical density of 0.12 m^{-1} for smoldering coal combustion, and 0.077 m^{-1} for flaming coal combustion. A prototype ionization type pump mode smoke detector, a submicron particle detector, was used to measure a number mean smoke particle diameter of 0.45 μm for smoldering coal combustion and 0.38 μm for flaming coal combustion. At an optical density of 0.022 m^{-1}, a comparison was made of the detectors' signal for the smoldering and flaming coal combustion experiments. The optical-type smoke detectors responded with greater intensity to smoldering than to flaming coal combustion; whereas the ionization smoke detectors responded with greater intensity to flaming than to smoldering coal combustion. As part of the smoke detector evaluation experiments, an odor monitor's response to the smoke was recorded. For the smoldering coal combustion experiments, the odor monitor alarm time was defined as the monitor's equivalent response to 1 ppm of H_2S, associated with combustion products from sulfur containing Pittsburgh seam coal. For the smoldering coal combustion experiments the odor monitor alarm time was earlier than the CO alarm time, whereas the odor monitor and CO alarm times were comparable for the flaming coal combustion experiments. A comparison of the odor monitor's alarm time with one of the ionization smoke detector's alarm time showed equivalency for smoldering coal combustion, whereas for flaming coal combustion the smoke detector alarmed prior to the odor monitor.

The smoke detectors used in the smoke chamber studies were incorporated into large scale diesel fuel fire experiments conducted under normal ventilation conditions in the Safety Research Coal Mine (SRCM) located at the Pittsburgh Research Center (2). In those studies a relative comparison was made of the smoke detector alarm time to that of a diffusion mode CO detector. Two diffusion mode smoke detectors, one ionization and one optical type, alarmed earlier than a diffusion mode CO detector. Based upon the measurement of the optical light transmission at the location of a pump mode ionization type smoke detector, it was determined that the smoke detector alarmed at an average optical density of 0.021 m^{-1} for the twelve experiments conducted.

Two ultrasonic ranging systems were used to demonstrate their response to smoke and heat in eighteen underground mine-fire experiments (3). In one of the experiments smoke candles instead of a diesel fuel fire were used to demonstrate that the ranging system responded to smoke in the absence of heat. In an experiment conducted in the intermediate scale fire tunnel with a coal fire, and a ranging system alarm defined as the average background signal plus ten standard deviations, the smoke optical density at the alarm was 0.025 m^{-1}.

REFERENCES

1. Edwards, J. C., and G. S. Morrow. Evaluation of Smoke Detectors for Mining Use, USBM RI 9586, 1995, 17pp.

2. Edwards, J. C., and G. F. Friel. Comparative In-Mine Evaluation of Carbon Monoxide and Smoke Detectors. USBM RI 9622, 1996, 11pp.

3. Friel, G. F., and J. C. Edwards. Mine Fire Detection by Ultrasonic Ranging Systems. DOE Pittsburgh Research Center RI 9624, 1996, 15pp.